NASA Contractor Report 165549

NASA-CR-165549
19820018563

HOT ISOSTATICALLY PRESSED MANUFACTURE OF HIGH STRENGTH MERL 76 DISK AND SEAL SHAPES

R. D. Eng and D. J. Evans

United Technologies Corporation
East Hartford, Connecticut 06108

May 1982

Prepared for

NATIONAL AERONAUTICS AND SPACE ADMINISTRATION
Lewis Research Center
Under Grant NAS3-20072

DISPLAY 28/2/1
82N26439*# ISSUE 17 PAGE 2377 CATEGORY 26 RPT#: NASA-CR-165549 NAS
1.26:165549 PWA/5574-123 CNT#: NAS3-20072 82/05/00 139 PAGES
UNCLASSIFIED DOCUMENT
UTTL: Hot isostatically pressed manufacture of high strength MERL 76 disk and seal shapes TLSP: Final Report
AUTH: A/ENG, R. D.; B/EVANS, D. J.
CORP: United Technologies Corp., East Hartford, Conn. CSS: (Commercial

TABLE OF CONTENTS

TABLE OF CONTENTS

SUMMARY

Project 2 of Contract NAS3-20072 began in September 1977. Its objective was to demonstrate the feasibility of using MERL 76, an advanced high strength direct hot isostatic pressed powder metallurgy superalloy, as a full scale component in a high technology, long life, commercial gas turbine engine. To be consistent with Pratt & Whitney Aircraft application of hot isostatically pressed, high strength powder metal disk alloys in such near term commercial engines, Project 2 was directed toward component testing including spin burst rig testing and engine demonstration testing of a JT9D first stage turbine disk. The specific goals of this project were as follows:

- Increase the JT9D disk rim temperature capability by at least 22C°(40F°) over disks produced from Superwaspaloy.
- Reduce the weight of JT9D high pressure turbine rotating components by at least 35 pounds by replacement of forged Superwaspaloy components with hot isostatic pressed MERL 76 components.
- Reduce JT9D disk manufacturing costs by at least 30 percent relative to Superwaspaloy disks.

Through an internally funded program, Pratt & Whitney Aircraft identified MERL 76 as an alloy capable of achieving properties comparable to Gatorized™ IN-100 in the as-HIP condition. The alloy has exhibited an improvement in cyclic life capability with improved resistance to corrosion and at a lower cost because of its HIP processibility.

In the previously completed Pratt & Whitney Aircraft MATE Project 1 under this same Contract, HIP processing procedures including powder manufacture and handling, container design and fabrication, and HIP consolidation techniques were established for another nickel base powder alloy, low carbon Astroloy which resulted in the technology base used to qualify astroloy turbine disks for the JT8D engine fleet. In addition to establishing tolerances for the HIP

cycle, inspection procedures including microstructural (thermally induced porosity tests), ultrasonic, and dimensional methods were demonstrated. The results of Project 1 established suitable manufacturing methods, including a process control plan, acceptance criteria and material specification, for fabrication of direct-HIP powder nickel alloys such as Low Carbon Astroloy for disk applications. Project 1 and the alloy development program conducted in house at Pratt & Whitney Aircraft, which established the chemical composition of the MERL 76 alloy, led to the logical extension of the work conducted under NAS3-20072, Project 2, "HIP Manufacture of MERL 76 Disk and Seal Shapes".

At the inception of the MATE Project 2, turbine disks and rotor seals were to be analyzed by evaluating a high strength powder alloy, MERL 76, direct HIP consolidated as in the JT10D disk configuration. After the initial group of HIP consolidations were fabricated, significant engine design changes and the projected unavailability of a JT10D experimental engine to test the manufactured MERL 76 components resulted in reorientation of the program. Consequently, although manufacturing procedures using JT10D MERL 76 turbine disks and tangential on-board injection (TOBI) rotor seals were identified and design allowable data using JT10D and JT9D disks were established, JT9D disk shapes were used for all component evaluation. The target component net sonic shape for the JT9D disk is presented in Figure 1.

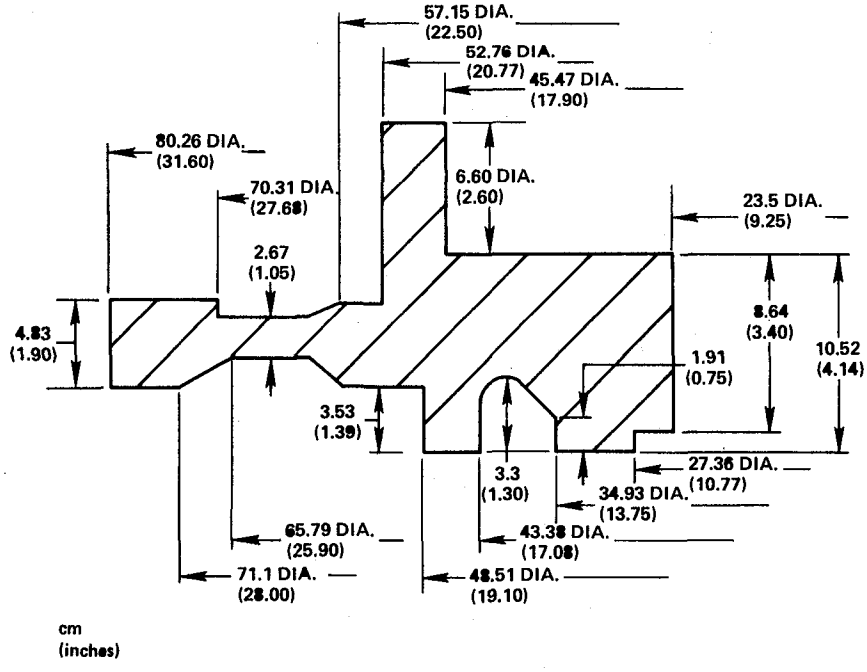

Figure 1 Target Shape for JT9D Disk

Concurrent with the program reorientation, a Pratt & Whitney Aircraft funded program determined that a modified MERL 76 composition (0.4% Hf, 1.2% Nb) gave greater latitude in the HIP consolidation temperature and improved stress-rupture properties without any adverse effect on mechanical properties. This modified chemistry was used to manufacture disk consolidations for the component evaluation portion of the program consisting of design data establishment, spin burst test, and experimental engine test. The modified MERL 76 composition is given in Table I.

TABLE I

COMPOSITION OF MERL 76

	Ni	Cr	Co	Mo	Al	Ti	Nb	Hf	B	Zr	C	Mn	S	P	Si	Fe	Cu	Bi	Pb	O	N
Min	R	11.9	18.0	2.8	4.85	4.15	1.20	0.30	0.016	0.04	0.015										
Max		12.9	19.0	3.6	5.15	4.50	1.60	0.50	0.024	0.08	0.03	0.02	0.01	0.01	0.10	0.30	0.07	0.5*	2.0*	100*	50*

*ppm
R = remainder

The objective of Task I was to select a heat treatment capable of achieving the desired properties for the alloy. The heat treatment selected was 1163°C(2125°F)/2 hrs./OQ + 871°C(1600°F)/0.67 hrs./AC + 982°C(1800°F)/0.75 hrs./ AC + 689°C(1200°F)/24 hrs/AC + 760°C(1400°F)/16 hrs/AC. Based upon the procedures utilized to manufacture ten HIP consolidated components in Task I, the manufacturing process was then finalized resulting in the establishment of a process control plan and acceptance criteria for MERL 76 HIP consolidated components as given in Appendix N. Using these established criteria, three remaining disk components were manufactured, one each for spin/burst rig test, experimental engine test, and design data generation.

A second requirement of Task I was to establish lower limit design properties for tensile (Figure 2), stress-rupture (Figure 3), 0.2% creep (Figure 4), and notched (Kt = 2.5) low cycle fatigue properties (Figure 5). In addition axial low cycle fatigue, fatigue crack propagation and low cycle fatigue crack threshold data were generated. During the course of measuring the mechanical properties, it was determined that several disks exhibited marginal rupture life and tensile ductility due to a prior particle boundary facture mode attributed to the presence of "golden" particles, presumably covered by hafnium oxide in the as-recieved powder. These "golden" particles were clearly observable at 30X using an optical microscope. For this reason, a binocular examination of the powder is included in the Process Control Plan (Appendix N).

In Task II, one disk was manufactured into a finish-machined JT9D 1st stage turbine disk and then spin tested. At four overspeed increments, growth measurements (Figure 6) were taken demonstrating that MERL 76 had acceptable growth and therefore adequate burst margin for rotating component applications.

In Task III, one disk was manufactured into a finish-machined JT9D 1st stage turbine disk which is scheduled for subsequent experimental test in a ground-based engine (Task IV) in December 1981 through January 1982. While the results of the disk's manufacturing process are presented in this report, the results of this engine test, which has not been conducted at the date of this writing, will be reported in Volume II of this contract (CR-165550) because of F.E.D.D. restrictions on category 2-type data.

Task V analyzed and compared the results of direct HIP MERL 76 to conventionally forged Superwaspaloy®. In adddition to displaying superior mechanical properties, direct HIP MERL 76 met the program objectives of increased rim temperature capability (Figure 7), reduced component weight (Figure 8), and at least 30% reduced material cost based on 1980 costs (Figure 9) when compared to Superwaspaloy®.

The results of this program have led to the conclusion that direct HIP MERL 76 disks are suitable for fabrication of components to be used in a commercial engine.

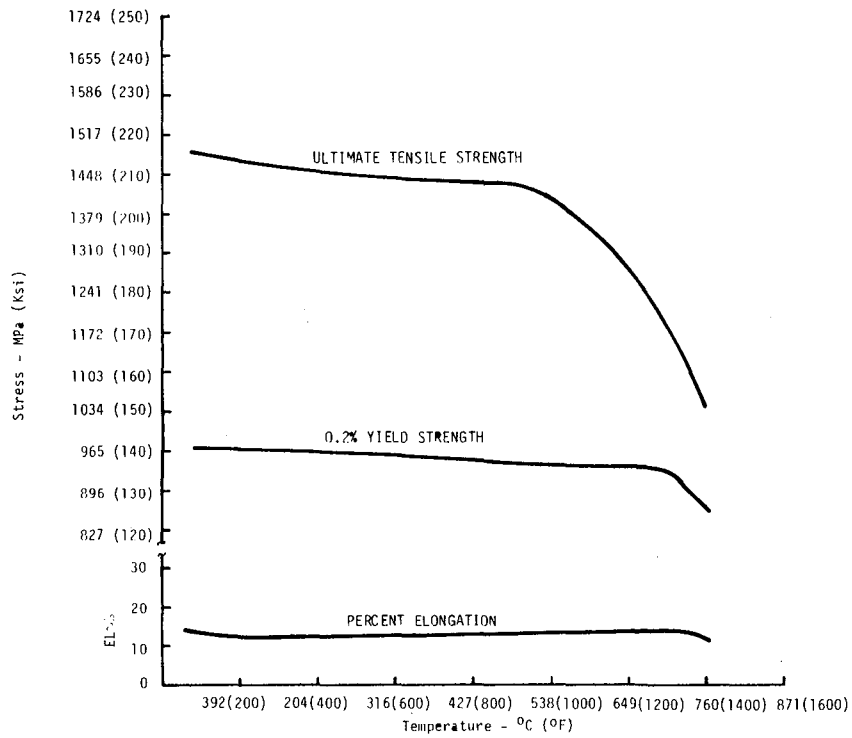

Figure 2 Lower Limit Tensile Properties of MERL 76

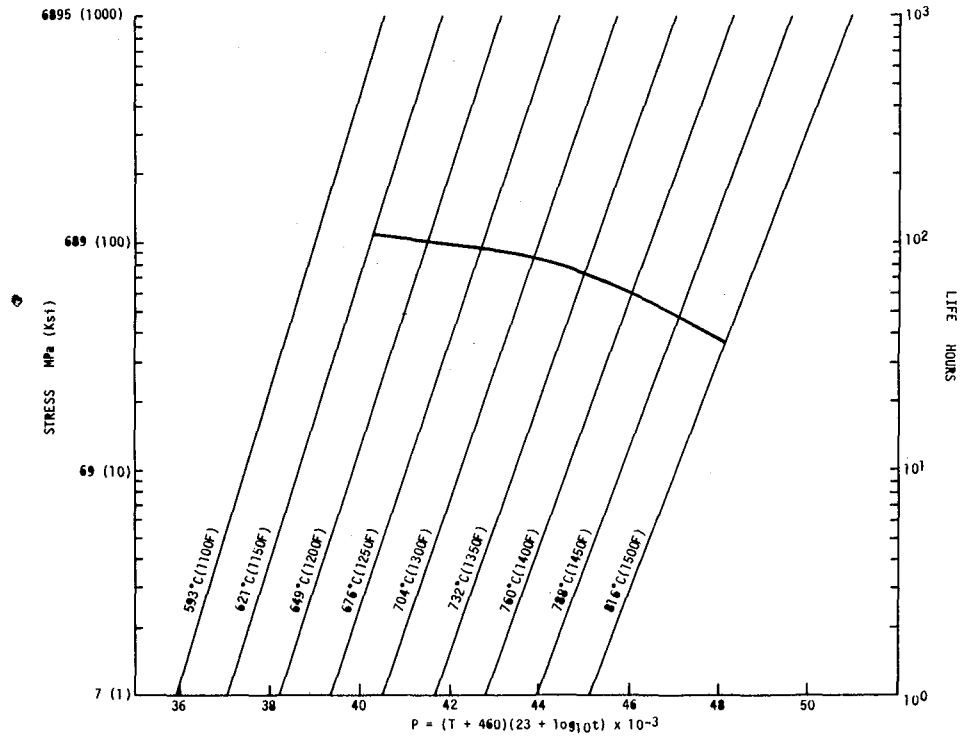

Figure 3 Lower Limit Stress-Rupture Properties of MERL 76

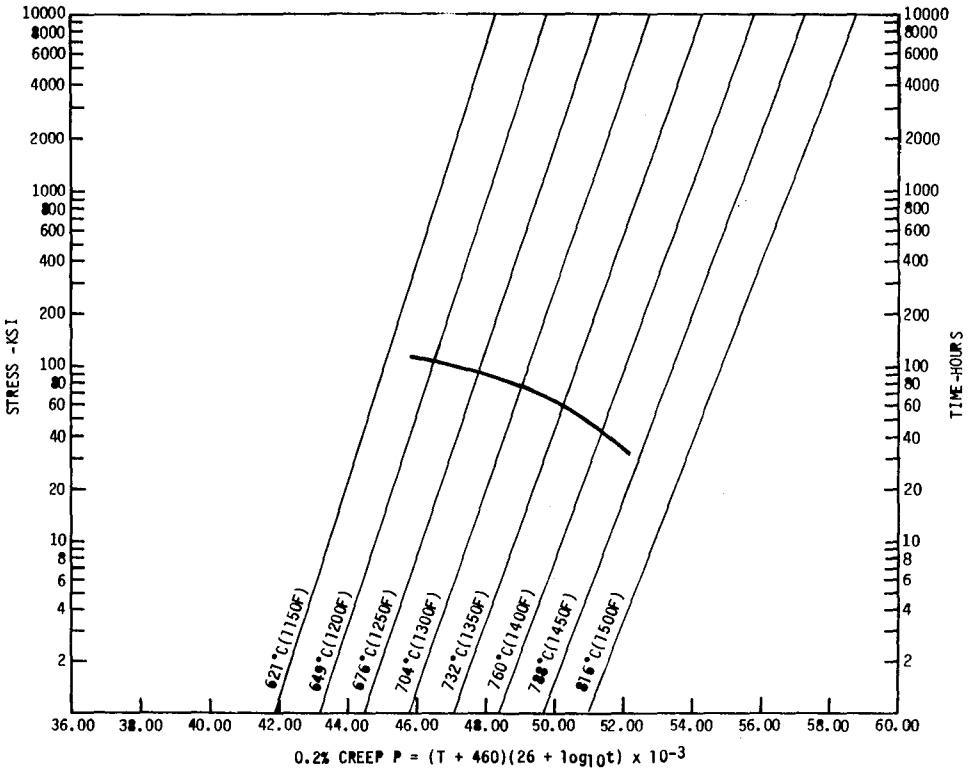

Figure 4 Lower Limit 0.2% Creep Properties of MERL 76

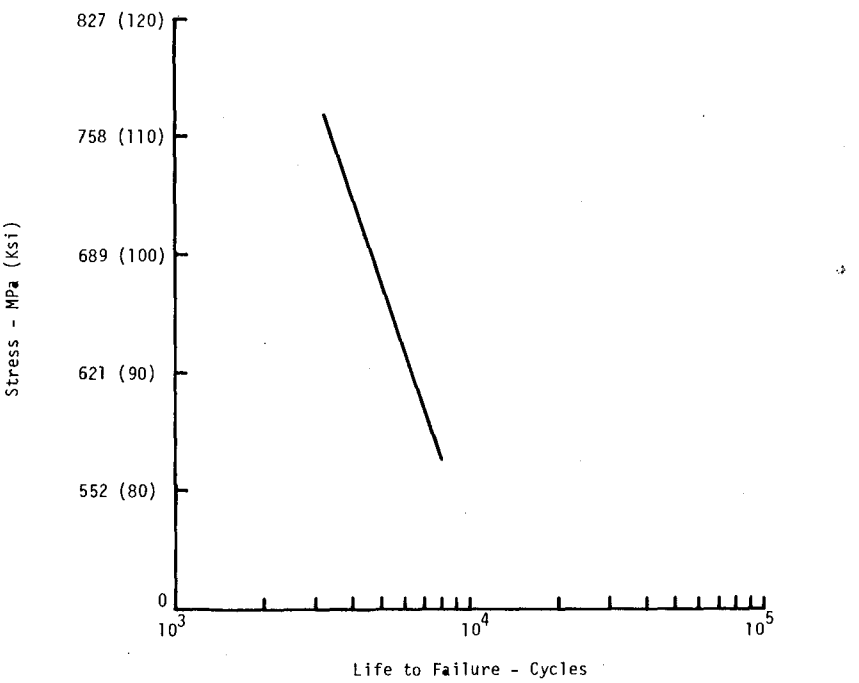

Figure 5 Lower Limit Notched (K_t=2.5) Low Cycle Fatigue Properties at 649°C(1200°F) for MERL 76 Temperature Range

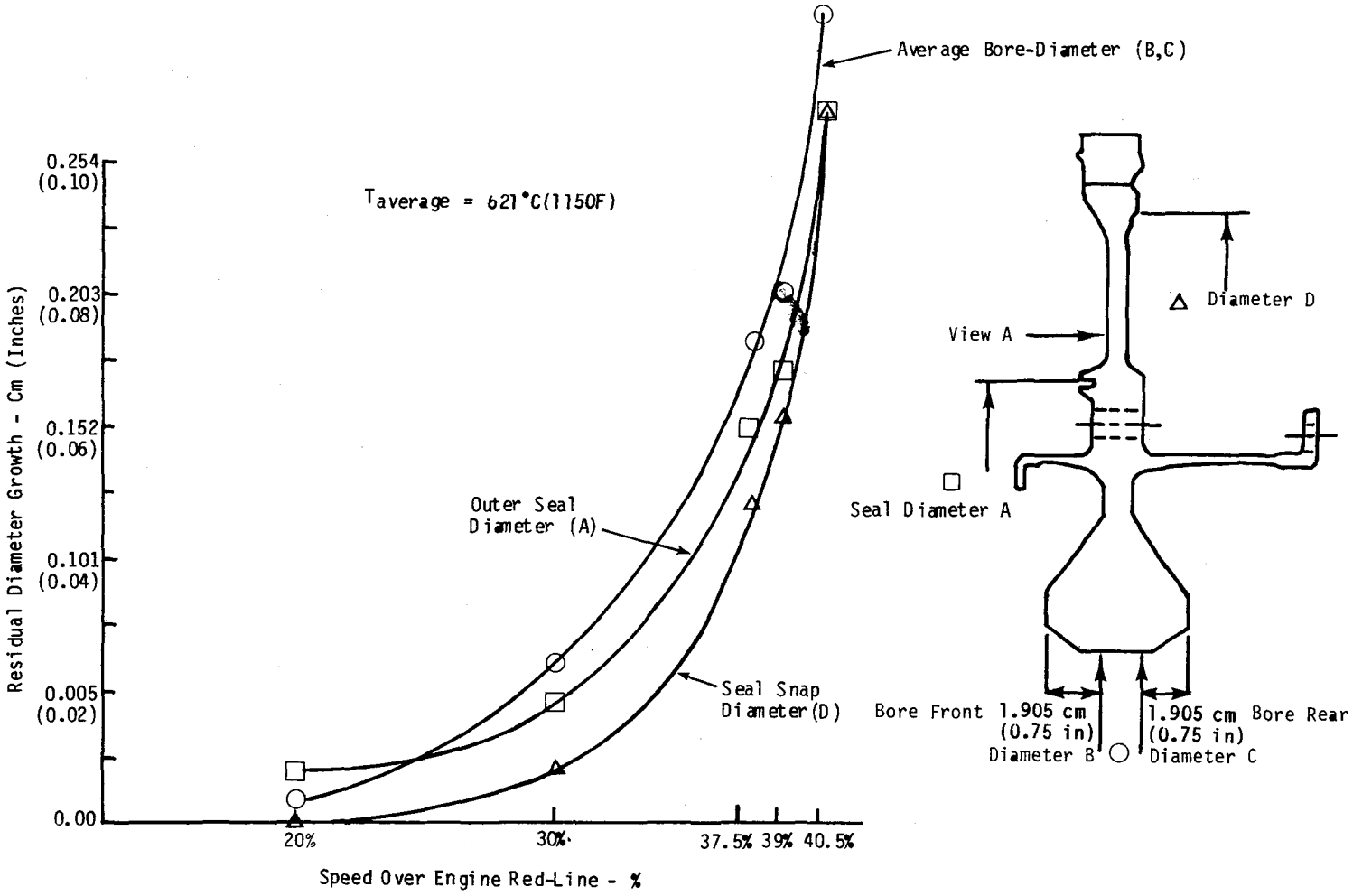

Figure 6 Growth at Various Speed Increments for a MERL 76 Disk

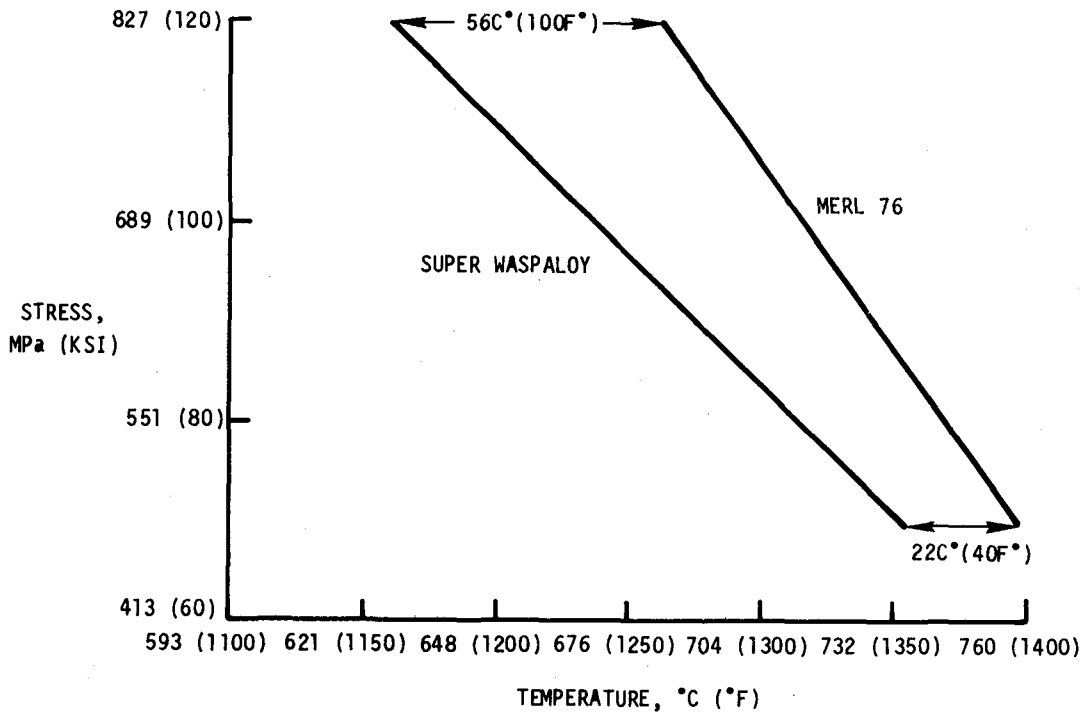

Figure 7 Increased Rim Temperature Capability of MERL 76 Compared to Superwaspaloy®

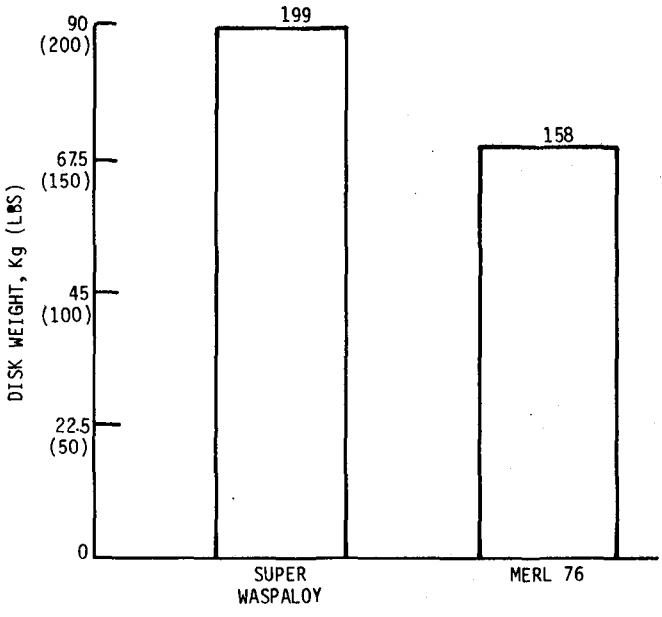

Figure 8 MERL 76 Reduces Component Weight When Compared to Superwaspaloy

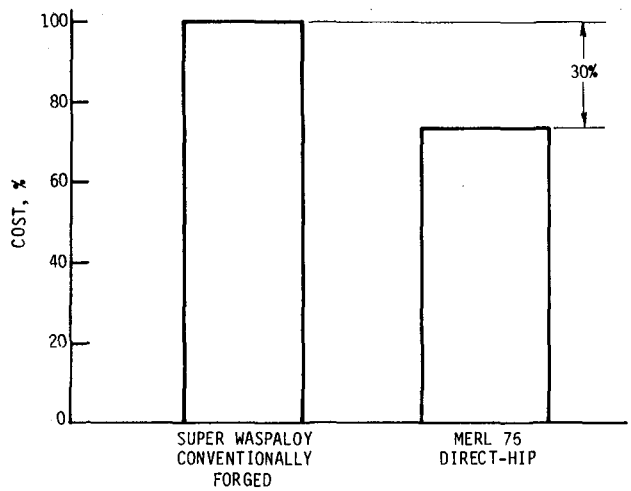

Figure 9 HIP MERL 76 Reduces Cost Based on Purchase of JT9D Turbine Forged Sonic Shapes in 1980

INTRODUCTION

The demand to improve engine operating economics has created a need to develop materials that can be fabricated into disk components that are able to withstand higher turbine inlet temperatures and greater rotor speeds. Since component durability contributes directly to maintenance costs and since this durability derives its capability from the fatigue characteristics of the material, developing new materials having greater strength and creep properties with superior cyclic properties would lower the operating costs of aircraft turbine engines. The material must be compatible with low cost fabrication techniques. The powder metallurgical approach was selected to develop the properties in these advanced disk designs. Direct hot isostatic pressing of the powder to a near sonic shape has been shown to be a particularly effective method of producing low cost disks.

To establish production disk fabrication for advanced aircraft powerplants, such as energy efficient engines, several factors, such as the alloy chemistry which is capable of achieving the required strengths, and the disk processing which will produce HIP net sonic shape must be considered. Through an internally funded program, P&WA identified an alloy capable of achieving properties comparable to Gatorized™ IN-100 in the as-HIP condition. Known as MERL 76, this alloy is of modified IN-100 base, with a nominal composition Ni-12.4 Cr-18.5 Co-3.2 Mo-0.75 Hf-1.65 Nb-5.0 Al-4.3 Ti-0.025 C-0.02 B-0.045 Zr.

The alloy has demonstrated the potential for improvement in cyclic fatigue life capability with improved resistance to corrosion and at a lower cost because of its HIP processibility over IN-100.

Under Project 1, manufacturing methods to produce direct HIP + heat treated Low Carbon Astroloy JT8D first stage turbine disks were established for the following areas:

- Powder manufacture and storage
- Disk shape container design and fabrication

- o Powder outgassing and transport from storage to disk shape container
- o HIP consolidation cycle tolerances

Based on the results of Project 1 and the alloy development program at Pratt & Whitney Aircraft, MERL 76 with a modified chemical composition was selected to demonstrate its feasibility as a full scale component in a high technology, long life, commercial gas turbine engine. The specific goals of project 2 were as follows:

- o Increase the JT9D disk rim temperature capability by at least 22C° (40F°) over disks produced from Superwaspaloy.

- o Reduce the weight of JT9D high pressure turbine rotating components by at least 35 pounds by replacement of forged Superwaspaloy components with hot isostatic pressed MERL 76 components.

- o Reduce JT9D disk manufacturing costs by at least 30 percent relative to Superwaspaloy disks.

The general approach that was followed to achieve these goals was to HIP MERL 76 to a JT9D first stage turbine disk configuration and demonstrate its component integrity through an engine test in an advanced commercial engine.

Project 2 comprised the following tasks:

Task I identified the manufacturing procedures necessary to produce MERL 76 turbine disks and tangential on-board injection rotor seals, and established design allowable data using these components. All turbine disks and rotor seals were manufactured by the Udimet Powder Division of Special Metals Corporation. These disks used a JT10D sonic shape and a JT9D sonic shape. An initial group of consolidations was used to establish and refine hot isostatic pressing conditions and a heat treatment to achieve target properties. The results of this initial group were used to refine the manufacturing process which led to the generation of a process control plan and acceptance criteria to HIP MERL 76 components. The next three disks were used to establish design allowable properties data.

Task II HIP consolidated and finish machined one disk for spin burst rig testing. The turbine disk was tested at five spin speeds to 140.5 percent overspeed at which point the rig failed before the disk. Task III HIP consolidated and finish machined one disk for a ground based JT9D experimental engine test. Task IV will subject one turbine disk to full scale JT9D experimental engine test, and Task V will provide the post-test analysis of the entire program. The post-engine test analysis, including visual, fluorescent penetrant, and dimensional inspection of the turbine disk engine tested in Task IV will be performed upon completion of an engine test and will be reported with the engine test data under separate cover.

Under AFWAL Contract F33615-77-C-5187, Pratt & Whitney Aircraft demonstrated the fabrication of gas turbine engine disks of MERL 76 by near net shape hot isostatic pressing. This work established the feasibility of reducing the consolidated disk weight through a refined container design and computer-aided dimensional analysis.

TECHNICAL PROGRAM

TASK I - MANUFACTURING PROCEDURES AND DESIGN ALLOWABLE DATA

Overview

Task I identified the manufacturing procedures necessary to produce MERL 76 HIP consolidated components and established design allowable data. In the original program (Figure 10), Task I consisted of the HIP manufacture of MERL 76 JT10D turbine disks and TOBI (tangential on-board injection) rotor seals (Figures 11-12). Because of significant design changes and the unavailability of a JT10D experimental test engine, the program was restructured as shown in Figure 13, to fabricate only disks after an initial group of three JT10D disks and three TOBI seals were consolidated. A total of seven turbine disks and three TOBI rotor seal components were consolidated in Task I which were used to establish and refine HIP process conditions and to develop a heat treatment to achieve target properties (Table II). Five of these disks had a JT10D sonic shape (see Figure 11) while the remaining two disks had a JT9D sonic shape (see Figure 1).

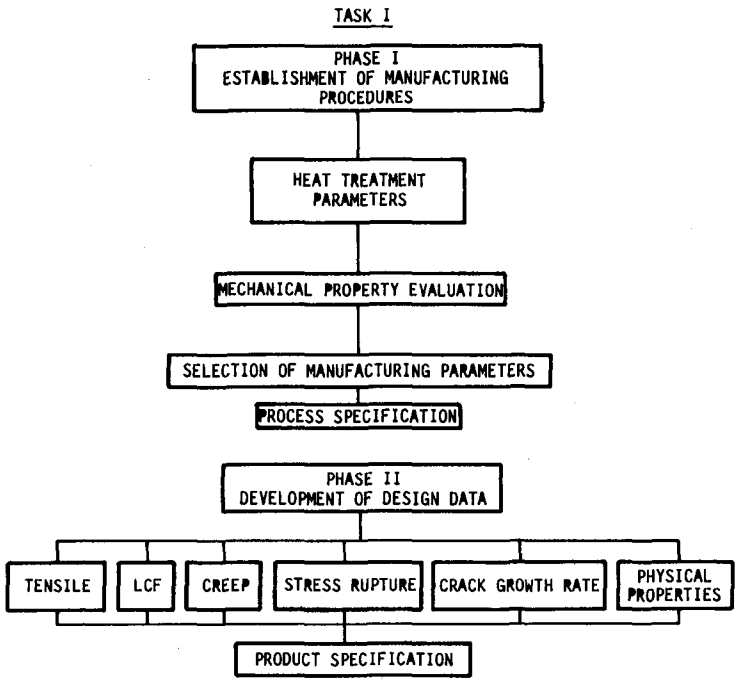

Figure 10 *Task I Flow Diagram - Phase I - Manufacturing Procedures, Phase II - Design Data*

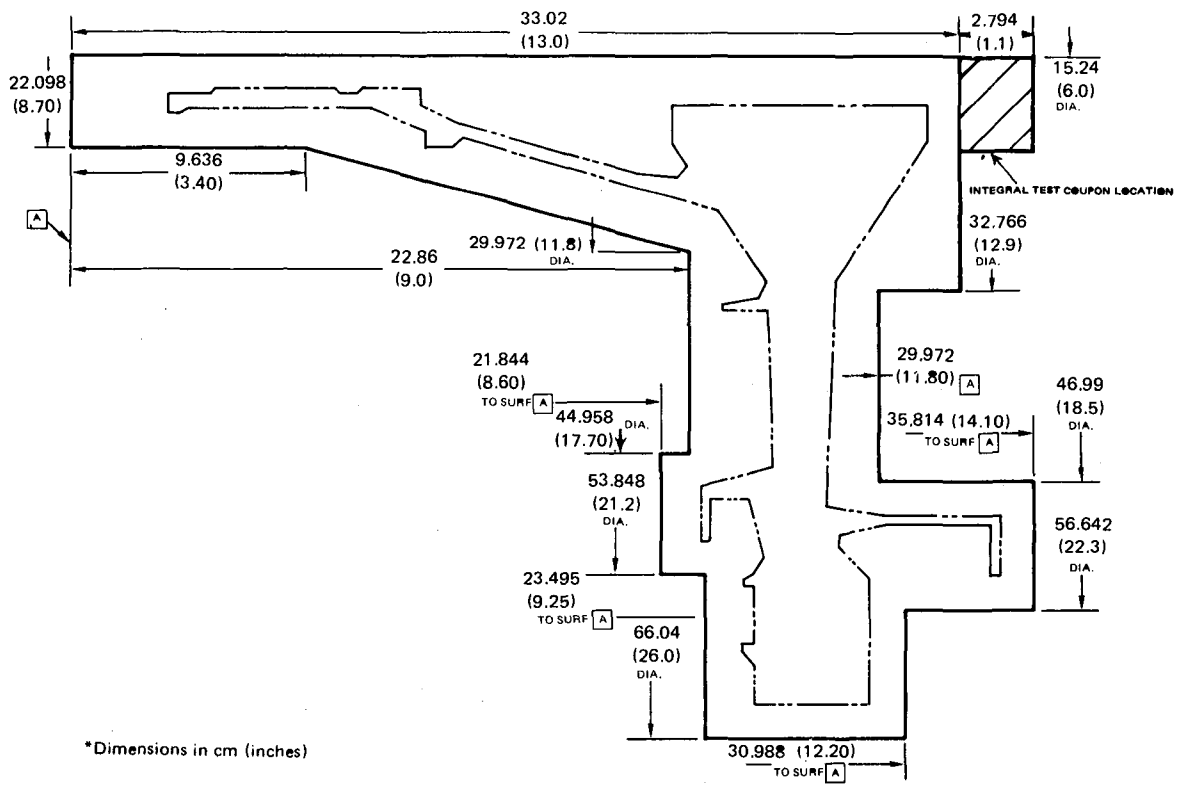

Figure 11 *Target JT10D As-HIP Shape - Turbine Disk ~625 lbs*

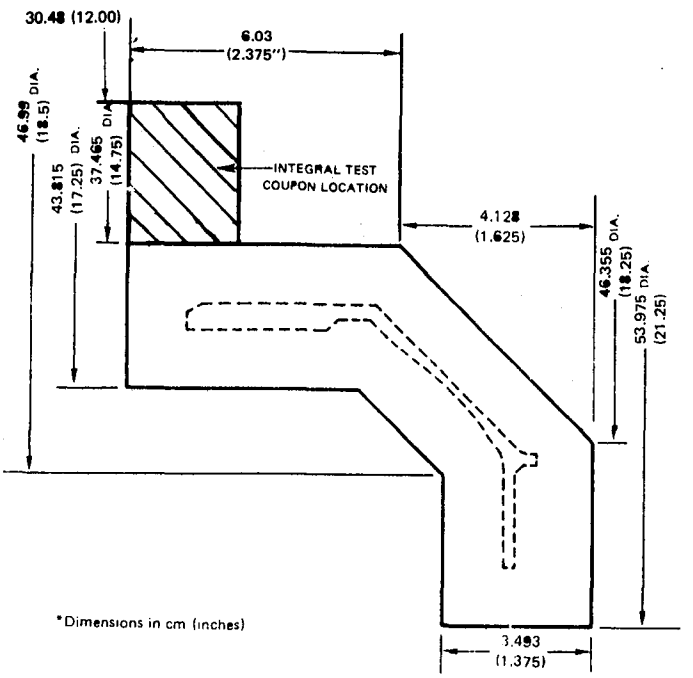

Figure 12 *Target JT10D As-HIP Sonic Shape TOBI Seal*

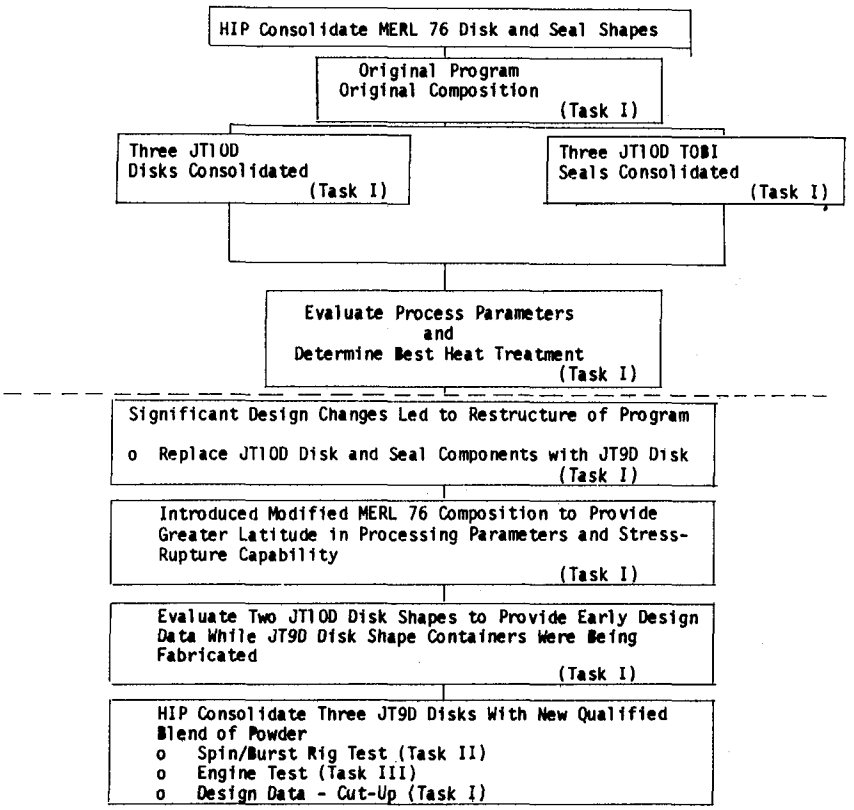

Figure 13 *Flow Chart of MERL 76 Disks and Seals Consolidated in the Restructured Program*

TABLE II

MECHANICAL PROPERTY REQUIREMENTS
FOR HIP MERL 76 POWDER SEALS AND DISKS

TENSILE GOALS

	0.2% Yield Strength MPa (Ksi)	Ultimate Tensile Strength MPa (Ksi)	Elongation (%)	Reduction in Area (%)
21°C (70°F) Tensile	1034 (150)	1482 (215)	15.0	15.0
704°C (1300°F) Tensile	1014 (147)	1172 (170)	12.0	12.0

STRESS-RUPTURE GOALS

	Life	Elongation (%)
732°C (1350°F)/ 638 MPa (92.5 Ksi)	23 hrs.	5

CREEP GOALS

	Time to 0.2% Elongation
704°C (1300°F)/ 552 MPa (80 Ksi)	100 hrs.

After the first group of three JT10D turbine disks and three TOBI seals were HIP consolidated in Task I, a P&WA funded program determined that a modified MERL 76 composition (Table III) would give greater latitude in the HIP consolidation temperature and improve stress-rupture life without any adverse effect on mechanical properties.[1] This modified composition had been selected for evaluation in Task I, Phase II (Design Data, see Figure 10) as well as in all succeeding tasks. To provide design data at an early date while JT9D shape containers were being fabricated, two JT10D disk containers were HIP consolidated using the modified composition. The evaluation of these two JT10D disks indicated that at elevated temperatures (>650°C/1200°F) tensile and stress-rupture properties were low due to contaminated powder.

In order to minimize the program schedule delay associated with the procurement of new powder, available powder was used in the first group of two JT9D consolidations so that dimensional data information could be applied to

(1) Evans, D. J. and Eng, R. D. "Development of a High Strength Hot Isostatically Pressed (HIP) Disk Alloy, MERL 76", to be published in Modern Developments in Powder Metallurgy, Vol. 14, pp. 51-63, 1981.

TABLE III
COMPOSITION OF MERL 76 VIM HEAT 7-11801

Element	MERL 76 Target Chemistry Original	Modified
Ni	R	R
Cr	11.9 - 12.9	11.9-12.9
Co	18.0 - 19.0	18.0 - 19.0
Mo	2.8 - 3.6	2.8 - 3.6
Al	4.85 - 5.15	4.85 - 5.15
Ti	4.15 - 4.50	4.15 - 4.50
Nb	1.50 - 1.80	1.20 - 1.60
Hf	0.060 - 0.90	0.30 - 0.50
B	0.016 - 0.024	0.016 - 0.024
Zr	0.04 - 0.08	0.04 - 0.08
C	0.015 - 0.03	0.015 - 0.03
Mn	< 0.02	< 0.02
S	<0.01	<0.01
P	<0.01	<0.01
Si	<0.10	<0.10
Fe	<0.30	<0.30
Cu	<0.07	<0.07
Bi	<0.5*	<0.5*
Pb	<2.0*	< 2.0*
O	<100.0*	< 100.0*
N	<50.0*	<50.0*

*ppm
R= remainder

the next iteration of container design. In this next and last iteration (Tasks II and III) of three JT9D disk shapes, at least two finish-machined disk components were required for component tests while the remaining disk was designated for design data (Task I).

Ingot and Powder Manufacture

In the entire program, nine heats of VIM material were used to manufacture 15 HIP consolidated components. The ingots were supplied by Special Metals and Howmet to the powder manufacturers, Udimet Powder Division of Special Metals and Homogeneous Metals Inc., respectively. The composition for each heat of material is given in Appendix A. Udimet atomized VIM ingots containing hafnium while HMI preferred to add the hafnium to the molten metal just prior to atomization.

After the first group of three JT10D turbine and three TOBI seals were manufactured, the composition of MERL 76 was slightly modified (1.4% Nb, 0.4% Hf) to provide much greater latitude in processing parameters. In order to conserve as much material as possible, new VIM ingots were cast using both

virgin elements and revert material (powder) of the original composition. Two VIM heats of MERL 76 composition (7-11802 and 7-11861) consisting of 55 percent virgin elements/45 per cent revert MERL 76 (original composition) powder were cast. The chemistry analysis of this modified composition of MERL 76 is reported in Appendix A.

The VIM ingots were converted to powder by argon atomization (Udimet) and hydrogen atomization (HMI). The resultant powder blend chemistry with the corresponding VIM ingot melt stock is also presented in Appendix A and Table IV. Target chemistry was met for all elements except for oxygen content in three blends. For blends that displayed an oxygen content of ~10 ppm over the allowable limit (100 ppm), acceptance was contingent upon the oxygen content of the HIP consolidation conforming to target requirements. The powder was accepted since adsorbed oxygen could be removed during dynamic vacuum degassing of powders. A fourth blend (BN 010680), which was atomized by HMI, initially exhibited inordinately high oxygen content (180 ppm). Since finer size powder tends to exhibit higher oxygen content, the sieve analysis results (Appendix B) which were determined concurrently with powder chemistry were next examined. Sieve analyses indicated that BN 010680 contained approximately 20% more finer mesh powder (-400) than typically measured for other -80 mesh MERL 76 powder analyzed. To determine the effect of this larger fraction of finer powder, additional oxygen analysis (Table V) was performed on three different mesh sizes: -100 mesh, +400 mesh, and -400 mesh. The analysis showed that the finer mesh (-400 mesh) displayed a considerably higher oxygen content (209 ppm vs. 74 ppm), thus confirming the relatively high oxygen level observed for the bulk (-80 mesh) analysis. The initial high oxygen result (180 ppm) could have been a result of segregation of powder wherein the sample consisted primarily of fine -400 mesh powder.

The powder was further characterized by scanning electron microscopy illustrating the dendritic structure of each particle as well as a number of irregular shaped particles (Figure 14).

TABLE IV

COMPOSITION OF HMI MERL 76 POWDER PLANNED FOR USE IN TASKS II/III

Element	Target	HMI 010680
Ni	R	R
Cr	11.9-12.9	11.9
Co	18.0-19.0	17.9
Mo	2.8-3.6	3.2
Al	4.85-5.15	4.9
Ti	4.15-4.50	4.3
Cb	1.20-1.60	1.32
Hf	0.30-0.50	0.42
B	0.016-0.024	0.018
Zr	0.04-0.08	0.07
C	0.015-0.03	0.024
N	50* Max	25*
O	100* Max	180*

*PPM
**Typical Analysis for -80 mesh MERL 76 powder

TABLE V

OXYGEN ANALYSIS

Sample No.	Mesh Size	PPM Oxygen
1	-100	143
		149
		140
		136
2	+400	68
		74
	-400	207
		209
3	HIP Consol-idation	144

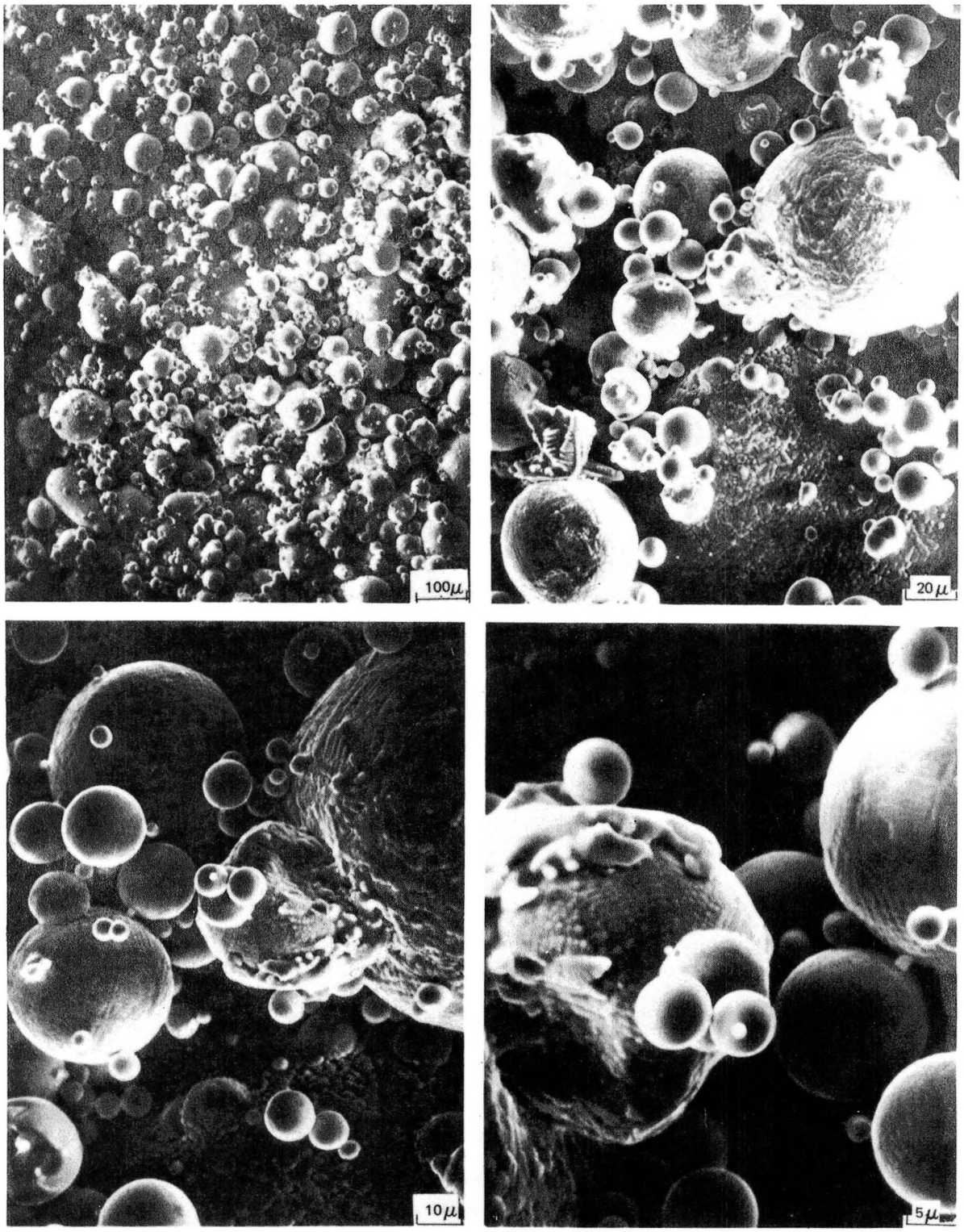

Figure 14 *Scanning Electron Micrographs of MERL 76 Powder Showing Predominantly Spherical-Shaped Particles. Note the Dendritic Structure in the Atomized Powder*

Container Fabrication and Filling

The Udimet Powder Division of Special Metals, Ann Arbor, Michigan, was selected as a major subcontractor for this project. Udimet participated as a subcontractor under the MATE Project 1, HIP Net Sonic Astroloy Disk program and produced the powder used by Pratt & Whitney Aircraft in its MERL 76 alloy selection program. Udimet was responsible for container fabrication, powder production, except for one blend which was atomized by Homogeneous Metals, Inc., consolidation, and post-consolidation evaluation including dimensional analysis and heat treatment.

The front and rear faces of each container were formed by shear spinning of a 0.203 cm (0.080 in) thick SAE 1008 sheet. The inner diameter bore segment of the JT10D disk components consisted of a 0.63 cm (0.25 in) wall thickness pipe. Shear spinning was accomplished in multiple steps utilizing metal tooling. The fill tube was made of 0.125 cm (0.049 in) wall, 0.90 cm (0.75 in) outer diameter seamless SAE 1015 tube.

Immediately prior to welding construction, each container detail was degreased and washed in acetone. Each detail was assembled in a fixture and GTA welded at the location shown in the schematic drawings (Figures 15-16) for the seal components and for both JT10D and JT9D components. During welding, the entire container was purged with argon to minimize oxidation of the steel. The assembled containers were then leak-checked by pressurizing to 137 MPa (20 psig) while submerged in a water-soap solution.

Each container was filled under vacuum with powder using a transport facility shown schematically in Figure 16. The powder was fed into the top of the powder transport facility via a tote bin and evacuated to $<15\,\mu m$ of Hg. As the powder was metered from the storage bin, it was vibrated to better expose the powder particles for vacuum outgassing. During container filling, the vacuum level in the powder transport facility was maintained at $<15\mu m$ Hg. After each container was filled with powder, the container was valved-off to maintain a vacuum and transferred to a station for hot vacuum outgassing at 316°C (600°F). After a pressure of 10^{-5} torr was achieved and maintained for

at least 12 hours, the container was sealed by crimping and fusion welding of the fill tube. Each HIP consolidation identity and corresponding powder weight and dynamic degassing parameters are given in Appendix C.

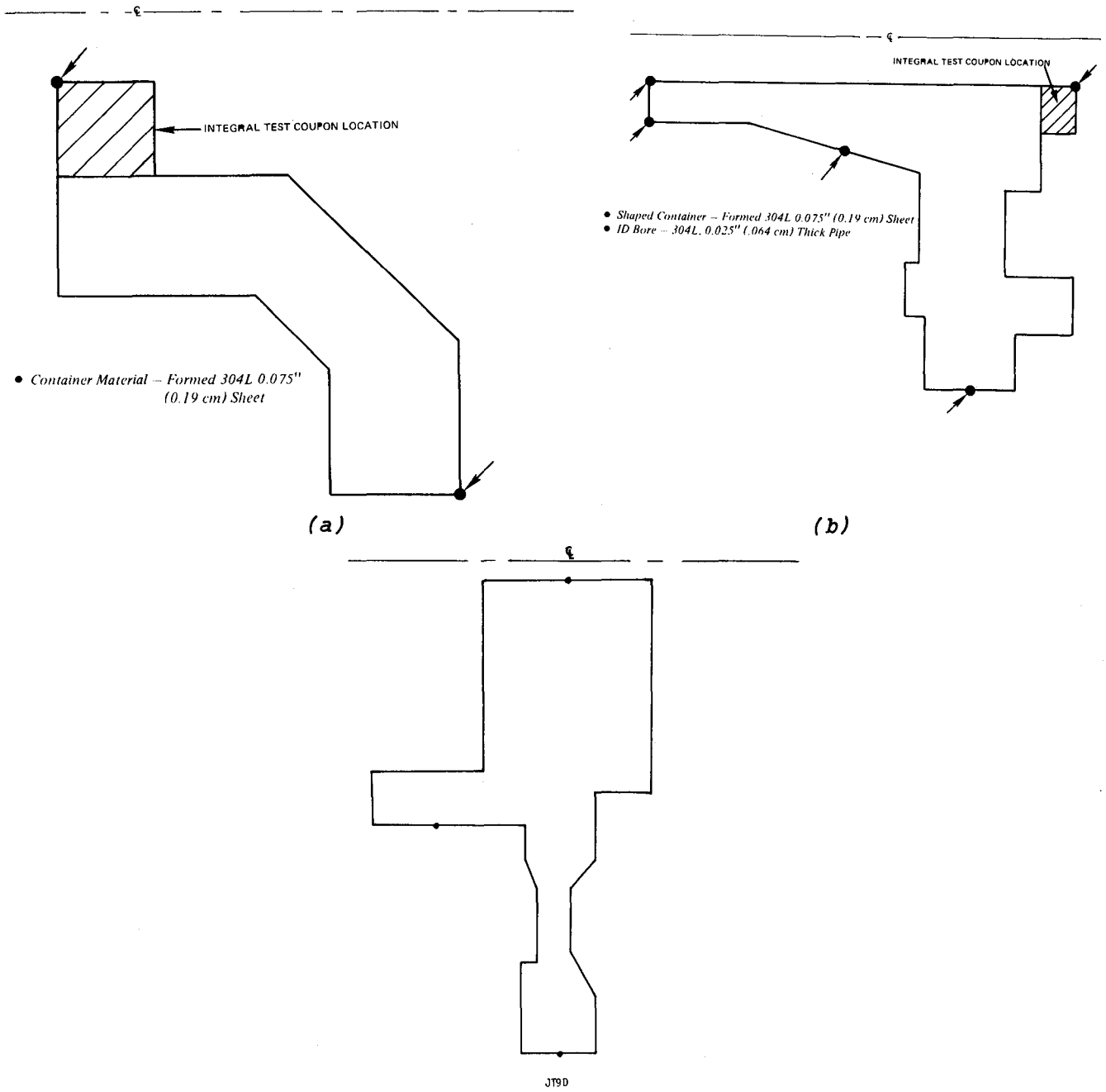

Figure 15 *Container Details for JT10D and JT9D Seal Components*
(a) Target as-HIP TOBI seal shape container showing location of two welds
(b) Target as-HIP disk shape container showing location of five welds
(c) Target as-HIP disk shape container showing locations of three welds

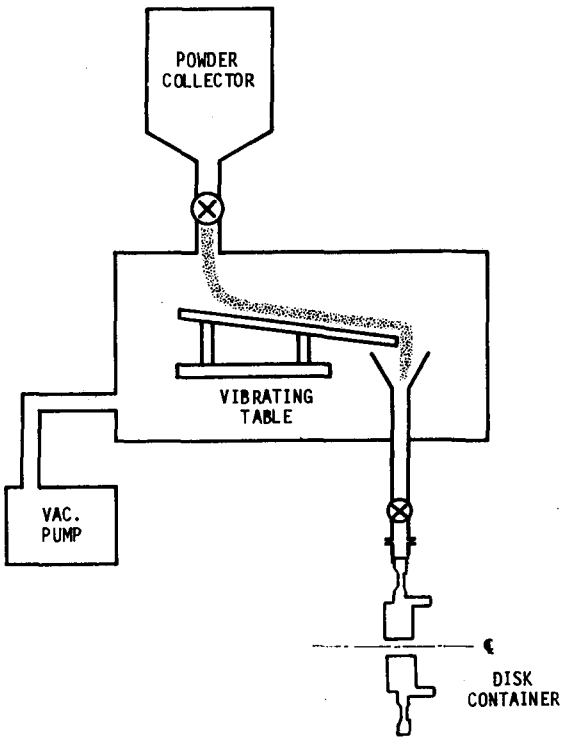

Figure 16 Powder Process Facility

HIP Consolidation and TIP (Thermally Induced Porosity) Testing

The initial group of five TOBI seals and three JT10D turbine disks of original MERL 76 chemistry (0.75 Hf, 1.6 Nb) was all HIP consolidated at 1169°C (2135°F)/103 MPa (15Ksi)/3 hours. The appearance of the as-HIP consolidated shapes of the JT10D disk and TOBI seals is shown in Figures 17-18. Of this first group of consolidations, the containers of two TOBI seals (s/n 34 S-1 and 35 S-3) failed prior to HIP consolidation. The failure of one seal was obvious because the container bulged, while the failure of the second seal was determined by a thermally induced porosity (TIP) test. A careful visual examination of the failed as-HIP seal consolidations showed a crack in the heat affected zone of the fill-tube/container weld. More care was taken in welding the subsequent replacement seals to assure sound full-penetration welds.

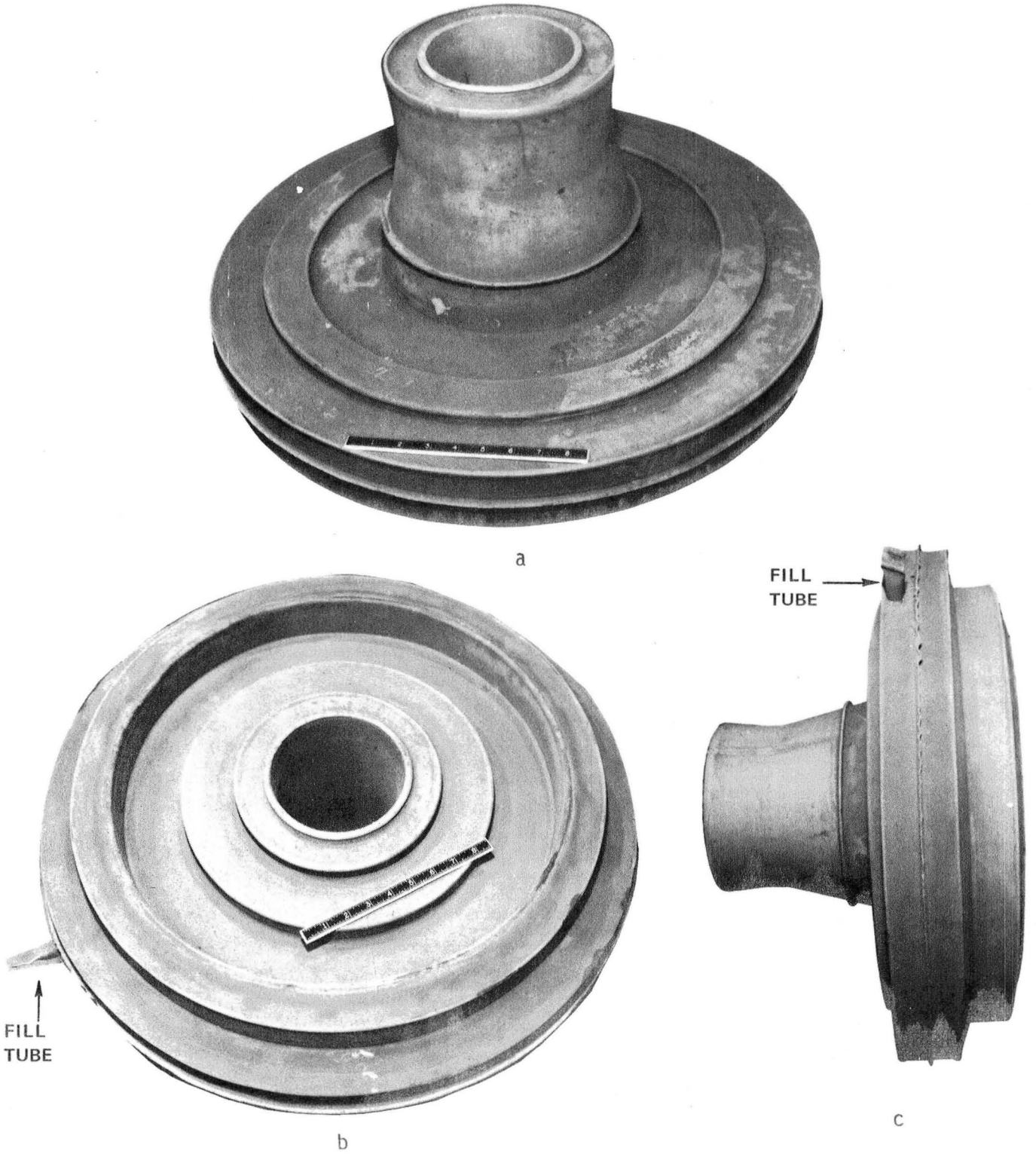

Figure 17 HIP Consolidation of Disk 34D-1

(a) Front view (b) Rear view (c) Side view

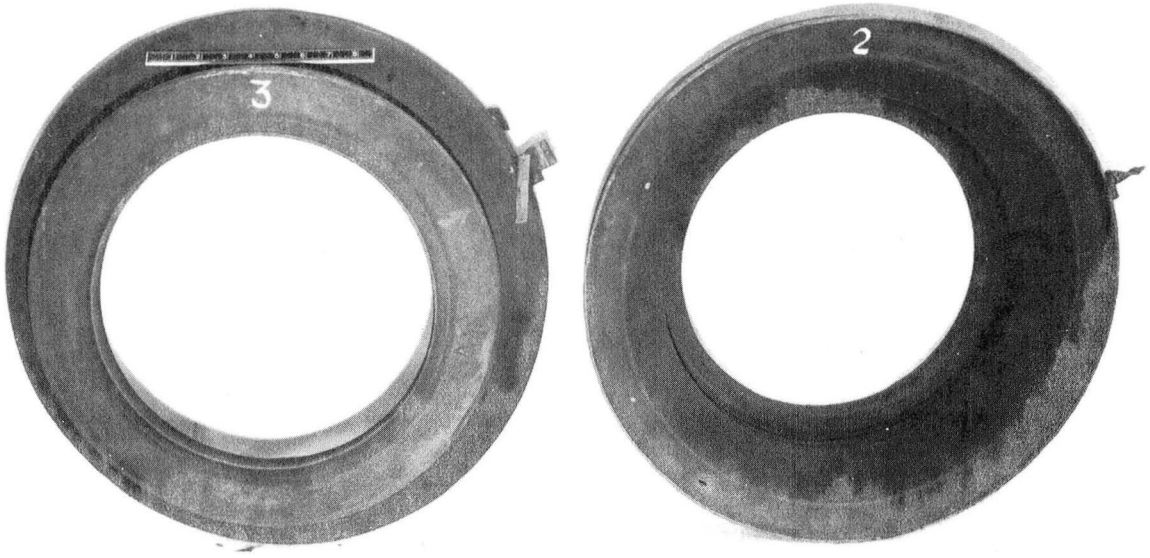

Figure 18 Front and Rear View of Seals 35S-3 (left) and 35S-2 (right)

After HIP consolidation, the fill-tube was removed to determine grain size while another portion was given a TIP (thermally induced porosity) test to determine the quality of the HIP consolidation. A TIP test consists of microexamination of a segment (usually the fill tube) etched with Kallings at 100X and AG21* at 1000X of the consolidation which had been exposed to a temperature near the HIP consolidation temperature. The level of porosity is determined by a point-count technique. The coalescence of gas during the high temperature exposure of the TIP test enables determination of the effectiveness of powder outgassing during container filling and the integrity of the container during HIP consolidation. Two types of porosity can be observed. Firstly, "hollow" particles are a result of inert gas entrapped during gas atomization in some of the particles. Secondly, porosity is observed at the prior particle boundaries (triple point) and is associated with container (or weld) failure prior to consolidation of the powders. Gas which seeps into the container can inhibit powder particle consolidation.

The grain size determination (Kalling's at 100X and AG21* at 1000X) was the first test conducted on the fill-tube. The grain size for each of the first group of five TOBI seals and three JT10D disks, which comprised original MERL

*AG21 mixture: 50 Lactic Acid - 30 HNO_3 - 2 Hf

76 chemistry (0.75Hf, 1.4Nb), ranged from ASTM 9-11. A micrograph showing a typical grain size and microstructure for this group of consolidations is shown in Figure 19. A second microexamination was conducted on a segment which was thermally exposed at 1170°C (2150°F)/4 hrs./AC. The resultant microstructure showed less than 0.3% porosity associated with "hollow" particles for all three disks and one of three TOBI seals. A typical microstructure after thermal exposure is given in Figure 20 illustrating sound HIP consolidation. For two seals (34 S-1, 35 S-3), the TIP tests indicated "triple point" porosity which suggested container failure prior to powder consolidation (Figure 21). Each disk that was consolidated and its resultant grain size is given in Appendix D.

Since the MERL 76 composition had been modified to permit HIP consolidation to a slightly coarser grain size for improved notch stress-rupture properties, disk 35D-3 was re-consolidated at 1196°C (2185°F)/103 MPa (15KSI)/3 hrs. to obtain coarser grain (ASTM 6-8) material. Testing of this disk was to provide data on coarse grained material earlier than scheduled. However, the grain size of the re-HIP consolidation was too large as shown in Figure 22. A close examination of this coarse grain microstructure revealed irregularly shaped eutectic gamma prime phases, indicating incipient melting had occurred (Figure 22(c). As a result of this brief study, the HIP consolidation temperature range was restricted to between 1169°C (2135°F) 1191°C (2175°F) to limit the maximum grain size (ASTM 6) for all subsequent consolidations, as well as to avoid further occurrence of incipient melting.

Accordingly, the remaining group of two modified JT10D and five JT9D turbine disks were HIP consolidated at 1182° (2160°F)/103 MPa (15KSI)/3 hours and yielded the desired grain size of ASTM 8-10.

TIP tests revealed that each of these consolidations was sound and free of "triple point" porosity suggesting that the container did not fail during HIP consolidation. The grain size and TIP test results that are typical for these consolidations are shown in Figures 23 and 24.

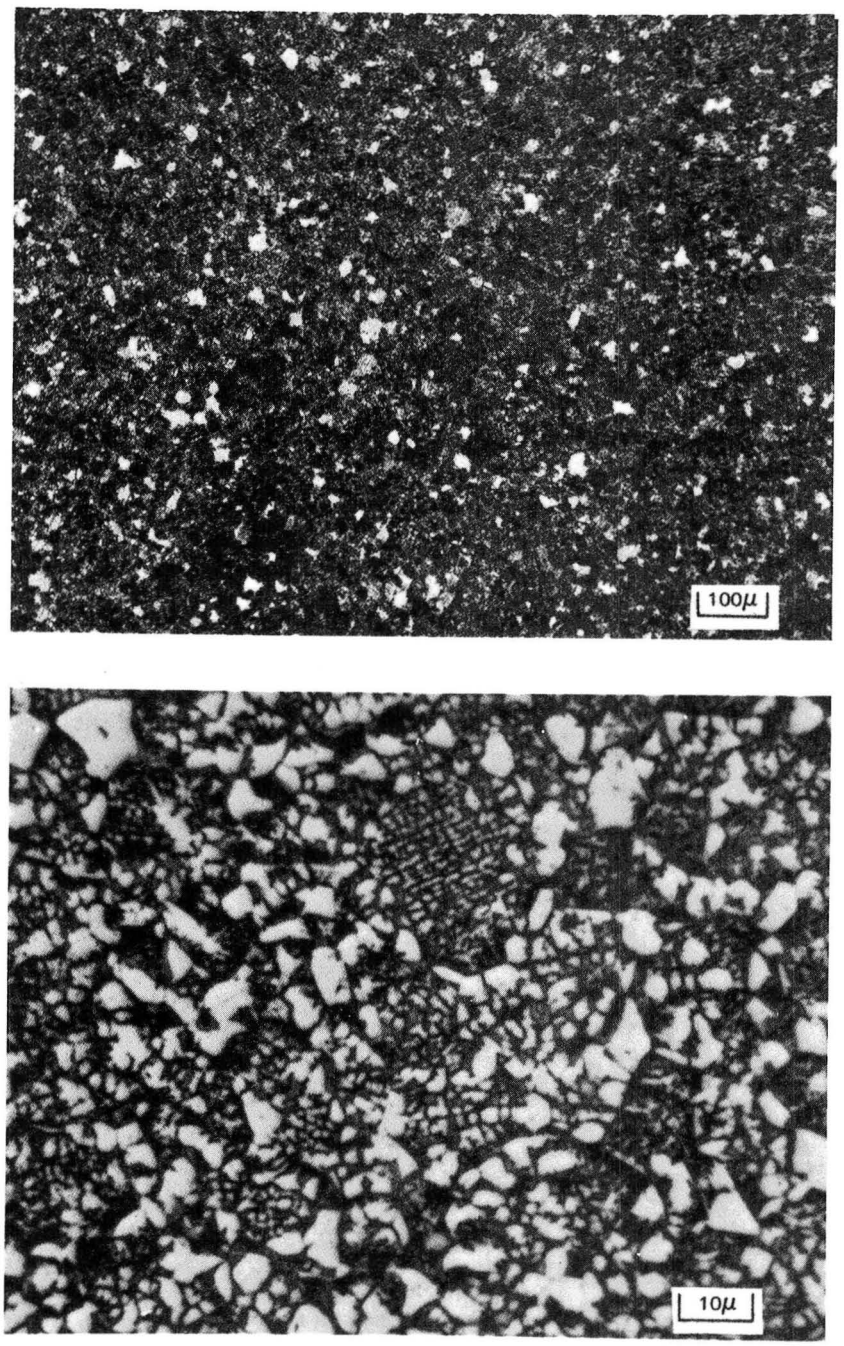

Figure 19 *Photomicrographs of Disk 34D-1 Showing the As-HIP (1169-1177°C (2135-2150°F)/103 MPa (15 ksi)/3 hrs) Microstructure of the Fill Tube. The Grain Size is ASTM 9-11.*

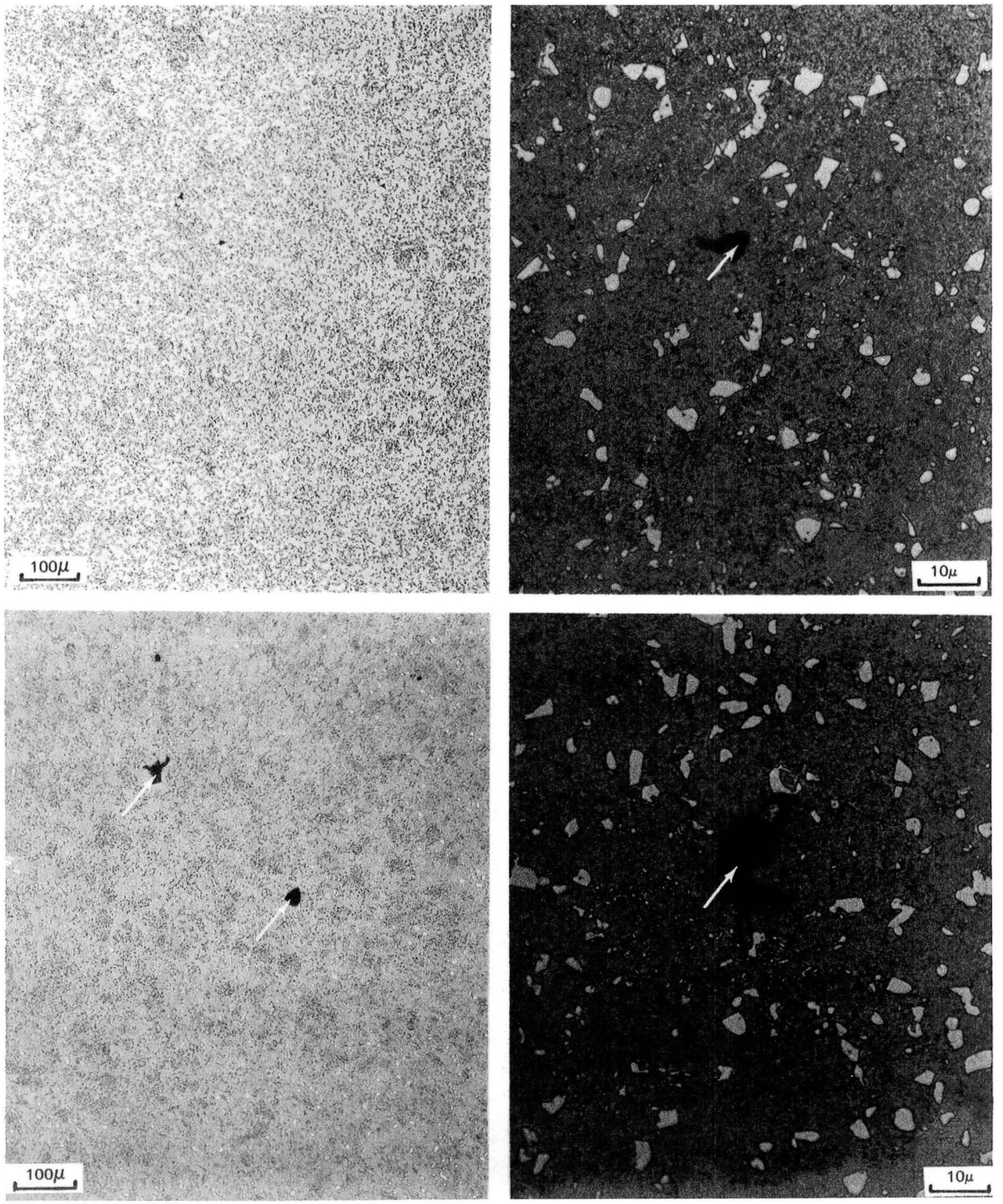

Figure 20 *Microstructure of the Fill Tube of Disk 35D-2 (Top) and 35D-3 (Bottom) Thermally Induced Porosity (TIP) Tested at 1170°C (2150°F)/4 hrs/AC. Less than 0.3% Porosity (Arrows) associated with hollow particles was observed.*

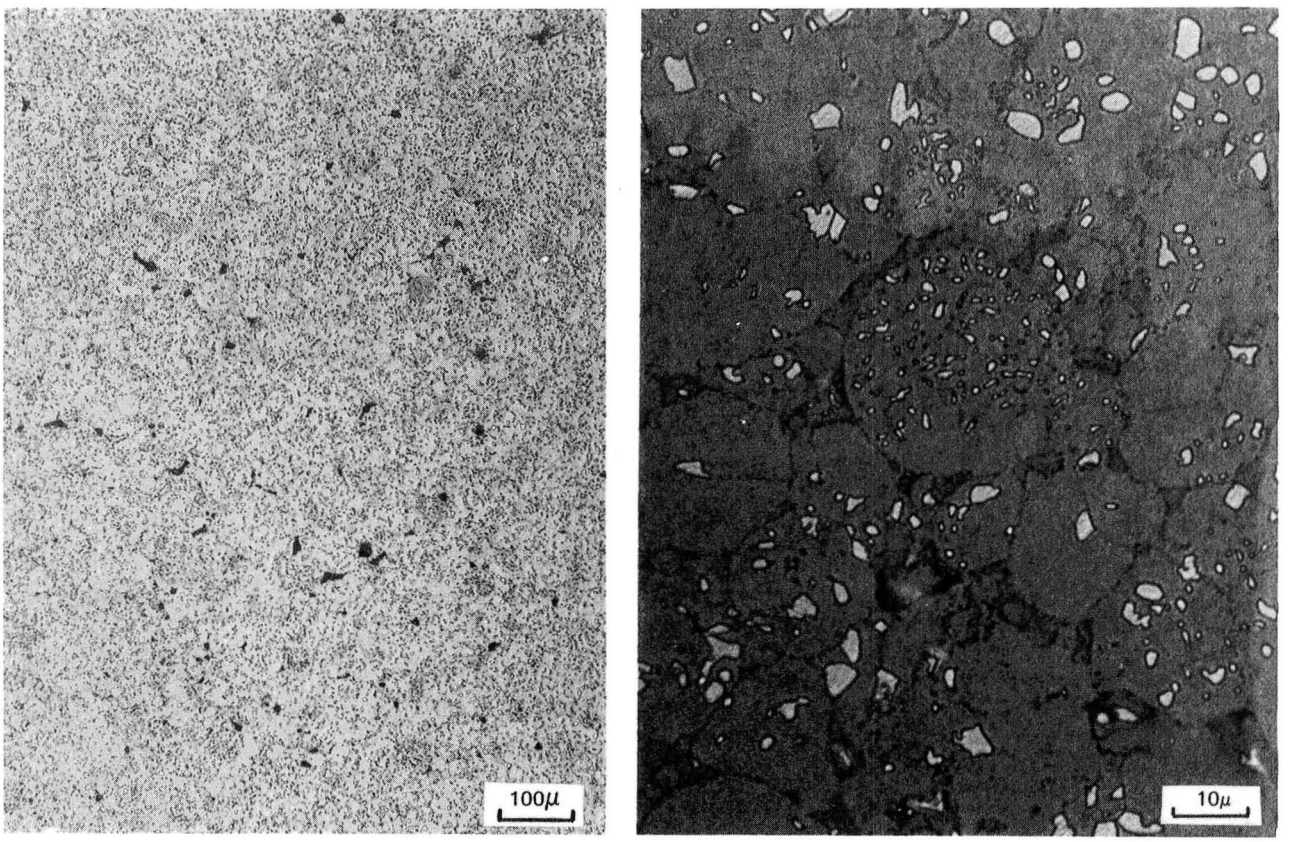

Figure 21 *Microstructure of the Fill Tube of Seal 35S-3 Thermally Induced Porosity (TIP) Tested at 1170°C (2150°F)/4 hrs/AC. Triple point porosity indicated that container failed prior to HIP consolidation.*

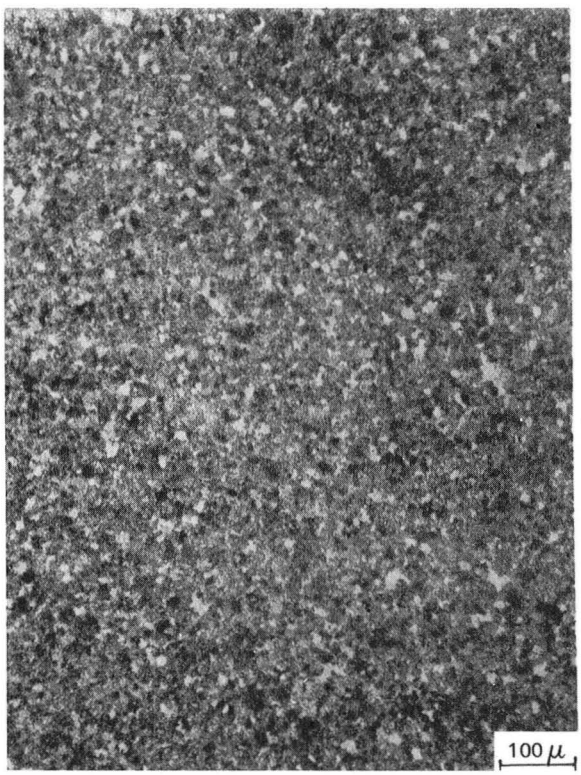

(A)

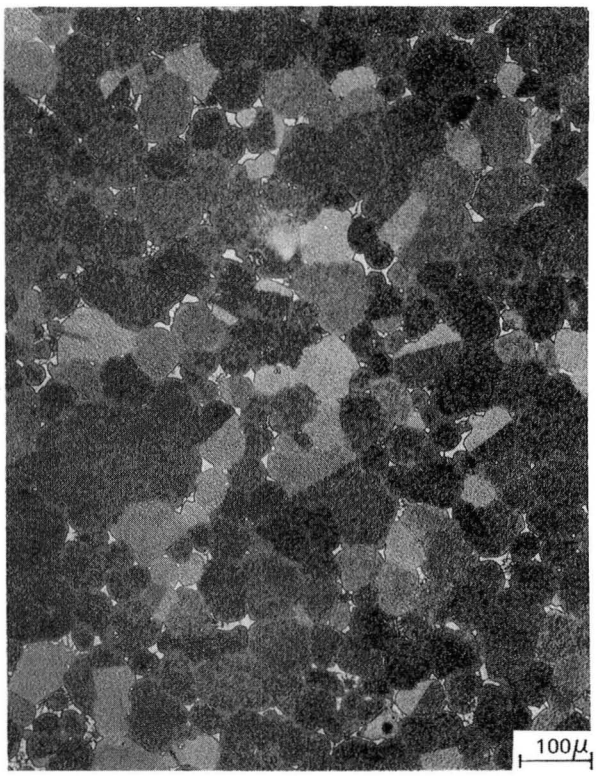

(B)

(C)

Figure 22 *As-HIP Microstructures of MERL 76 Disk 35D-3*

a. Initial HIP at 1169°C (2135°F)-1177°C (2150°F)/ 103 MPa (15 ksi)/3 Hrs. Grain Size - ASTM 10-11

b. & c. Re HIP at 1169°C (2185°F)-1204°C (2200°F)/ 103 MPa (15 ksi)/3 Hrs. Grain Size ASTM 4-6. Note the irregularly shaped gamma prime indicating incipient melting has occurred.

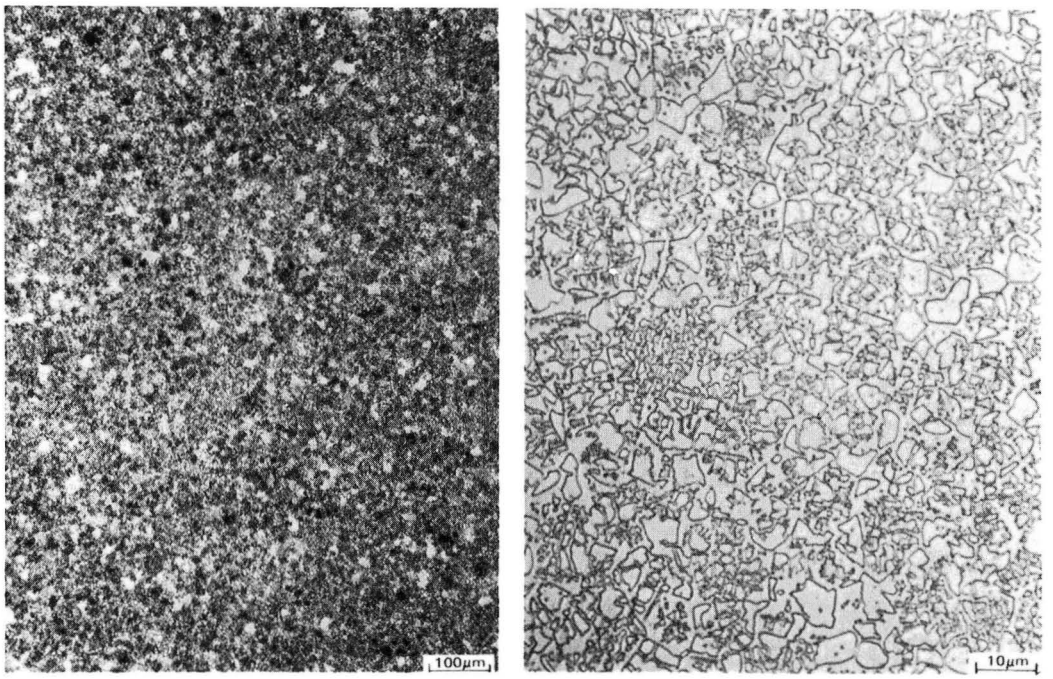

Figure 23 *As-HIP Microstructures of Disk 160-3 Showing a Grain Size of ASTM 8-10 Was Achieved*

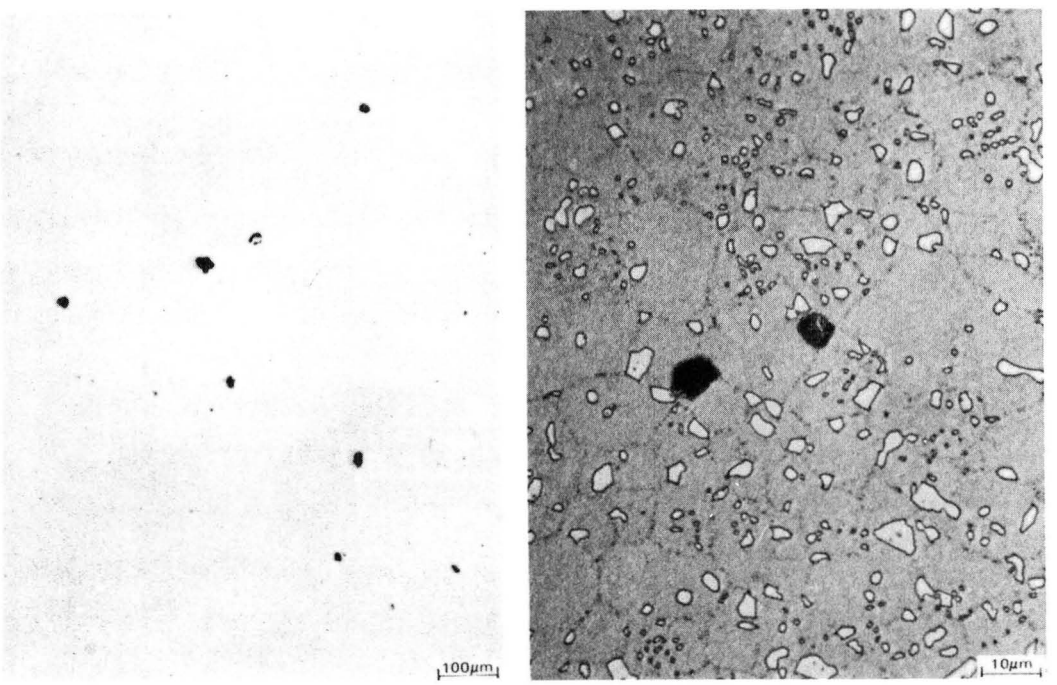

Figure 24 *Microstructure of Material Removed from the Fill-Tube of Disk 160-1 and Heat Treated at 1174°C (2145°F)/4 hrs/AC Showing Only the Thermally Induced Porosity Related to "Hollow" Particles*

Dimensional Analysis

An important aspect of direct HIP technology is the accuracy to which a HIP consolidation can approach a target sonic shape and yet still yield a usable component. Accordingly, dimensional data were determined utilizing a high accuracy automated mechanical measuring system in conjunction with an automated computer system for recording data on paper tape. The data collected were then transmitted to a second computer which contained a program to process the dimensional data.

A vertical probe with three degrees of motion was manually placed on the face of each disk. Multiple scans were taken approximately 30° apart on the circumference of each component. One face was measured in a single set-up and the disk was then inverted to measure the opposite face. Only one of the first group of three full-size JT10D consolidation and two of the three TOBI seals were dimensionally analyzed indicating that the consolidations were approximately 25.4 cm (0.100 in.) over target shape.

More detailed dimensional analysis was performed on the disks which were finish-machined for subsequent engine and rig test. Although the as-HIP consolidation did not yield a sonic shape, two of the three disks in this group yielded a finish-machined disk as will be discussed in greater detail later in Tasks II and III. The lack of dimensional control on this group of disks may have been related to the use of relatively large size alumina balls (~1.25 cm/.5 in) rather than tooling to support the disks during HIP consolidation Although previous consolidation utilized both metal tooling and smaller size alumina balls (~ .64 cm/.25 in), no significant differences in shrinkage behaviour were observed.

Non-Destructive Inspection

Ultrasonic inspection was conducted to determine the quality of consolidation by utilizing the following components:

- o Tektronix Mk III/7603 oscilloscope
- o 1.27 cm (0.5 in) X 10 MHz transducer focused at 7.6 cm (3 in)
- o 1.91 cm (0.75 in) X 5 MHz transducer focused at 20.3 cm (8 in)
- o 2 (2/64") diameter flat-bottom hole test blocks

Sonic inspections were conducted on components in the fully heat treated condition with containers intact but grit blasted to remove the oxide scale. No rejectable sonic indications were found.

Additional non-destructive tests were conducted on the two JT9D disks which were designated for spin/burst rig tested (Task II) and for experimental engine testing (Task III) in a land-based engine. After machining to as close to sonic shape as possible, both disks underwent chemical etch for grain size and surface discontinuities examination and then followed by fluorescent penetrant inspection. No rejectable indications were observed. After machining to final dimensions per blueprint, both disks were given a light anodic etch to examine for any residual can material and then another fluorescent penetrant inspection. Again, no rejectable indications were found.

Heat Treatment Selection

It has been reported that strength is affected by such factors as section size, geometry, and mass for gamma prime strengthened nickel-base super alloys. For alloys such as Low Carbon Astroloy[2], these factors are influenced by cooling rate response during solution and aging heat treatments. This effect was thus the first factor investigated in developing the recommended heat treatment for MERL 76.

---

(2) Eng, R.D. and Evans, D.J. "Manufacture of LC Astroloy Turbine Disk Shapes by HIP" Mate-Project 2, NASA CR-135409, March 1978.

o Solution Heat Treat Selection

To select a cooling rate from the solution heat treat the effect on tensile strength of four different cooling rates was evaluated. The different quenches used were: oil quench, 177°C (350°F) salt quench, 343°C (650°F) salt quench and forced air cool from a 1163°C (2125°F) solution temperature. Primary evaluation was made on quarter sections of a large disk (10.2 cm/4in. thick, 314 Kg/690 lbs), while the effect of an oil quench or a forced air cool cycle was verified on a smaller TOBI seal component (54Kg/120 lbs). The selection of the 1163°F (2125°F) solution temperature was based on a prior solution heat treatment evaluation of MERL 76 conducted at Pratt & Whitney Aircraft. Mechanical properties were determined by removing specimens from both thick (bore) and thin (hub) regions from each quarter section and from the relatively thin section of the TOBI seal. Each quarter section and the TOBI seal received the same two-step precipitation hardening cycles. The best age cycle was evaluated after the best cooling rate was established in this initial heat treat evaluation. The cycle was applied after each of the solution heat treat cycles as shown below:

(A) 1163°C (2125°F)/2 hrs./RAC + 649°C (1200°F)/24 hrs./AC + 760°C (1400°F)/16 hrs./AC.

(B) 1163°C (2125°F)/2 hrs. furnace cool at 55C°(100F°) per hour to 1121°C (2050°F)/0.5 hr./oil quench + 649°C (1200°F)/24 hrs./AC + 760°C (1400°F)/16 hrs./AC.

(C) 1163°C (2125°F)/2 hrs. furnace cool at 55C°(100F°) per hour to 1121°C 92050°F)/0.5 hr./salt quench at 343°C (650°F)/AC + 649°C (1200°F)/24 hrs./AC + 760°C (1400°F)/16 hrs./AC.

(D) 1163°C (2125°F)/2 hrs. furnace cool at 55C°(100F°) per hour to 1121°C (2050°F)/0.5 hr./salt quench at 177°C (350°F)/AC + 649°C (1200°F)/2400 hrs./AC + 760°C (1400°F)/16 hrs./AC.

(E) 1163°C (2125°F)/2 hrs./OQ + 649°C (1200°F)/24 hrs./AC + 760°C (1400°F)/16 hrs/AC.

Elevated temperature tensile results indicated a strong effect of cooling rate on tensile strength which was prominently demonstrated for thick sections tested at temperatures from (621°C(1150°F)- 704°C(1300°F)). Figure 25 indicates that the highest tensile strengths were achieved for material given an oil quench followed by a 343°C(650°F) or 177°C(350°F) salt quench. Both salt quenches gave similar strengths but were approximately 35 MPa (5 ksi) lower. A forced air cool yielded the lowest strengths, approximately 70 MPa (10 ksi) lower than oil quenched thick section materials. For material tensile tested at room temperature, the cooling rate effect on strength was not as prominent. In fact, material given either an oil quench or 177°C (350°F) salt quench gave better properties than the 343°F (650°F) and forced air cool which displayed a strength deficiency of 35 MPa (5 ksi) and 55 MPa (8 ksi), respectively, as also shown in Figure 25. A few stress-rupture specimens for each heat treatment were tested to observe any obvious trends. Testing at 732°C (1350°F)/655 MPa (95 ksi) indicated that the rupture strength did not appear to be significantly dependent upon cooling rate (see Figure 25A). A detailed compilation of both tensile and stress-rupture properties is given in Appendix E.

For thin section material, an oil quench still gave the best tensile strength but the difference between both salt quenches and forced air cool were minimal as shown in Figure 26. Test results from the rapid air cooled TOBI seal are included in the discussion of thin sections. The one group of specimens that gave anomalously high tensile strengths for material given a forced air cool can be explained by specimen location. The group of two specimens were removed from near the surface rather than from the center of the cross section as in the case for all other specimens. Figure 26A shows that stress rupture strengths of thin section were not significantly affected by cooling rate. Detailed tensile and rupture strengths are included in Appendix E.

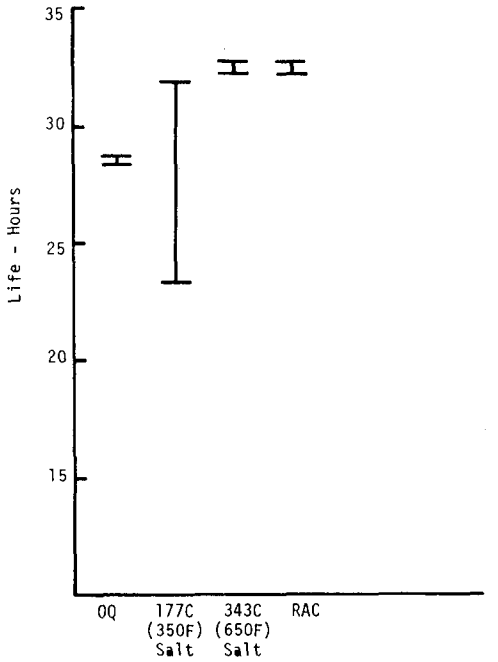

(A)

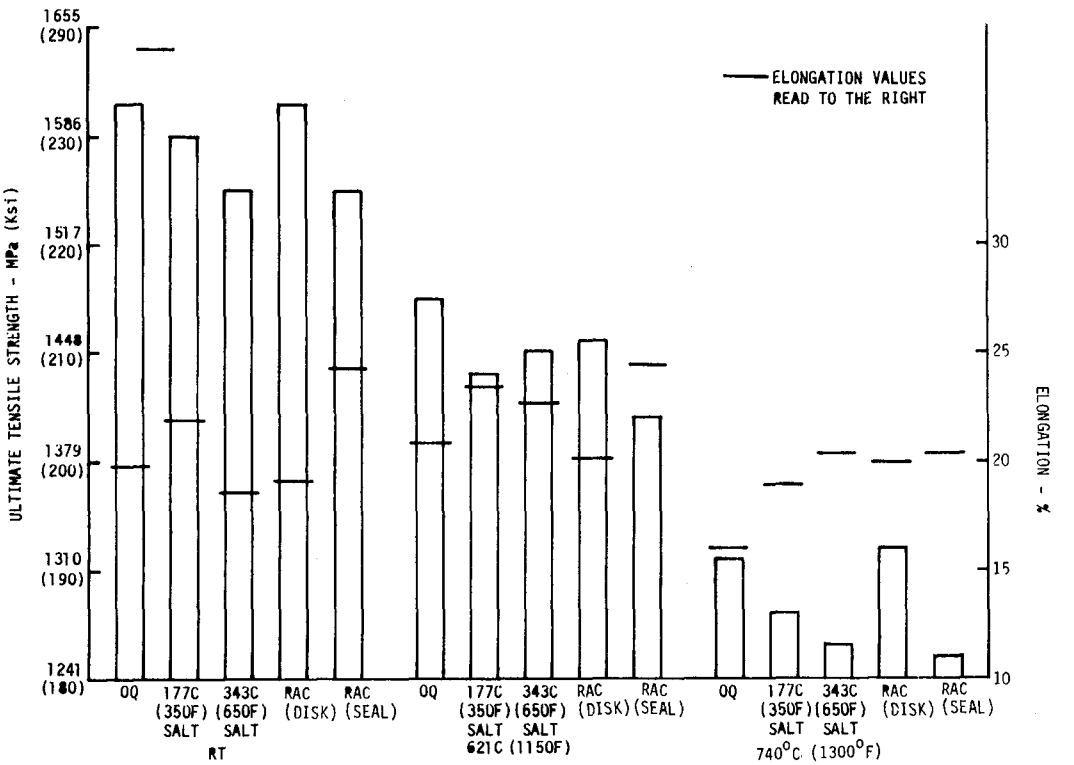

(B)

Figure 25 Mechanical Properties of MERL 76

A Effect of Rate of Quench from Solution Treatment on Stress Rupture Life

B Effect of Quench Rate from Solution Treatment on Tensile Strength of Thick Sections

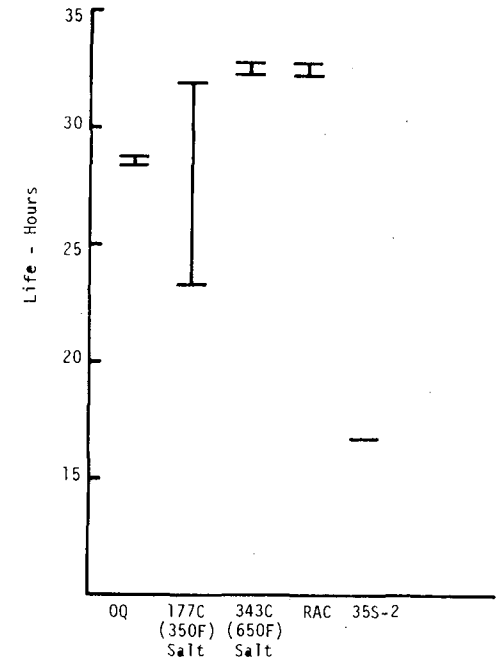

(A)

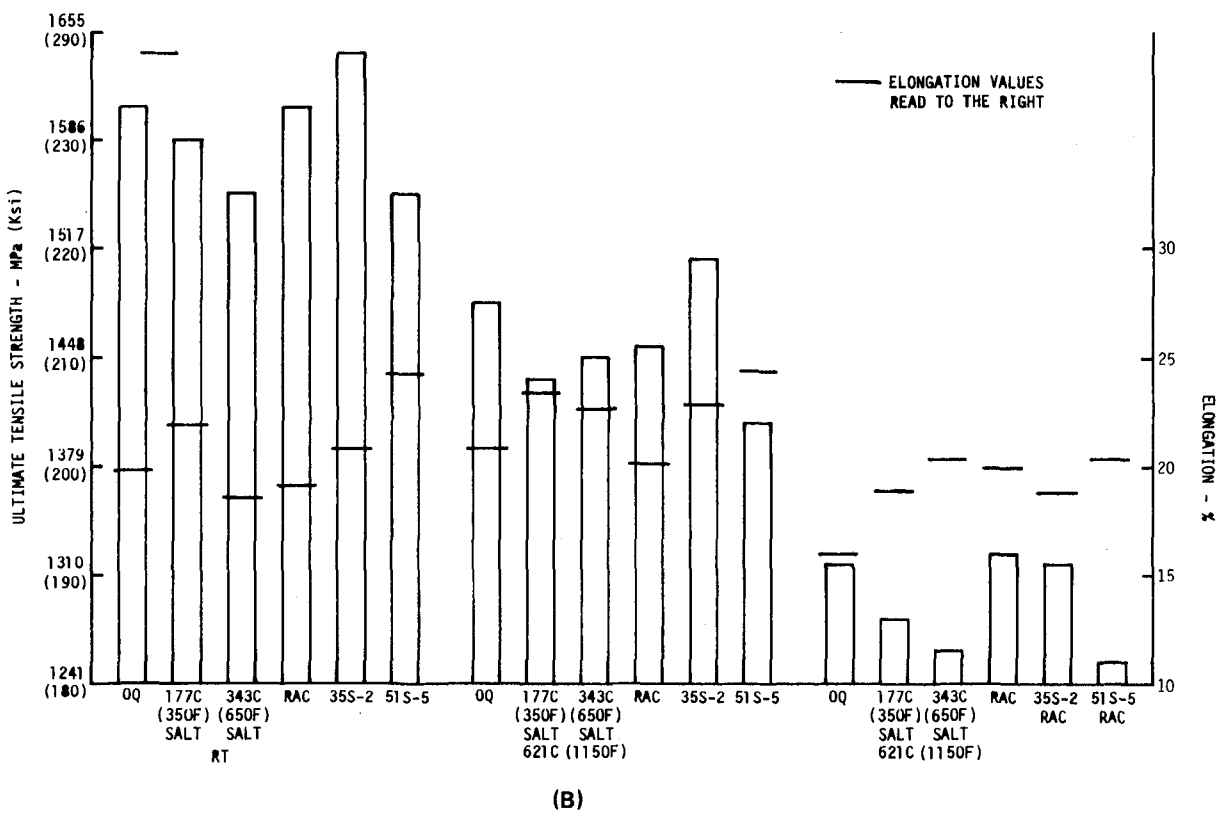

(B)

Figure 26 Mechanical Properties of MERL 76
(A) Effect of Quench Rate From Solution Treatment on Stress-Rupture Life. (B) Effect of Quench Rate From Solution Treatment on Tensile Strength of Thin Sections.

A comparison of tensile strength for both thin (38 cm/1.5 in) and thick (10.2 cm/4 in) section material is shown in Figure 27. The oil quench gave the best strength for both section sizes while material given a forced air cool displayed the lowest strengths (93 MPa/135 ksi at 621°C/1100°F) for thick section. Both salt quenches produced similar strengths (104 MPa/148 ksi) for thin sections but the 177°C(350°F) gave slightly better properties for 10.2 cm (4 in thick) material.

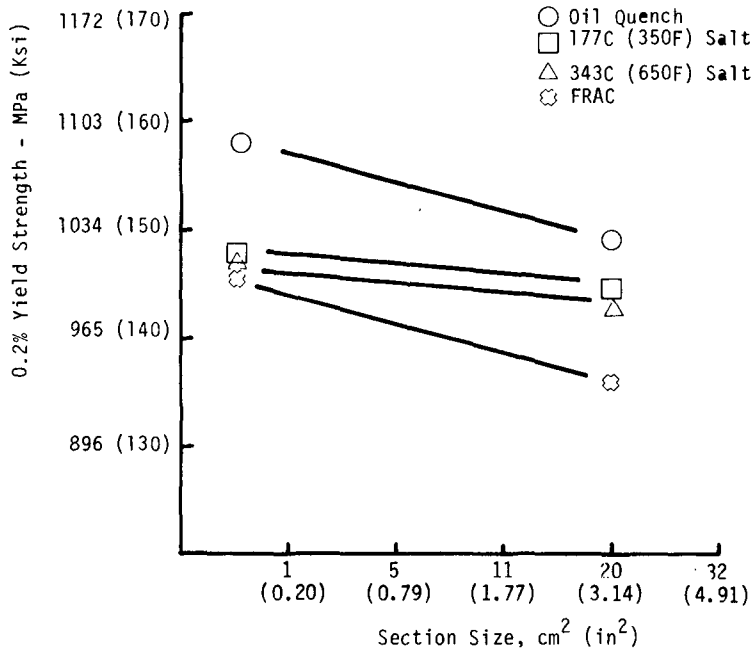

Figure 27 *621°C(1150°F) Tensile Strength as a Function of Cooling Rate and Section Size*

To assess the microstructural response to the various cooling rates, specimens were removed from the bore (thick) and hub (thin) section of each of the four fully heat treated, disk quarter sections. Figures 28-30 indicate that the matrix cooling gamma prime for the material forced air cooled (heat treat A) was coarsest (0.5 μm) while that for 163°C (325°F) salt quench (heat treat D) and oil quench (heat treat B) was finest (0.1 μm). The 343°C (650°F) salt quench (heat treatment C) provided an intermediate size (0.2 μm) matrix cooling gamma prime. Based upon these observations, the cooling rate for these relatively large sections (10.2 cm/4 in. thick) can be listed in descending order as follows:

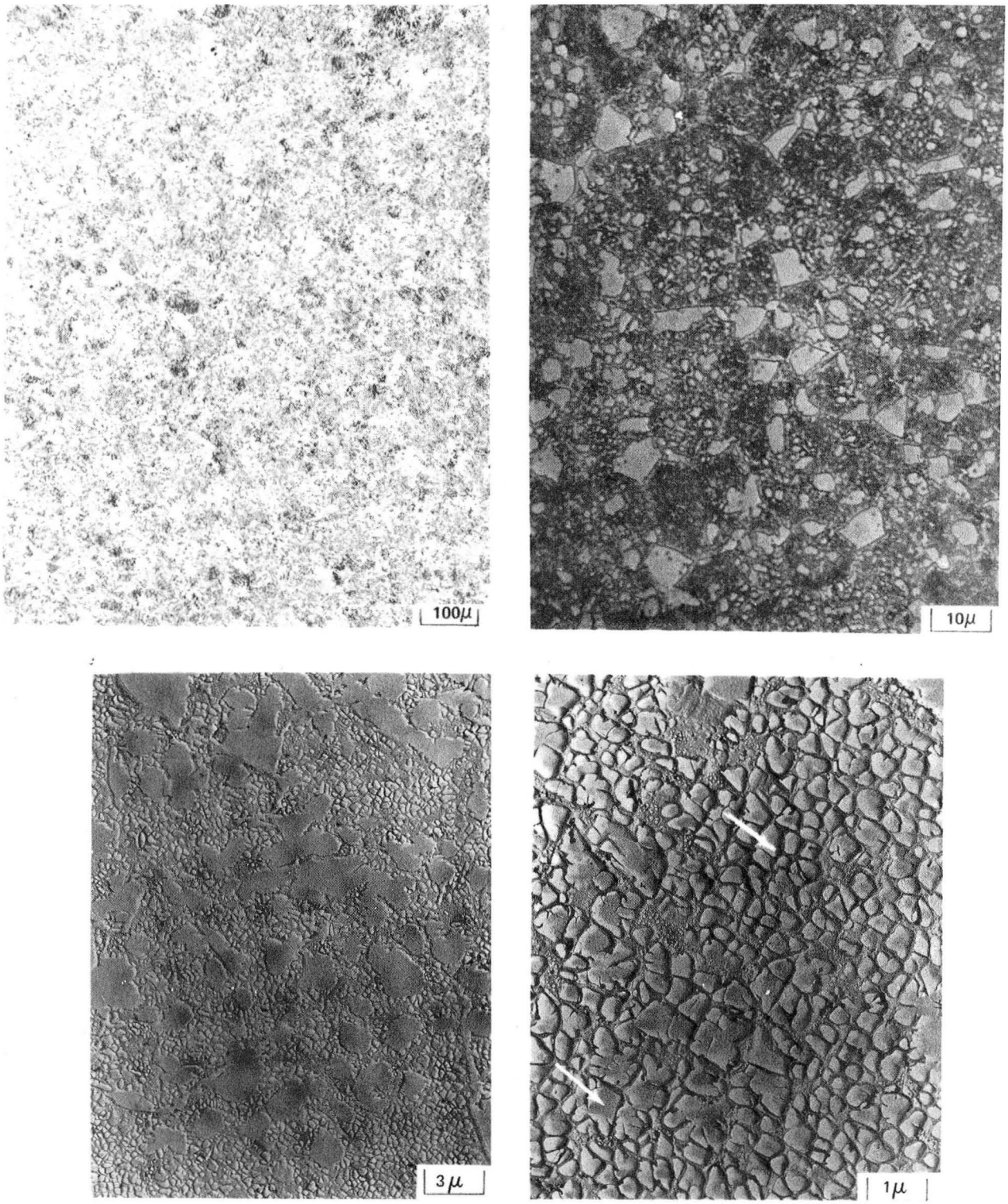

Figure 28 *Micrographs of the Bore (Thick) Region of a Quarter Section of Disk 34D-1 Heat Treated at 1163°C(2125°F)/2 hrs/RAC + 649°C (1200°F)/24 hrs/AC + 760°C (1400°F)/16 hrs/AC Showing the Matrix Cooling Gamma Prime Size (Arrows) To Be About 0.5 μm*

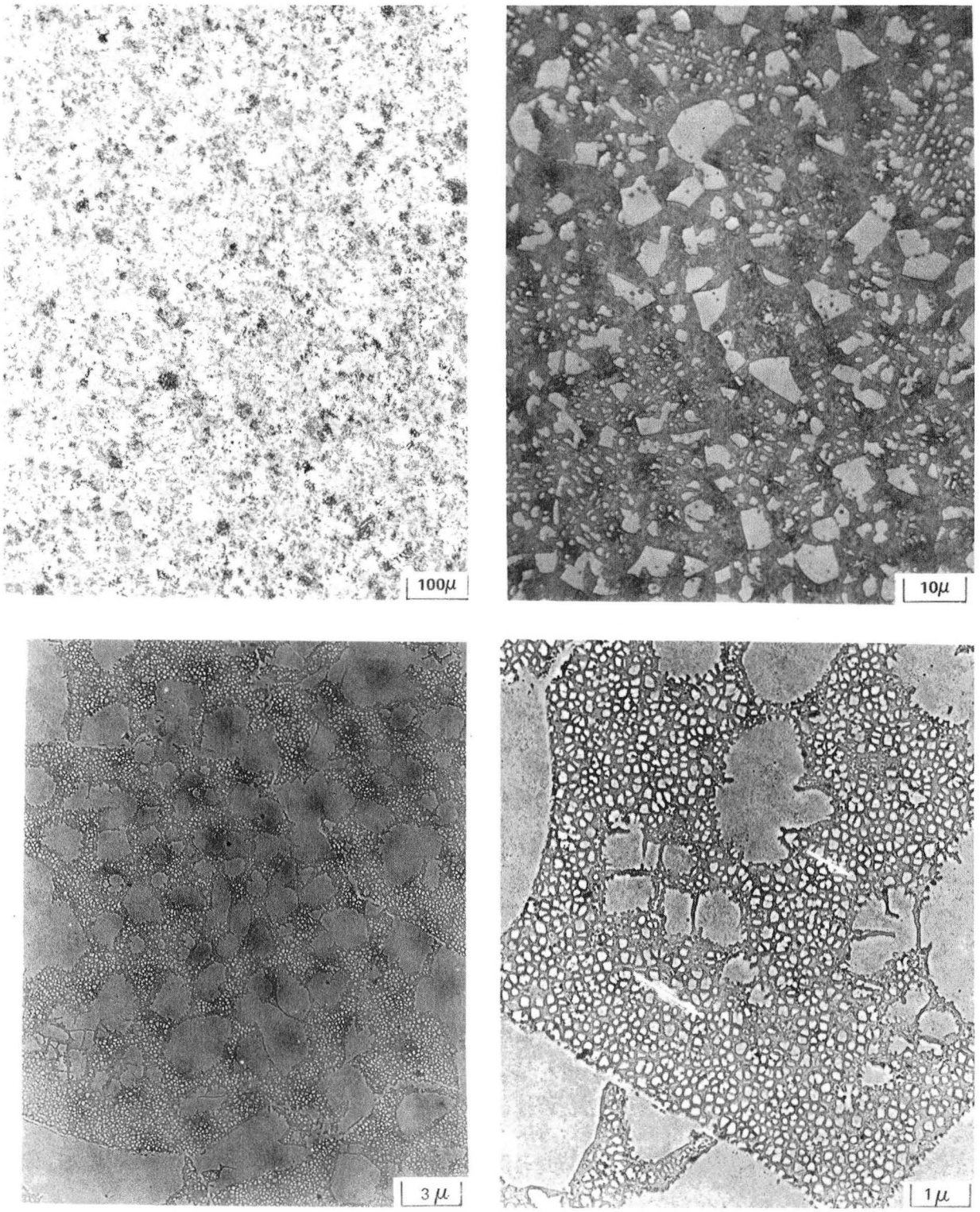

Figure 29 *Micrographs of the Bore (Thick) Region of a Quarter Section of Disk 34D-1 Heat Treated at 1163°C (2125°F)/2 hrs Furnace Cool at 55C°(100F°) Per Hour to 1121°C (2050°F)/0.5 hr/Salt Quench at 177°C (350°F)/AC + 649°C (1200°F)/2400 hrs/AC + 760°C (1400°F)/ 16 Hrs/AC Showing a Matrix Cooling Gamma Prime (Arrow) of Approximately 0.1 μm*

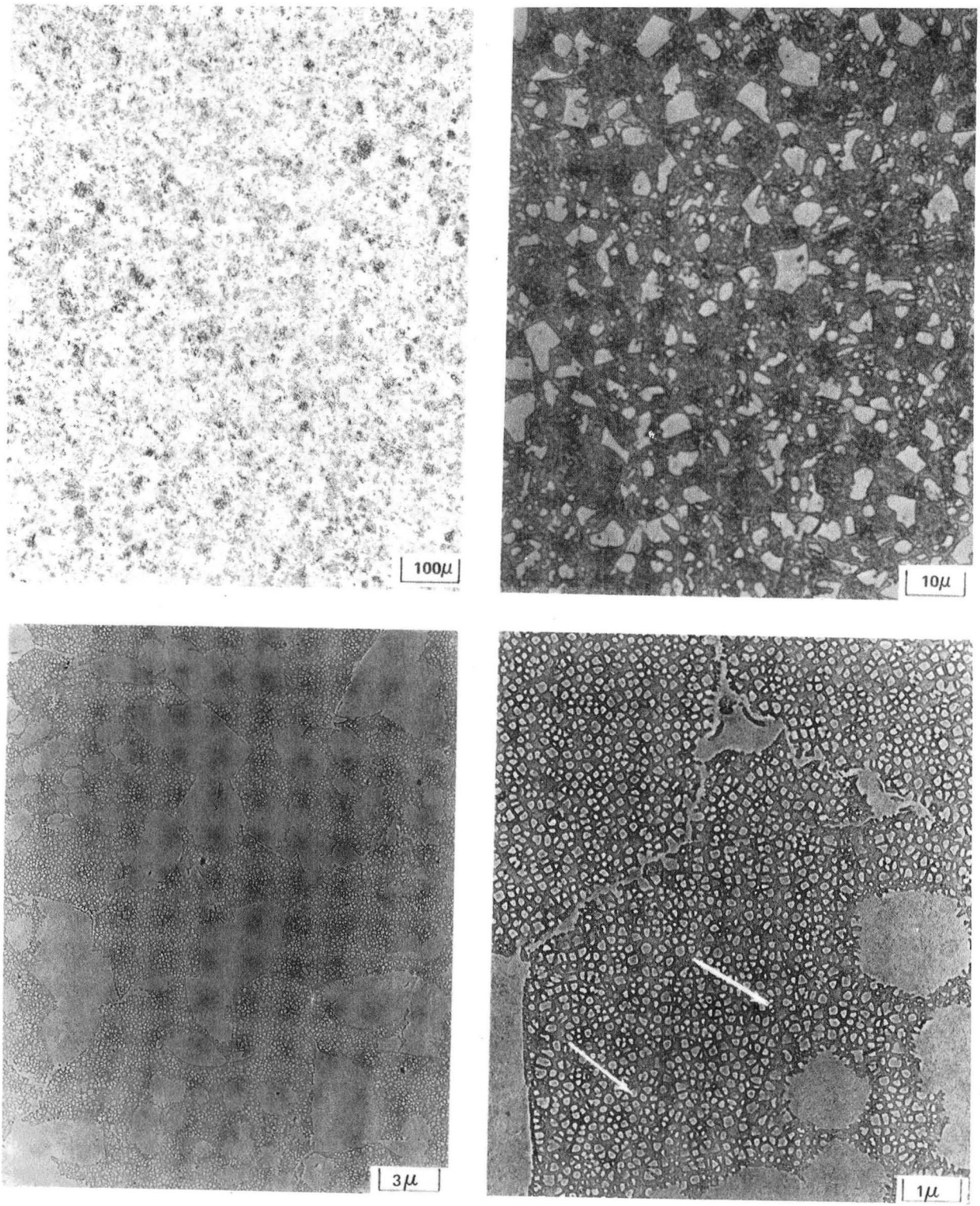

Figure 30 *Micrographs of the Bore (Thick) Region of a Quarter Section of Disk 34D-1 Heat Treated at 1163°C (2125°F)/2 hrs Furnace Cool at 55C°(100F°) Per Hour to 1121°C (2050°F)/0.5 hr/Oil Quench + 649°C (1200°F)/24 hrs/AC + 760°C (1400°F)/16 hrs/AC Showing a Matrix Cooling Gamma Prime Size (Arrow) of Approximately 0.1 μm*

- o Oil quench and 177°C (350°F) salt quench* (fastest)
- o 343°C(650°F) salt quench
- o Forced air cool (slowest)

Similar relationships between microstructure and cooling rates were observed for the thin hub sections (3.8 cm/1.5 in. thick) as shown in Figures 31-33. The matrix cooling gamma prime for thinner (hub) section was proportionately finer than that for the thick (bore) section. The difference in matrix cooling gamma prime size between the 343°C(650°F) salt quench and 163°C(325°F) and oil quench appeared negligible (0.15 μm vs. 0.1 μm).

A comparison of thin with thick section microstructure showed that the matrix cooling gamma prime was generally more uniformly precipitated in thin sections. This is probably attributable to the much faster cooling rates for thin sections.

The microstructure for TOBI seal 35S-2 (thin section) given an oil quench (heat treat B) is given in Figure 34. Electron micrographs show a high volume of extremely fine, barely resolvable gamma prime which contributed to the observed high tensile strength.

o Stabilization/Aging Cycle

Having selected oil quench as the best cooling rate from the solution heat treat temperature, the next step in heat treatment selection was to determine the post-solution heat treat cycle which achieved a good balance between strength and ductility. In this evaluation, a two step sequence (649°C(1200°F)+ 760°C(1400°F) with exposure times of up to 48 hours was selected with the rationale that the initial lower temperature step would provide nuclei for the subsequent higher temperature precipitation hardening step. The second approach was to evaluate a stress relief cycle for any

---

* The cooling rates were considered comparable for approximately 10.2 cm (4 in) thick section size since the difference in matrix cooling gamma prime size and properties were slight.

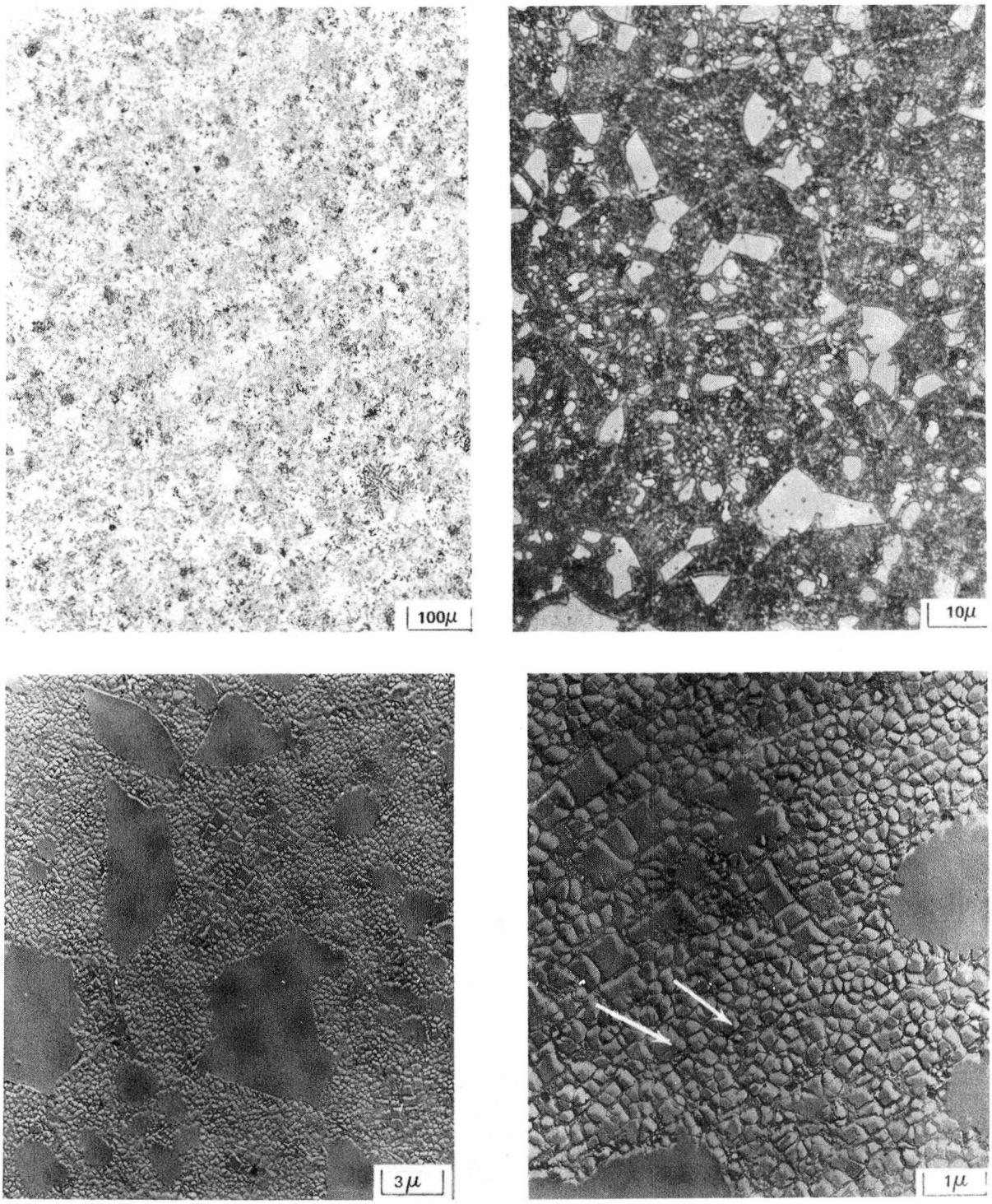

Figure 31 *Micrographs of the Hub (Thin) Region of a Quarter Section of Disk 34D-1 Heat Treated at 1163°C (2125°F) 2 hrs/RAC + 649°C (1200°F)/24 Hrs/AC + 760°C (1400°F/16 hrs/AC Showing a Matrix Cooling Gamma Prime (Arrow) of Approximately 0.3 μm*

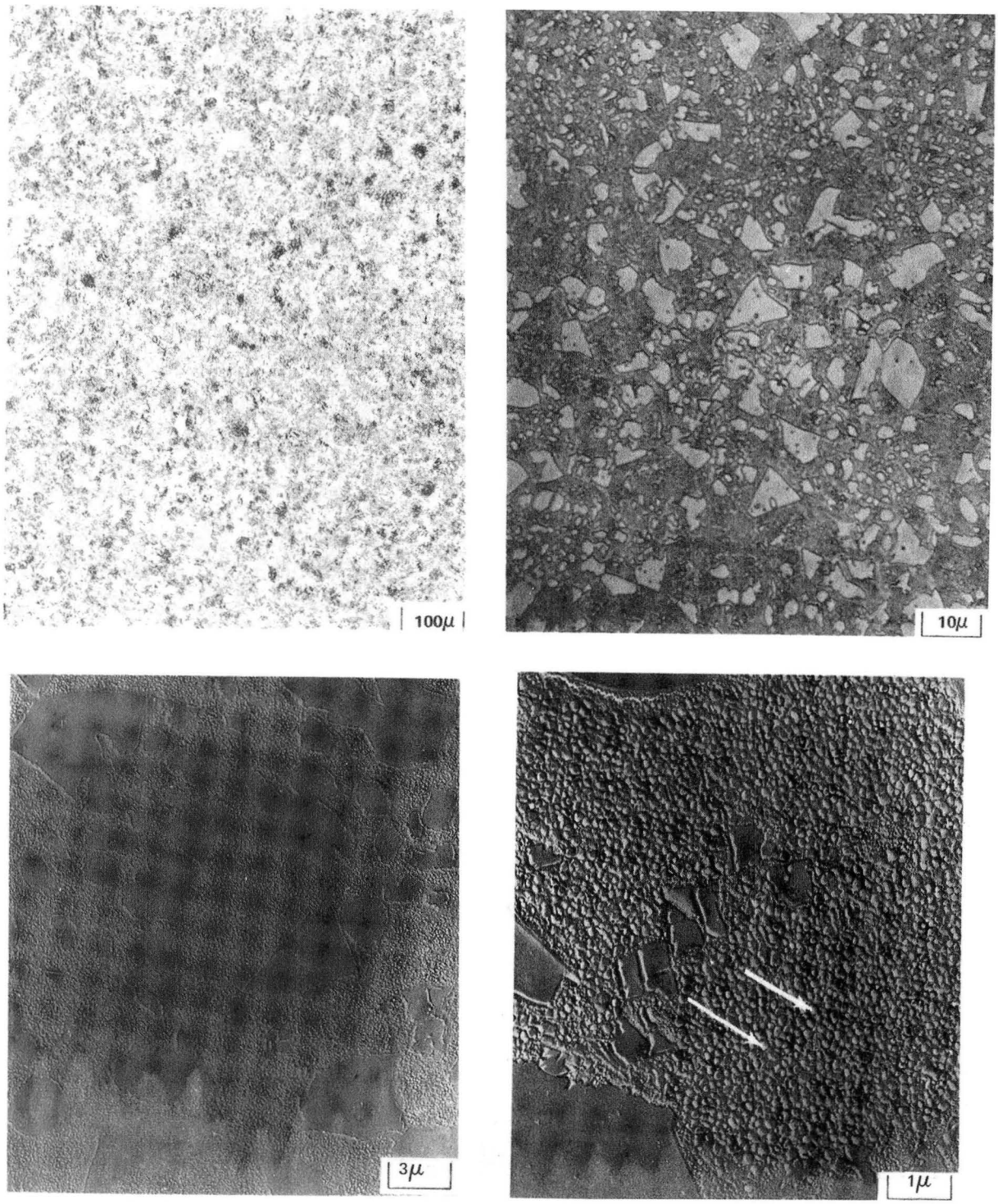

Figure 32 *Micrographs of the Hub (Thin) Region of a Quarter Section of Disk 34D-1 Heat Treated at 1163°C (2125°F)/2 hrs Furnace Cool at 55C°(100F°) Per Hour to 1121°C (2050°F)/0.5 hr/Salt Quench at 177°C (350°F)/AC + 649°C (1200°F)/2400 hrs/AC + 760°C (1400°F)/ 16 hrs/AC Showing a Matrix Cooling Gamma Prime Size (Arrow) of 0.1 μm*

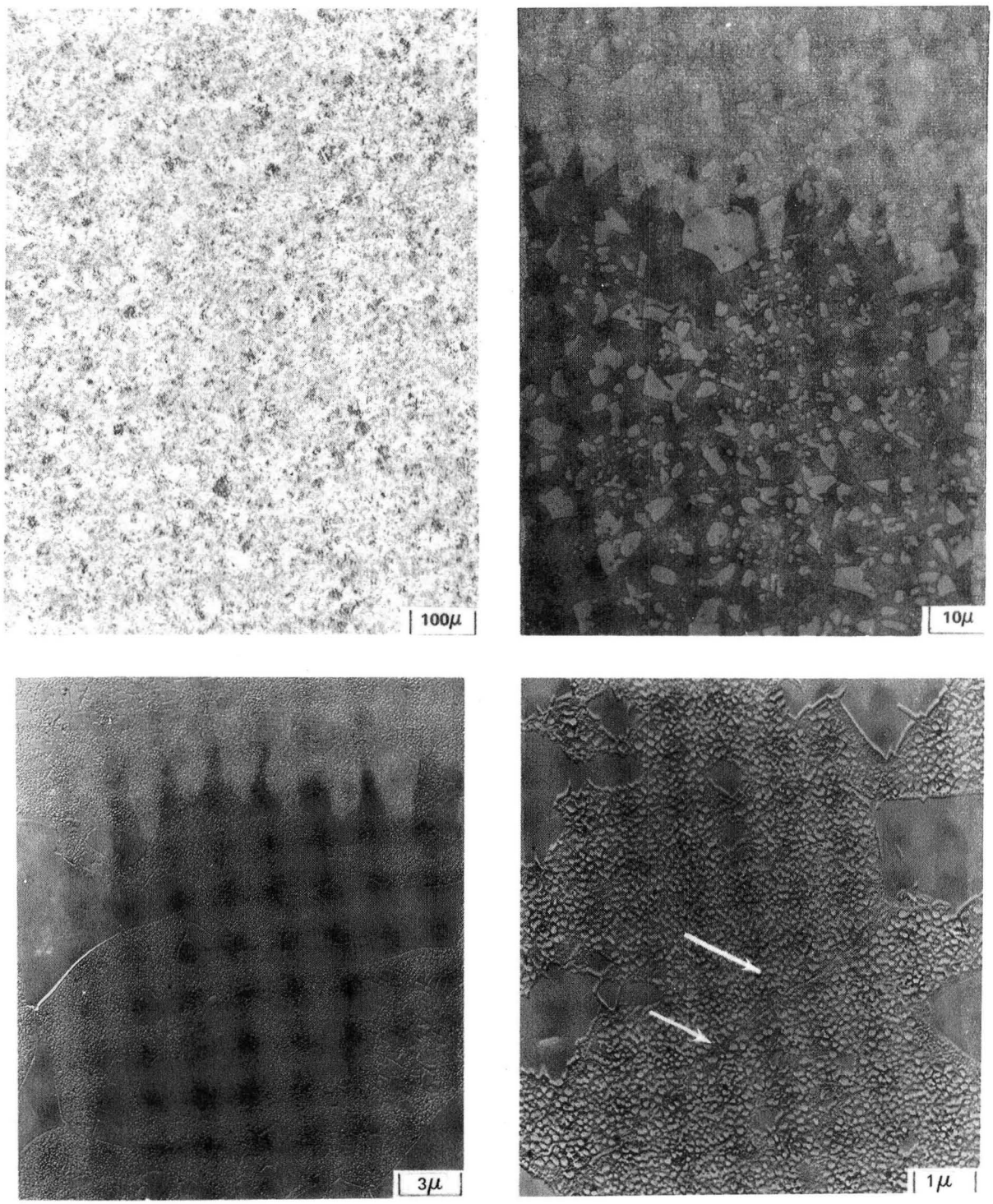

Figure 33 *Micrographs of the Hub (Thin) Region of a Quarter Section of Disk 34D-1 Heat Treated at 1163°C (2125°F)/2 hrs Furnace Cool at 55C°C(100F°) Per Hour To 1121°C (2050°F)/0.5 hr/Oil Quench + 649°C (1200°F)/24 hrs/AC + 760°C (1400°F)/16 hrs/AC Showing a Matrix Cooling Gamma Prime Size (Arrow) of 0.1μm*

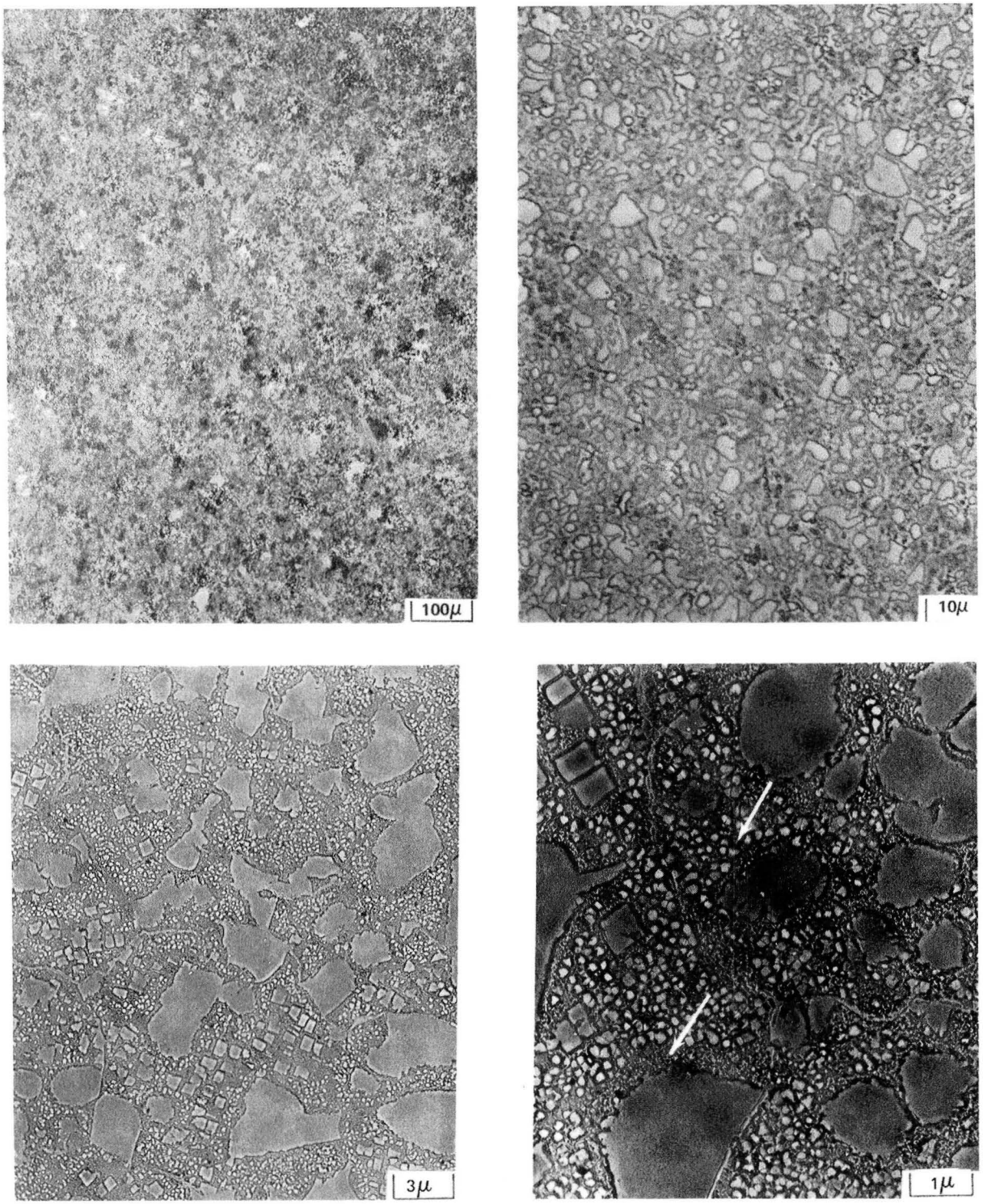

Figure 34 *Micrographs of TOBI Seal 35S-2 Heat Treated at 1163°C (2125°F)/2 hrs Furnace Cool at 55C°(100F°) Per Hour to 1121°C (2050°F)/0.5 Hr/Oil Quench + 649°C (1200°F)/24 hrs/AC + 760°C (1400°F)/16 hrs/ AC Showing a High Volume of Matrix Gamma Prime (Barely Resolvable) As Indicated by Arrows*

residual stresses that may have been retained from oil quenching. Tensile and stress-rupture specimen blanks were removed from the oil quenched disk 35D-3 (1163°C(2125°F) for 2 hrs/OQ). These blanks were given one of the aging heat treatments shown in Table VI.

TABLE VI

AGING HEAT TREATMENTS APPLIED TO DISK 35D-3

Identification	Heat Treatment
a	649°C (1200°F)/24 + 760°C (1400°F)/8
b	649°C (1200°F)/24 + 760°C (1400°F)/16
c	649°C (1200°F)/24 + 760°C (1400°F)/48
d	649°C (1200°F)/8 + 760°C (1400°F)/16
e	649°C (1200°F)/24 + 788°C (1450°F)/8
f	649°C (1200°F)/24 + 816°C (1500°F)/8
g	760°C (1400°F)/48
h	871°C (1600°F)/0.67 + 982°C (1800°F)/0.75 + 649°C (1200°F)/24 + 760°C (1400°F)/16
i	871°C (1600°F)/1 + 649°C (1200°F)/24 + 760°C (1400°F)/16
j	649°C (1200°F)/24 + 760°C (1400°F)/16 + 871°C (1600°F)/1

The specimens given the direct two-step age were the first group to be analyzed. Figure 35 summarizes the 621°C (1150°F) tensile strengths displayed after the various heat treat cycles. A 760°C (1400°F) age provided the highest ultimate and yield strength compared to either the 788°C (1450°F) or 816°C (1500°F) aging cycle. The strength was further increased by 35 MPa (5 ksi) when the exposure time at 760°C (1400°F) was increased to 16 hours. Incorporating an intermediate exposure of 871°C (1600°F) and 982°C (1800°F) for a stress relief for the quenched material in the direct two-step age did not adversely affect the properties, Figure 35(c). The average tensile properties for all test temperatures and for all aging cycles evaluated are given in Figures 36-41. The results indicate heat treatments consisting of an intermediate age cycle (871°C(1600°F)/1hr - 982°C(1800°F)/.75 hr followed by a two-step precipitation age at 649°C (1200°F)/24 hrs + 760°C (1400°F)/16 hrs. (i.e., h identified in Table VI) produced the best combination of strengths for all test temperatures used. A detailed compilation of the tensile results is given in Appendix F.

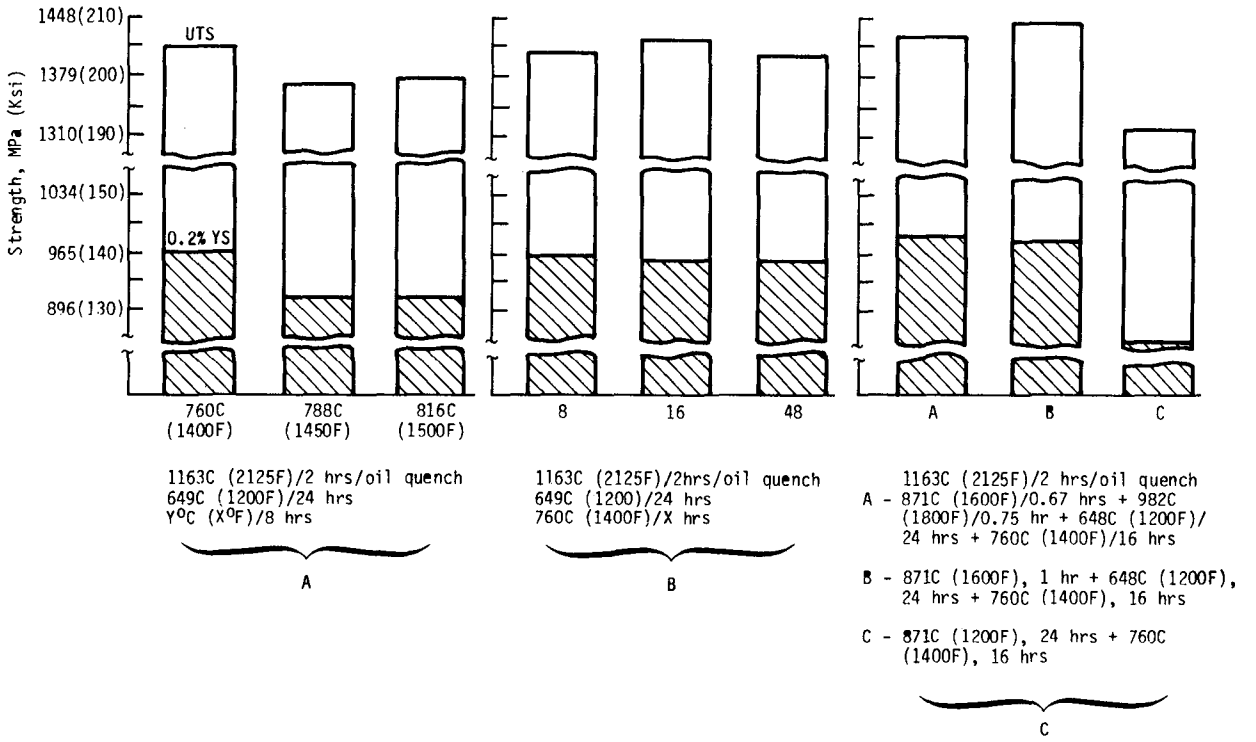

Figure 35 Tensile Strengths After Various Heat Treatments

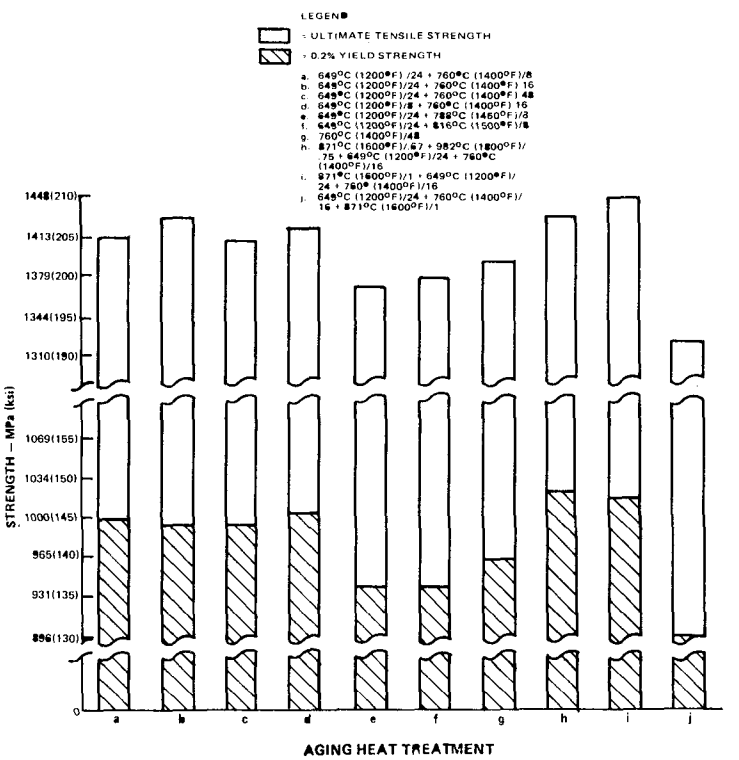

Figure 36 Average 621°C (1150°F) Tensile Strength of Specimens Removed From Bore of Disk 35D-3 Solution Heat Treated at 1163°C (2125°F)/ 2 hrs/OQ + Aged at Various Cycles

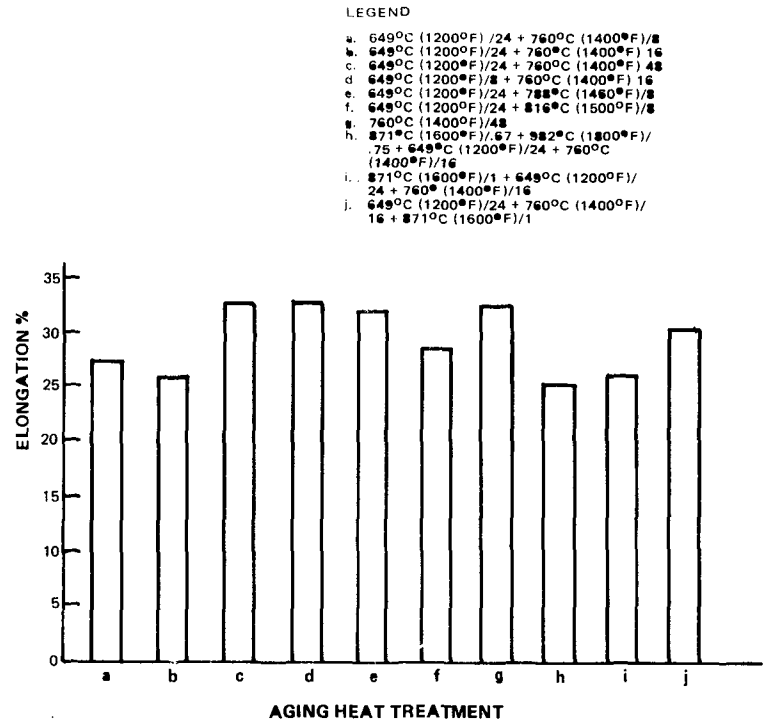

Figure 37 *Average 621°C (1150°F) Tensile Elongation of Specimens Removed from Bore of Disk 35D-3 Solution Heat Treated at 1163°C (2125°F)/2 hrs/OQ + Aged at Various Cycles*

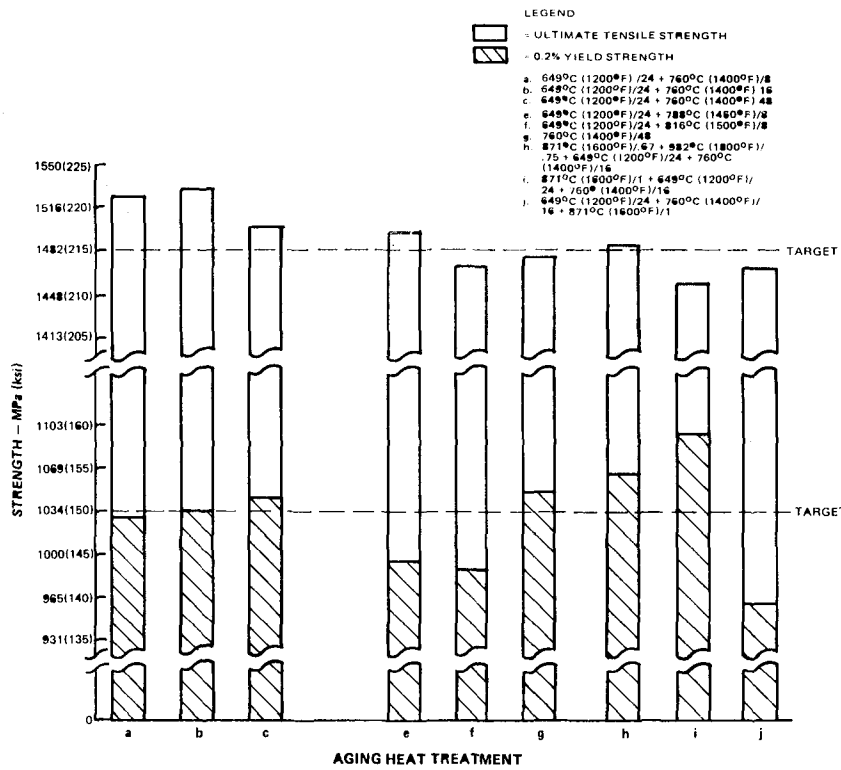

Figure 38 *Average Room Temperature Tensile Strength of Bore Specimens Removed From Disk 35D-3 Solution Heat Treated at 1163°C (2125°F)/2 hrs/OQ + Aged at Various Cycles*

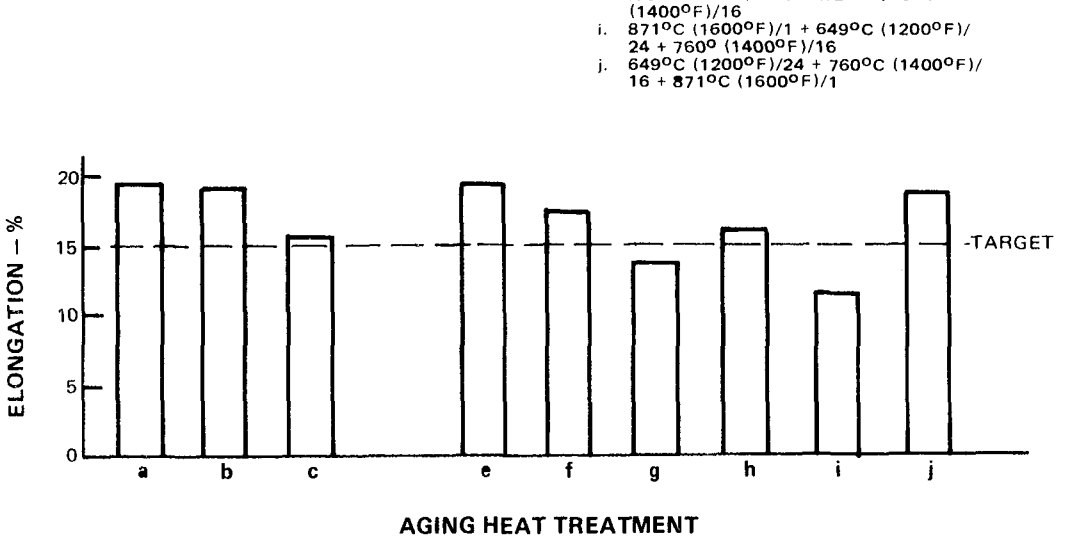

Figure 39 *Average Room Temperature Elongation of Bore Specimens Removed from Disk 35D-3 Solution Heat Treated at 1163°C (2125°F)/2 hrs/ 0Q + Aged at Various Cycles*

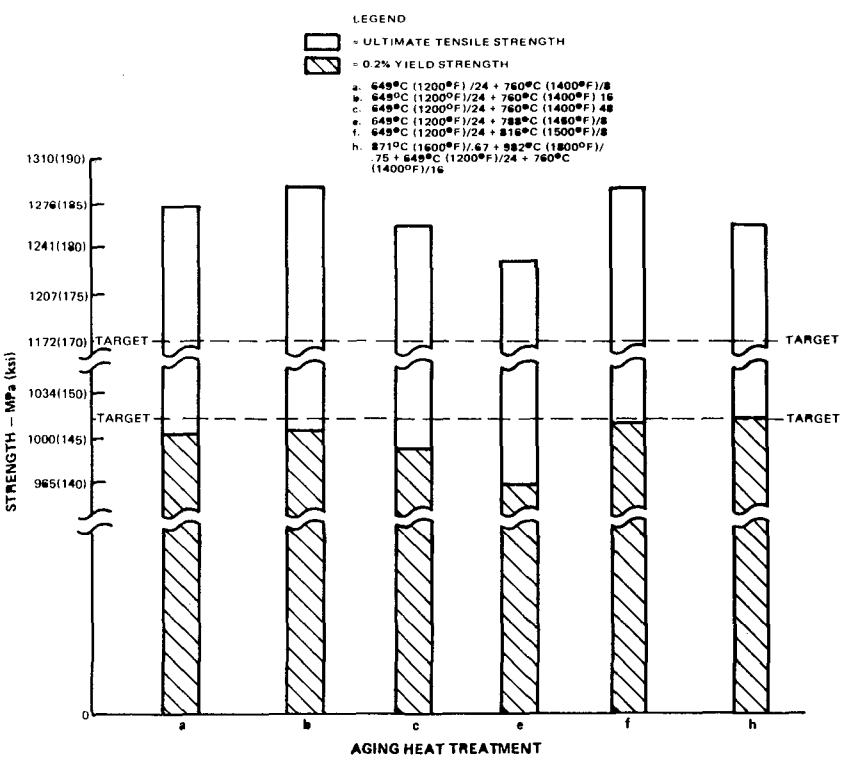

Figure 40 *Averaged 704°C (1300°F) Tensile Strength of Specimens Removed from Bore of Disk 35D-3 Solution Heat Treated at 1163°C (2125°F)/2 hrs 0Q + Aged at Various Cycles*

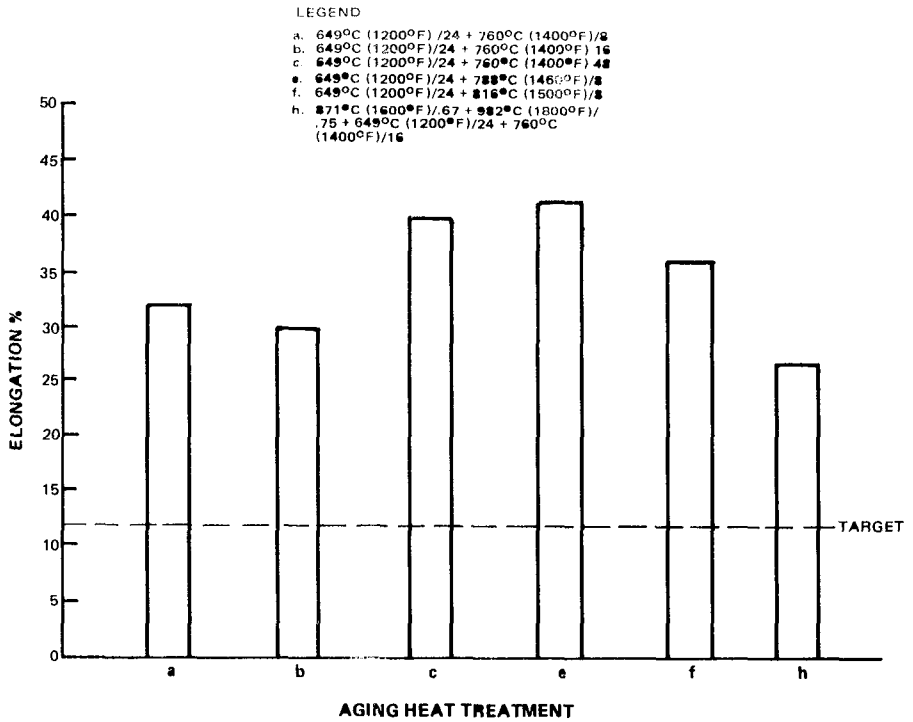

Figure 41 *Average 704°C (1300°F) Elongation of Specimens Removed from Bore of Disk 35D-3 Solution Heat Treated at 1163°C (2125°F)/2 hrs/OQ + Aged at Various Cycles*

Stress-rupture testing was conducted for a few select heat treatments. Material given either a direct two-step age or a stabilized + direct age displayed comparable rupture lives as shown in Table VII.

TABLE VII

DISK 35D-3 STRESS RUPTURE PROPERTIES
732°C (1350°F)/655 MPa (95.0 ksi)

Identification	Life - Hrs.	% EL	Specimen Location
c-A	25.9	NOTCH Failure	Bore
c-B	44.8	9.1	Bore
j-2A	56.3	NOTCH Failure	Rim
j-2B	42.8	NOTCH Failure	Rim
h-41	47.6	9.6	Rim
h-42	43.2	NOTCH Failure	Rim
i-45	49.4	13.4	Rim
i-46	41.4	NOTCH Failure	Rim
Target Min	23.0	5.0 at 732°C(1350°F)/638 MPa (92.5 ksi)	

c. 649°C(1200°F)/24 + 760°C(1400°F)/48

h. 871°C(1600°F)/.67 + 982°C(1800°F)/.75 + 649°C (1200°F)/24 + 760°C(1400°F)/16

i. 871°C(1600°F)/1 + 649°C(1200°F)/24 + 760°C (1400°F)/16

j. 649°C(1200°F)/24 + 760°C(1400°F)/16 + 871°C (1600°F)/1

Based upon the results of the heat treat evaluation of the large disk, only three post-solution heat treat cycles were applied to the smaller TOBI seal component for confirmation of the best post solution heat treat cycle. Seal 51S-5 was solution heat treated at 1163°C (2125°F)/2/RAC) and then aged at conditions b, h and i given in Table VI. Tensile specimens were removed from the tangential direction and tested at RT, 621°C (1150°F) and 704°C (1300°F). Figures 42-44 indicates that heat treatments h and i (Table VI) again gave the best properties confirming the trends observed for disk 35D-3. A detailed presentation of TOBI seal test data is given in Appendix G.

As a result of this evaluation in Phase I of Task I, a process control plan and acceptance criteria was tentatively established. This criteria, initially established, is essentialy those shown in Appendices M and O except for the addition of a visual inspection of the powder after powder contamination was observed in one blend of powder used in the design data portion (Task I, Phase II) of this program. For the components made for design data, spin burst test and engine test, the process control plan and acceptance criteria were used.

An important feature of this process control plan was the heat treating procedure, particularly for the solution cycle, to assure that the desired properties are achieved. For this reason, solution heat treating of all components was accomplished by utilizing furnaces with oil tanks adjacent to the furnace doors. The elapsed time between removal of the disk from the furnace and insertion nominally ranged from 15-30 seconds in the automatic mode. However, longer quench delay times were achieved by operating the furnace quench controls on the manual mode as for disk 35D-2. Cracking was prevented in the oil quench sequence by instituting a delay hold time of 90 seconds before the part was immersed in oil. Temperature tolerance for solution heat treatment was ±14C°(±25F°) and ±8C°(±15F°) for the stabilization and age cycles.

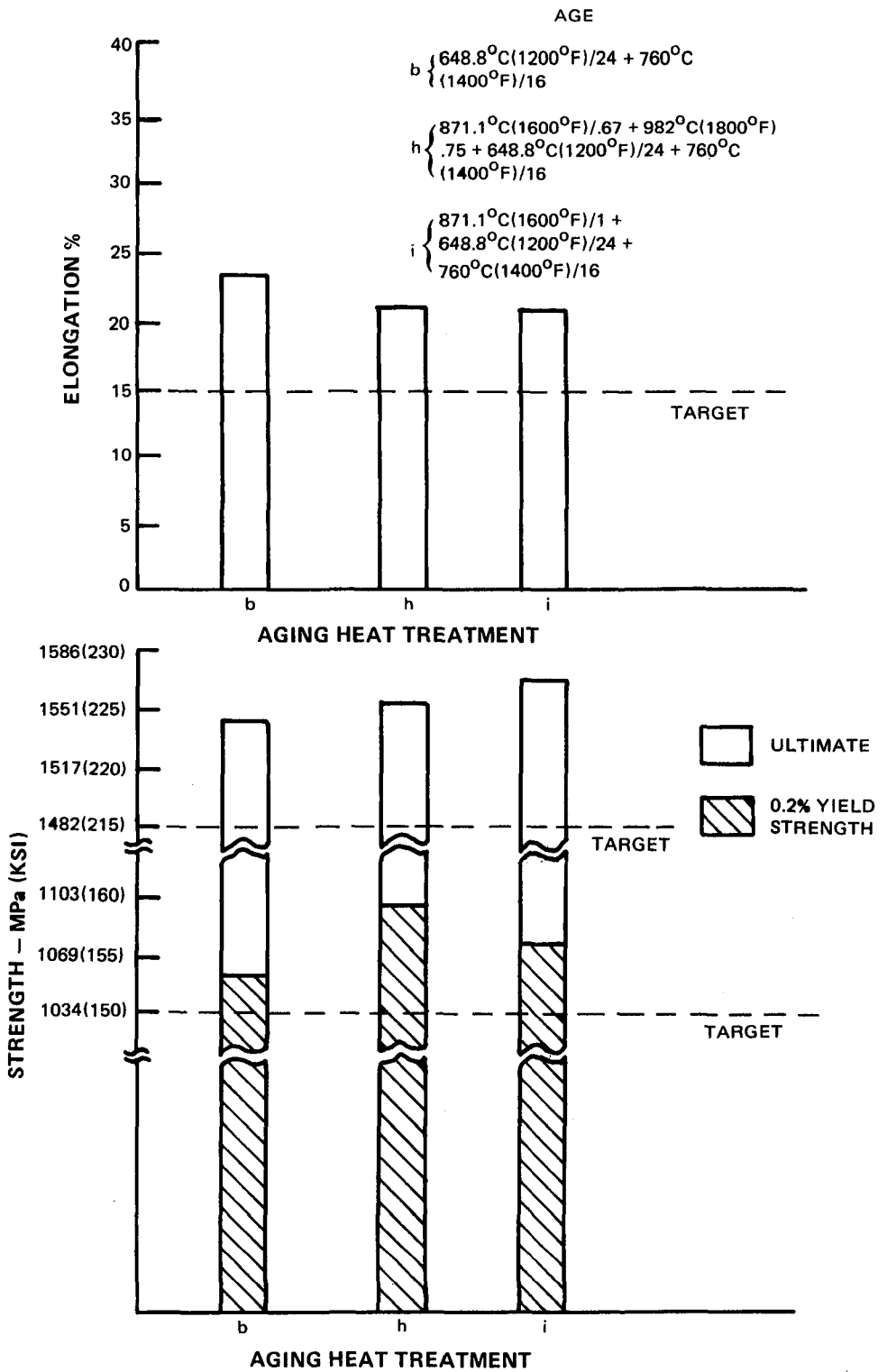

Figure 42 ***Average Room Temperature Tensile Strength of Specimens Removed*** *from TOBI Seal HIP at 1182°C(2160°F)/103.42 MPa (15 ksi) 3 hrs + 1171°C(2140°F)/2 hrs/RAC + Age at Various Cycles*

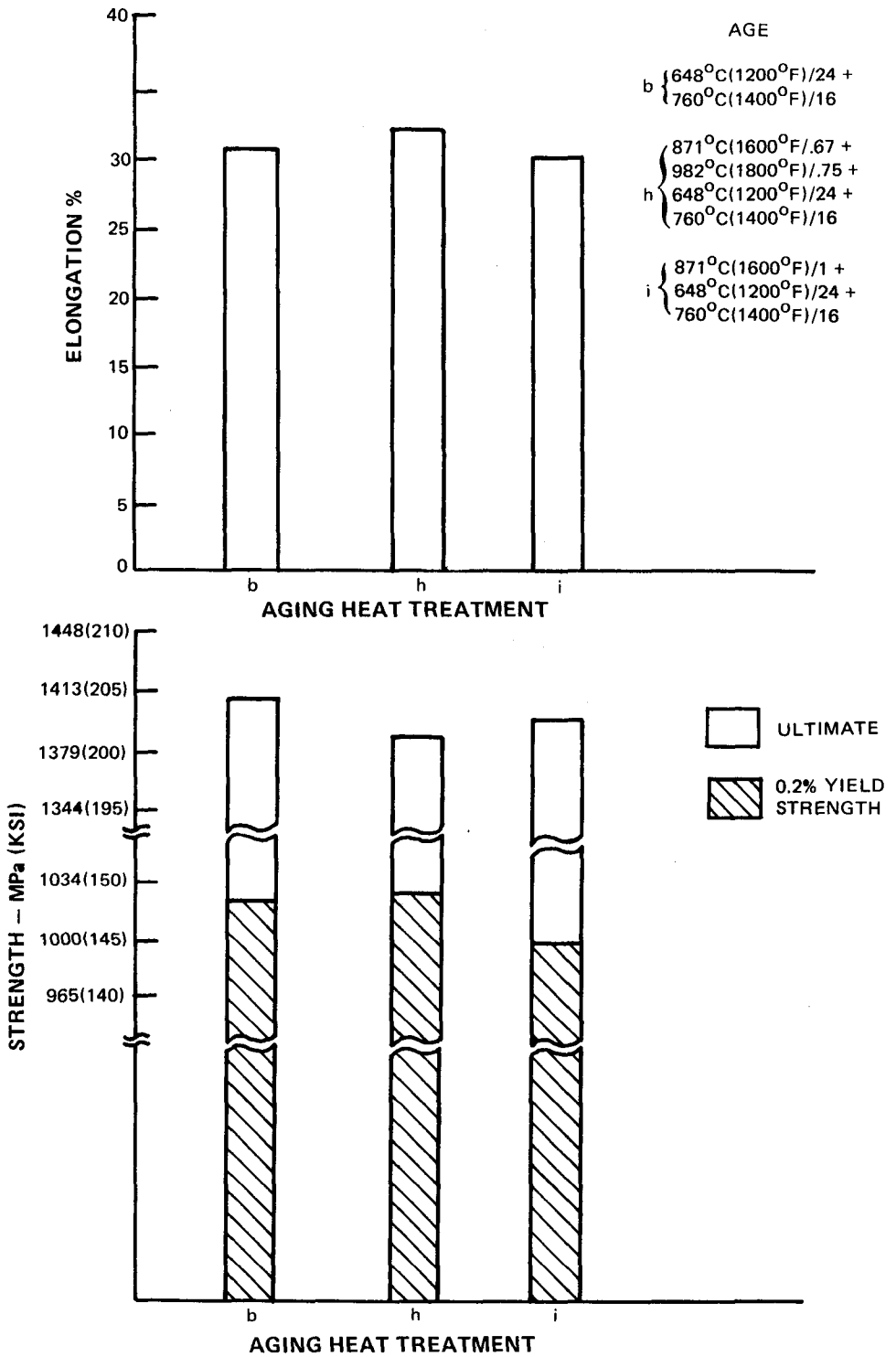

Figure 43 *Average 621.1°C (1150°F) Tensile Strength of Specimens Removed from TOBI Seal HIP at 1182°C(2160°F)/103.42 MPa (15 ksi)/3 hrs. + 1171°C (2140°F)/2 hrs./RAC + Age at Various Cycles*

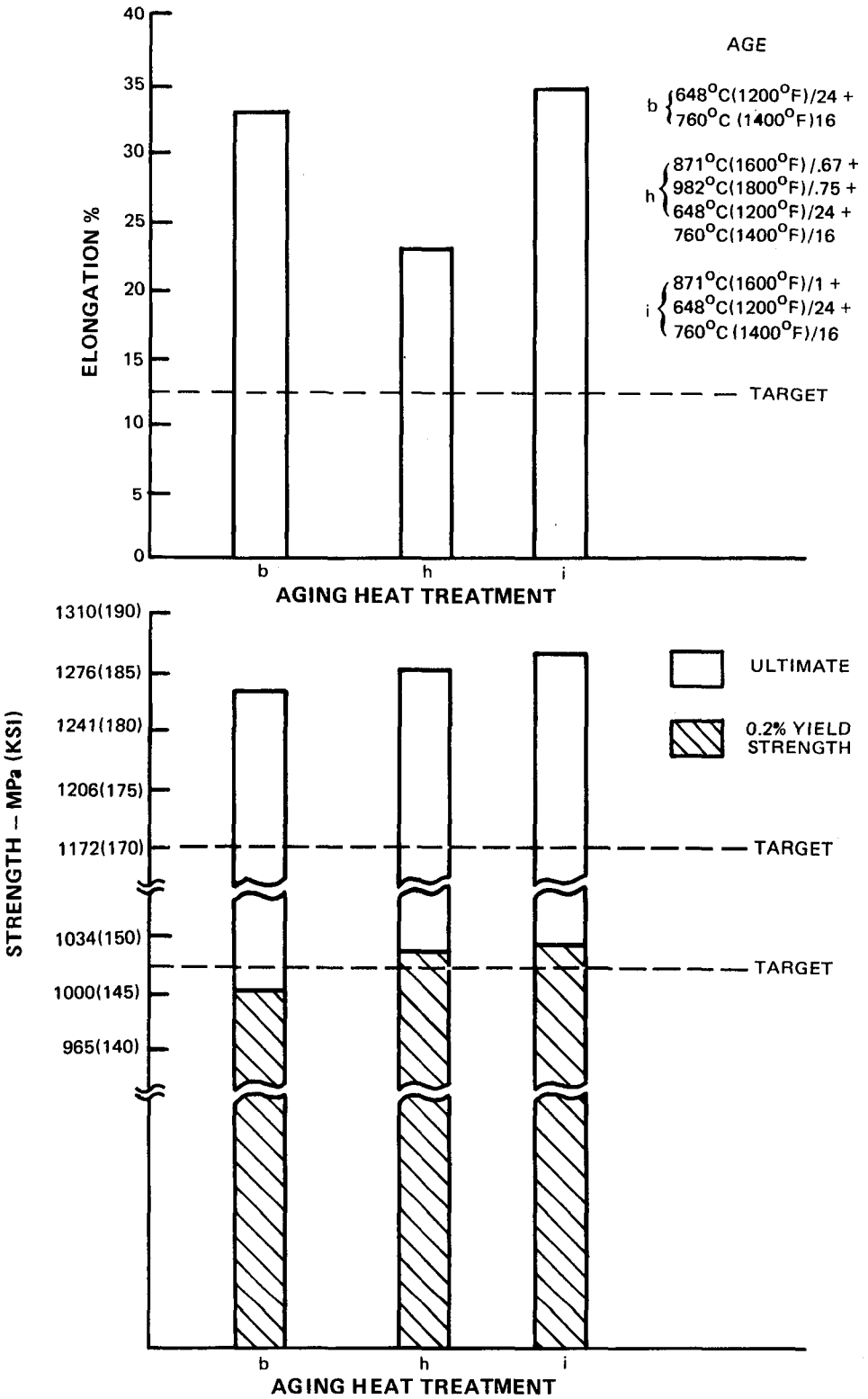

Figure 44 *Average 704°C (1300°F) Tensile Strength of Specimens Removed from TOBI Seal HIP at 1182°C(2160°F)/103.42 MPa (15 ksi)/3 hrs. + 1171°C (2140°F)/2 hrs/RAC + Age at Various Cycles*

TASK I, PHASE II - DEVELOPMENT OF DESIGN DATA

The purpose of Phase II was to develop the data necessary to permit the design of a JT9D first stage turbine disk using MERL 76. The properties that were characterized were those associated with the mechanical properties, physical properties and chemistry of specimens machined from three HIP disks.

Mechanical Properties

Critical mechanical properties that control the performance of a disk component vary with the location in the disk. Furthermore, since the disk experiences a spectrum of conditions during a flight cycle, material properties must be determined over a range of temperatures and stresses. For design purposes, it is necessary to establish that these material properties can meet the minimum design requirements.

In all disk locations, it is important to achieve adequate tensile properties to ensure that localized yielding will not occur. Additionally, tensile strength and ductility are important factors when disk components are subjected to overspeed conditions. For these reasons, tensile properties over a wide temperature range were defined.

In the turbine blade attachment location, stress-rupture properties of the disk component becomes an important consideration. Properties must be determined over a range of temperatures to establish properties under thermal transient conditions that may occur during service.

In the hotter rim sections of a disk, time dependent deformation can occur under operating stresses. This creep deformation must be minimized to preserve the dimensions of the disk.

The life of the disk component is usually determined by the fatigue properties. A fatigue failure of a disk can lead to extensive damage and even destruction of an engine. Both smooth and notch section properties are required because of the complex geometry of a disk component. In order to establish the basic fatigue capability of the material, axial and bolt-hole

specimens were tested. These tests establish the fatigue crack initiation behavior of the material in situations where a fatigue crack nucleates and grows from a surface. By measuring fatigue crack growth rates in addition to establishing LCF threshold stress intensity levels, initiated cracks may be prevented from propagating to a critical size.

Test Program

Tensile, stress-rupture and creep tests were conducted according to standard ASTM procedures. Test specimens were machined with tangential and radial orientations from various locations (i.e., rim, web, bore) of disks 102-1, 102-2, and 160-2. The location and the corresponding identity of each test specimen is indicated in Figures 45 and 46. Tensile specimens (Figure 47) were removed from the bore, web, and rim of the disks. Combination smooth and notched bar stress-rupture specimens (Figure 48) were removed from the bore and rim in the tangential direction while creep-rupture specimens (Figure 49) were removed from web-radial and rim tangential locations of the disk.

Fatigue tests, consisting of Sonntag-type axial specimens, bolt-hole, threshold stress intensity, and crack growth were performed according to Pratt & Whitney Aircraft procedures.

Smooth and notched Sonntag specimens (Figure 50) were tested in a 10,000 pound capacity servo-controlled, closed-loop, hydraulic driven fatigue rig. A function generator supplied a sine wave load signal set at 30 Hz frequency. The amplified output of the load cell was monitored using the amplitude measuring device and oscilloscope to determine the maximum and minimum loads. The specimens were heated using an induction unit rated at 2.5 kw output at 450 kHz nominal frequency. Test temperature was controlled by thermocouples which were tack welded to the specimen above and below the gage section with one used for controller input and one for monitoring by a precision potentiometer. Fluorescent penetrant inspection methods were used to establish life to 1/32 inch crack. In this procedure, penetrant fluid is applied to the notch with the specimen held at a load less than the maximum test load. The notch is then wiped clean and observed with an ultraviolet light while the load is released forcing the penetrant from any existing crack.

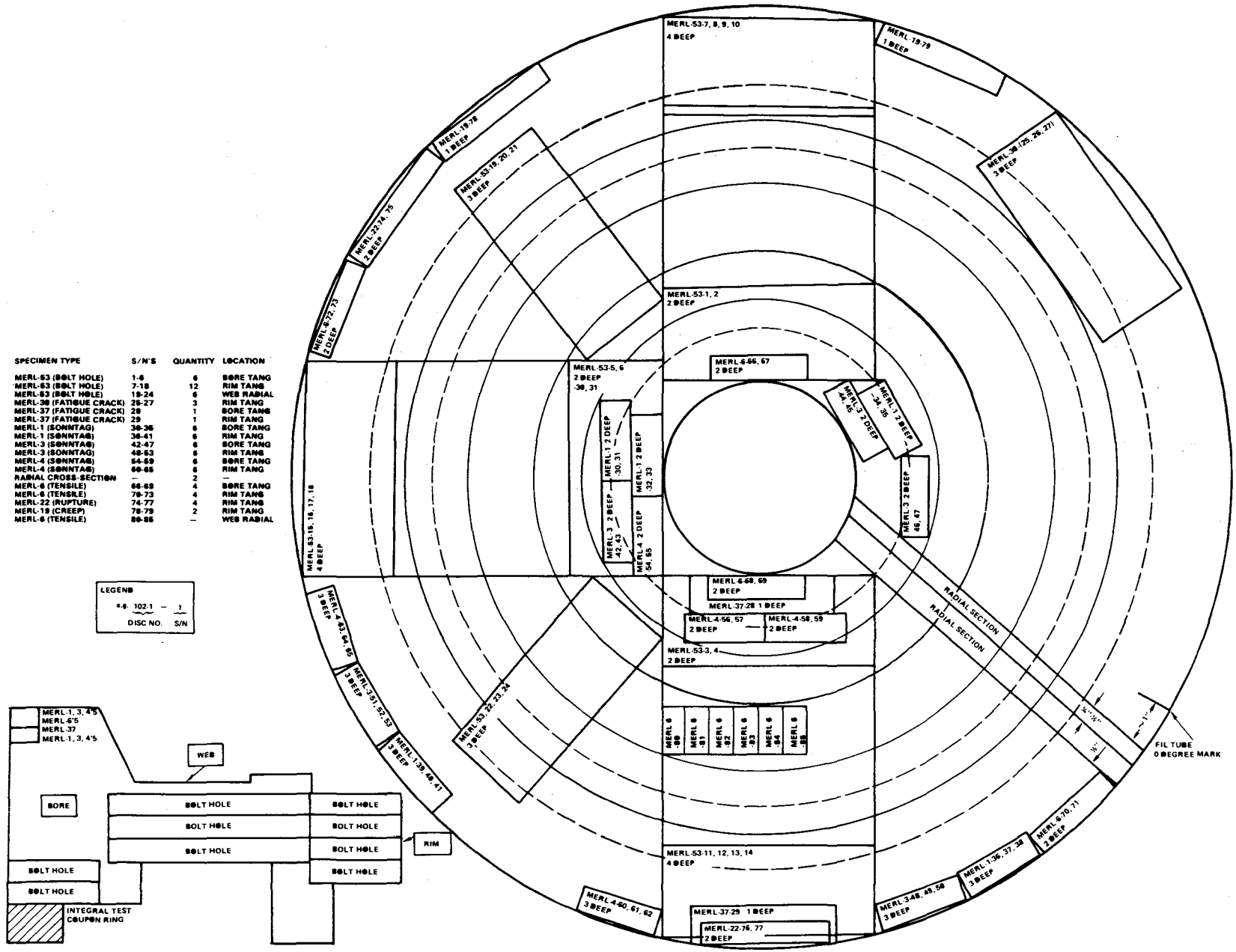

Figure 45 Identification and Location of Test Specimens Machined From Disks 102-1 and 102-2

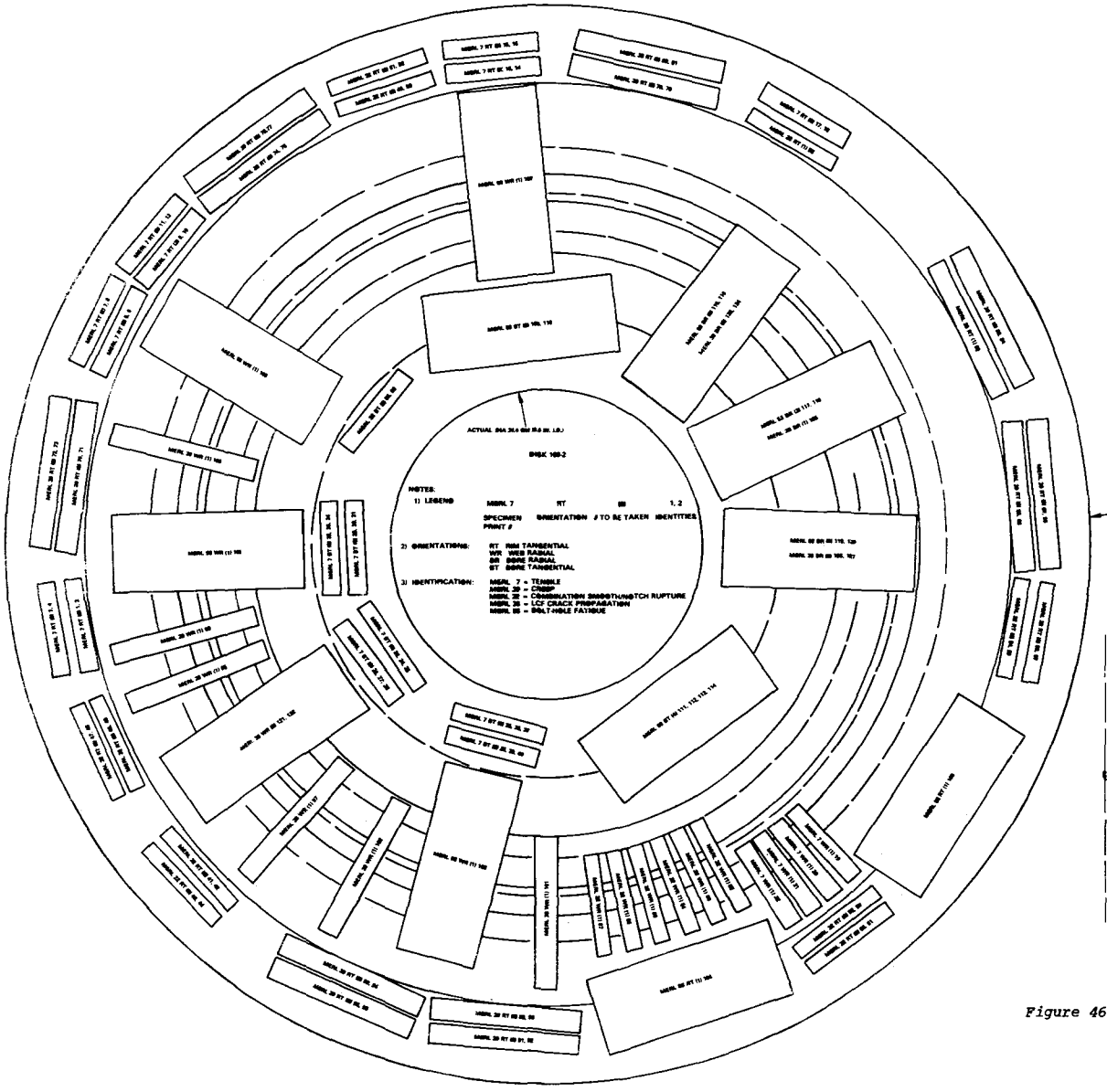

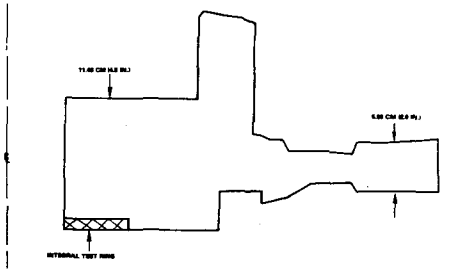

Figure 46 *Identification and Location of Test Specimen Machined From Disk 160-2*

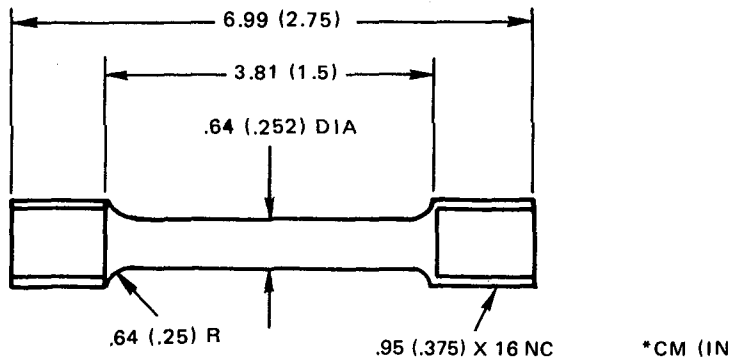

Figure 47 Tensile Test Specimen

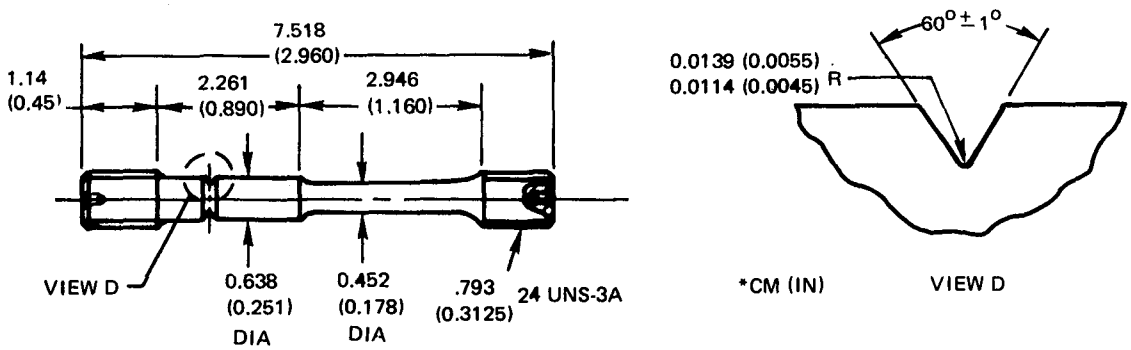

Figure 48 Combined Smooth Notch Bar (K_t = 3.9) Stress-Rupture Specimen

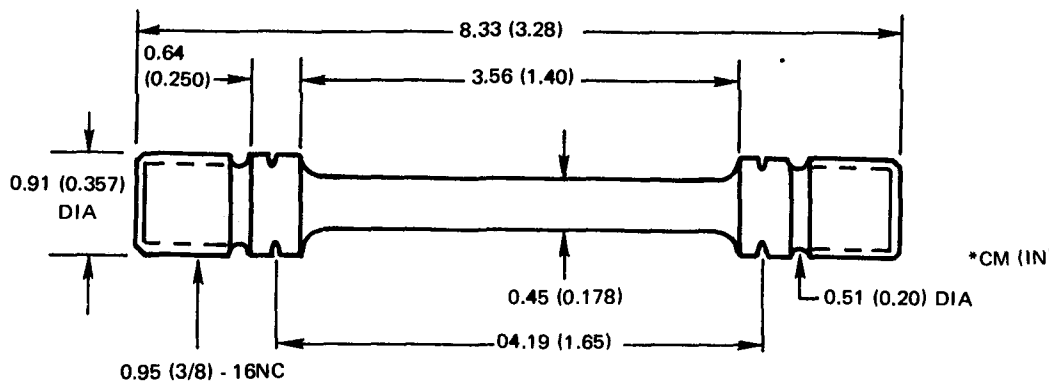

Figure 49 Creep Specimen

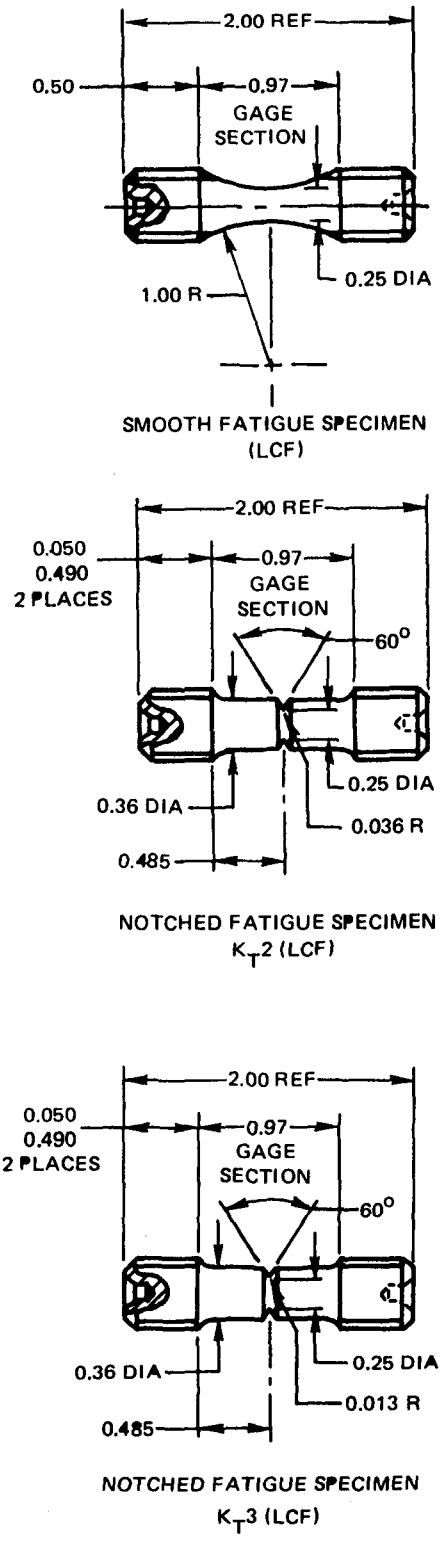

Figure 50 *Low Cycle Fatigue Sonntag Specimens*

Notched (K_T = 2.5) low-cycle fatigue bolt hole specimens (Figure 51) were subjected to testing conducted at 482°C (900°F), and at stress levels of 621 MPa (90 ksi), 568 MPa (85 ksi), and 552 MPa (80 ksi). A cycle of ten seconds at load and 10 seconds at no load was utilized. The cross-sectional area of each specimen was accurately measured to allow grouping of similar specimens for testing as a four specimen gang at the same stress. A single resistance furnace was used to heat all four specimens of the gang and the test temperature was monitored by attaching thermocouples to the gauge of each specimen.

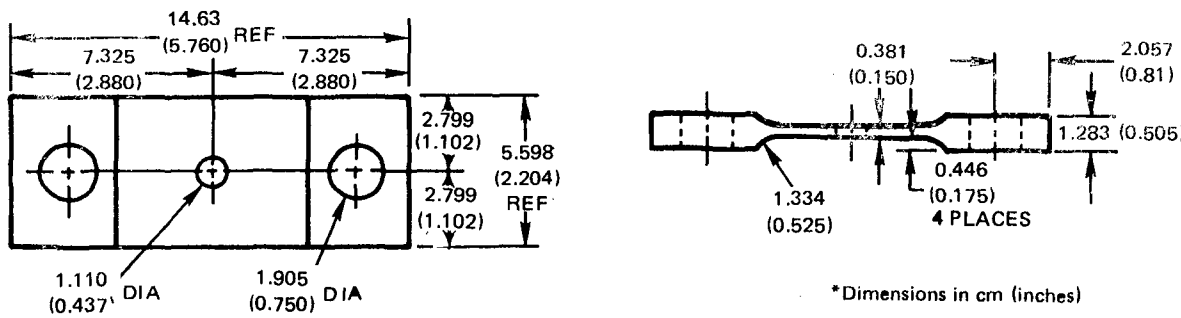

Figure 51 Bolt-Hole (K_t = 2.5) Low Cycle Fatigue Specimen

Fatigue crack threshold specimens (Figure 52) were tested with a Sonntag machine rated at a 2000 pound capacity and an 1800 cpm loading rate with a resistance furnace. Specimens were precracked at room temperature. The precrack length was controlled by using a strain gage bonded to both ends of the EDM slot in the center crack panel to shut off the rig after the crack initiates and grows beyond the slot. Each specimen was heated to the test temperature. The load (ΔK level) was increased as required to produce crack growth and then reduced until growth stopped for a minimum of 10^6 cycles. The upload/download procedure was repeated several times to gain confidence in the initially measured ΔK level. Crack length measurements were made using acetate replicas which were then measured using a microscope.

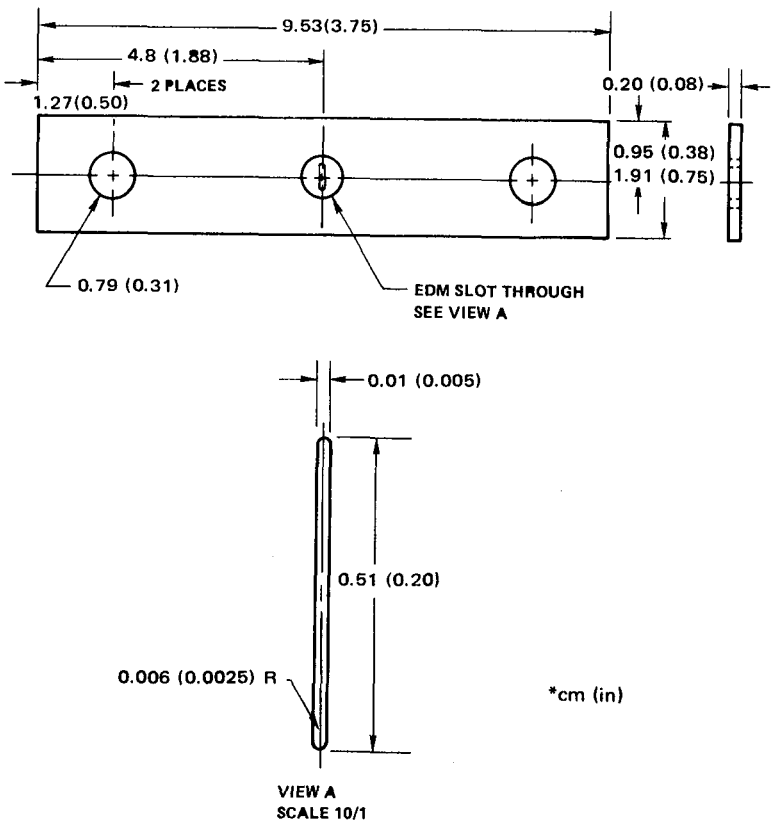

Figure 52 Fatigue Crack Threshold Specimen

Fatigue crack growth specimens (Figure 53) were tested at 427°C (800°F) and 538°C (1000°F) at a stress ratio R = 0.8 (minimum stress/maximum stress) at ten cycles per minute. A hydraulic driven push-pull rig was used for this test. The load-unload cycle was controlled by a timer and specimens were heated with a two-zone resistance furnace. The temperature of the specimen was controlled and monitored by the two thermocouples attached above and below the notch in the specimen. During the test, the crack length was monitored with a calibrated optical telescope system containing a micrometer slide.

The initial calculated ΔK value contained a sufficient stress to initiate and propagate a crack from the EDM slot.

$$\Delta K = \Delta\sigma \sqrt{\pi a}\, f(a/b)$$

$\Delta\sigma$ = alternating gross stress applied

a = half specimen width

$f(a/b)$ = finite width correction factor

The crack length was measured, using an optical telescope mounted on a micrometer slide.

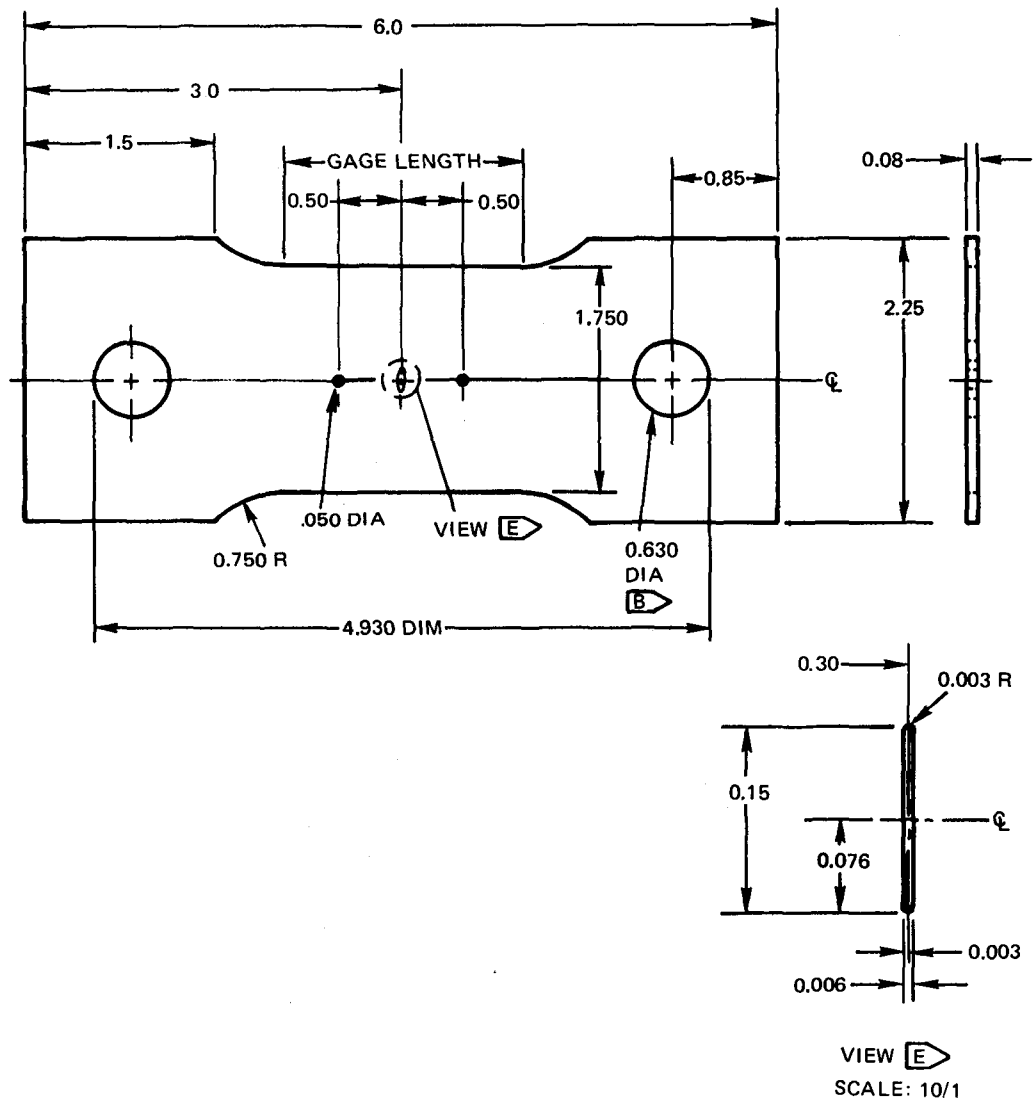

Figure 53 Fatigue Crack Growth Specimen

Integral Test Coupon Properties

To verify mechanical property response of the HIP components, an integral test coupon was provided within the design of the HIP container. For JT10D and JT9D disk components, the integral test coupon ring was located at the bore inner diameter - front face. Testing of the integral test coupon ring included tensile, stress-rupture, interstitial oxygen and nitrogen tests, and microstructural analysis as specified in the acceptance criteria.

Integral test ring properties were determined for the two JT10D (102-1, 102-2) and the JT9D (160-1) design data disks. For the two JT10D consolidations (102-1 and 102-2), room temperature and 649°C (1150°F) tensile properties exceeded target goals while at 704°C (1300°F), tensile ductility appeared to be very close to target (Table VIII). Corresponding stress-rupture testing indicated that levels were lower than target. Subsequent analysis revealed a powder contamination problem as discussed at the end of the fatigue property section. These specification tests on the integral rings were instrumental in determining the quality of HIP consolidation. For the next design data consolidation (160-2), tensile and rupture properties all exceeded target levels as shown in Table IX indicating that this consolidation was sound.

Test Results

Tensile Properties

The temperature dependence of tensile properties for MERL 76 was determined for the temperature range between room temperature and 760°C (1400°F) as shown in Figure 54. The shape of this curve was defined by testing material from a JT9D disk, S/N 160-2. Additional tensile properties were determined for two other disks (JT10D). A compilation of all the tensile data is given in Appendix H. The tensile strengths determined for the JT10D consolidation appears to be stronger than that for JT9D. However, the specimens removed from the JT10D disks were located nearer to the disk surface than those for the JT9D disk as shown in the test specimen layout given in Figures 45-46. Specimens positioned closer to the surface experienced a more rapid cooling rate and hence, greater strengths.

TABLE VIII

INTEGRAL TEST RING PROPERTIES
OF JT10D DISKS

Tensile Results

Consolidation Disk Number	Temperature °C (°F)	0.2% YS MPa (ksi)	UTS MPa (ksi)	El %	RA %
102-1	RT	1077 (156.3)	1401 (203.4)	22.5	27.5
102-1	621 (1150)	1058 (152.8)	1382 (200.6)	23.7	26.5
102-2	621 (1150)	1066 (154.7)	1394 (202.3)	21.9	25.4
102-1	704 (1300)	1056 (153.3)	1235 (179.2)	12.0	17.1
	704 (1300)	1069 (155.1)	1235 (179.2)	15.2	19.1
Target	RT	1034 (150.0)	1481 (215.0)	15.0	15.0
	621 (1150)	965 (140.0)	1337 (194.0)	12.0	12.0
	704 (1300)	965 (140.0)	1171 (170.0)	12.0	12.0

Note: 102-1 and 102-2 contain "golden" particles

Stress-Rupture Results

Consolidation Disk Number	Test Conditions	Life-Hrs.	% El
102-1	732°C/448 MPa (1350°F/65 ksi)	208.2	N
		35.2	N
102-2	732°C/655 MPa (1350°F/95 ksi)	20.3	5.1
		15.1	N
102-2	704°C/655 MPa (1300°F/95 ksi)	33.8	N
Target	732°C/655 MPa (1350°F/95 ksi)	23	5

TABLE IX

INTEGRAL TEST RING PROPERTIES OF JT9D DISK (160-2)

Tensile Results

Heat Code	Temperature °C (°F)	0.2% YS MPa (ksi)	UTS MPa (ksi)	EL %	RA %
160-2	RT	1056.3 (153.2)	1587.2 (230.2)	24.3	19.7
	RT	1057.0 (153.3)	1581.7 (229.4)	24.4	25.4
	621 (1150)	1022.5 (148.3)	1399.0 (202.9)	17.0	15.4
	621 (1150)	1034.9 (150.1)	1410.0 (204.5)	21.4	21.1
Target	RT	965 (140)	1481 (215)	15.0	15.0
	621 (1150)	965 (140)	1337 (194)	12.0	12.0

Combined (Smooth/Notch) Stress Rupture Properties

Heat Code	Temperature °C (°F)	Stress MPa (ksi)	Hours to Failure	Type of Failure	EL %	RA %
160-2	732 (1350)	655 (95)	42.0/39.9*	-N/S-	6.1*	13.4*
	732 (1350)	655 (95)	49.0/44.6*	-N/S-	7.1*	5.6*

*Ater notch failure, specimens were remachined and tested as smooth bar.

INTERSTITIAL GAS ANALYSIS

	Oxygen (ppm)	Nitrogen (ppm)
160-2	94	27

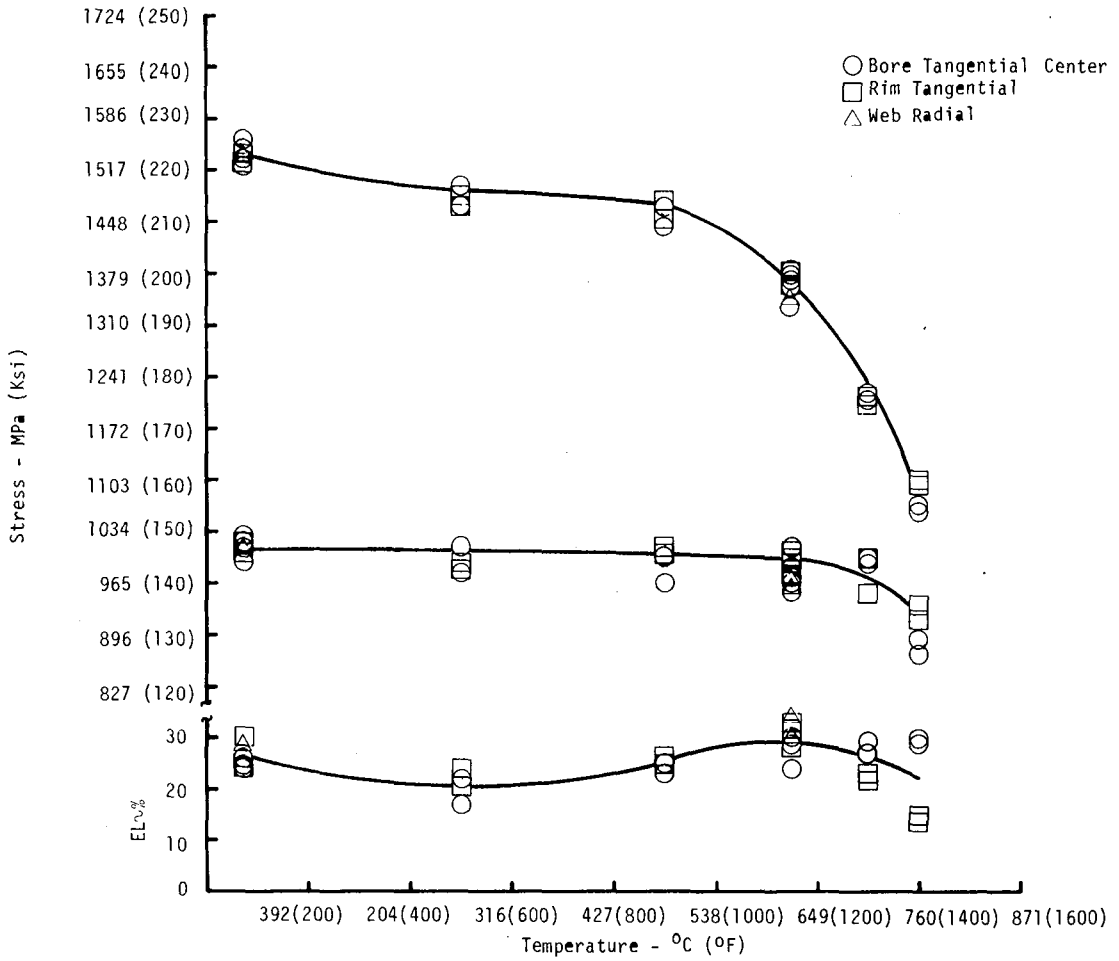

Figure 54 Temperature Dependence of Tensile Properties

The fracture surfaces from several of the tensile specimens were examined via scanning electron microscopy (SEM). While transgrannular failure mode was observed for specimens tested at RT and 482°C(900°F) (Figure 55), a mixed mode of transgranular/intergranular was observed at 621°C(1150°F) and then entirely intergranular mode at 704°C(1300°F) (Figure. 56).

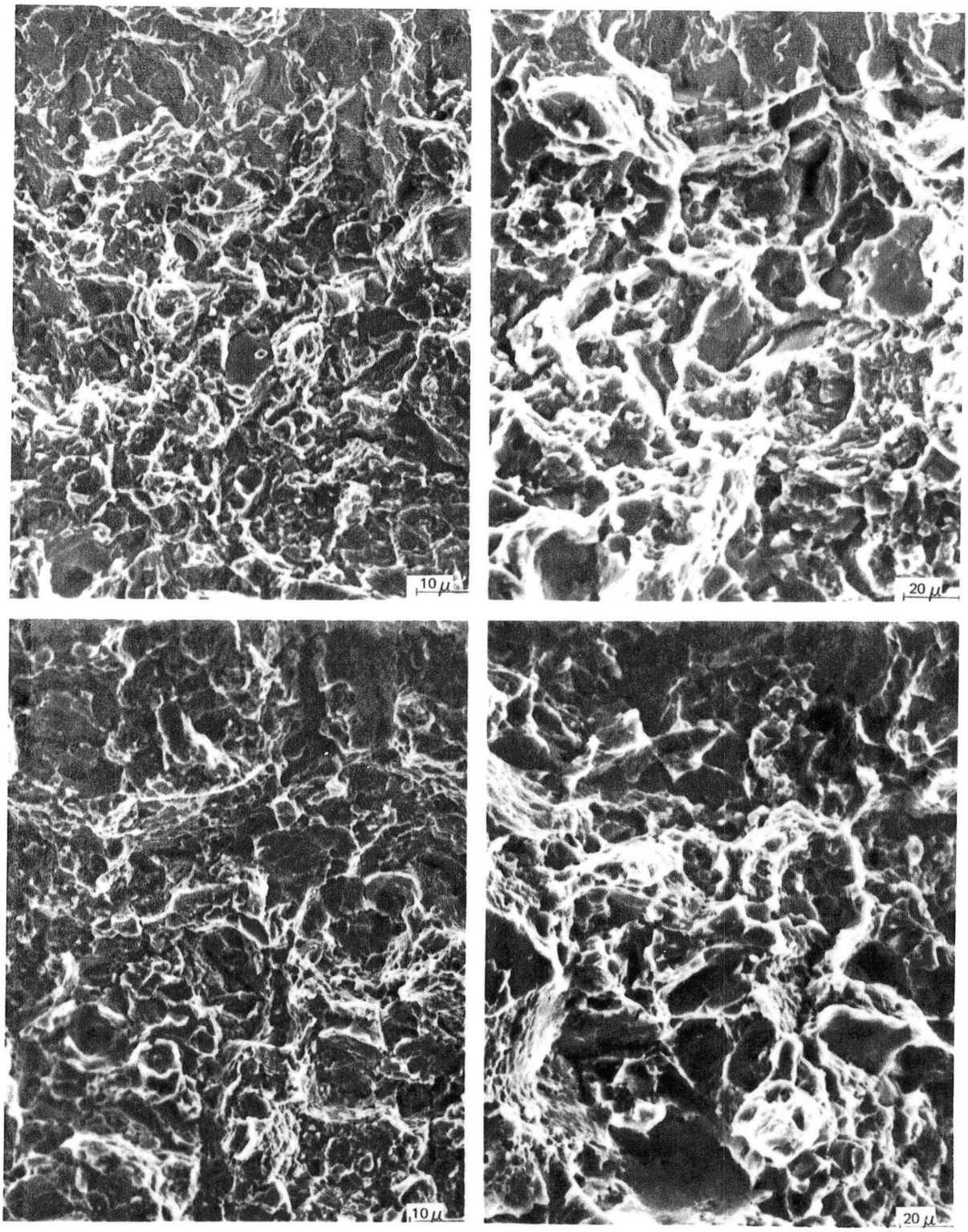

Figure 55 *Scanning Electron Micrographs Showing Predominately Transgranular Mode of Failure for MERL 76 Tensile Specimens Tested as Follows: Top: Room Temperature; Bottom: 482°C (900°F)*

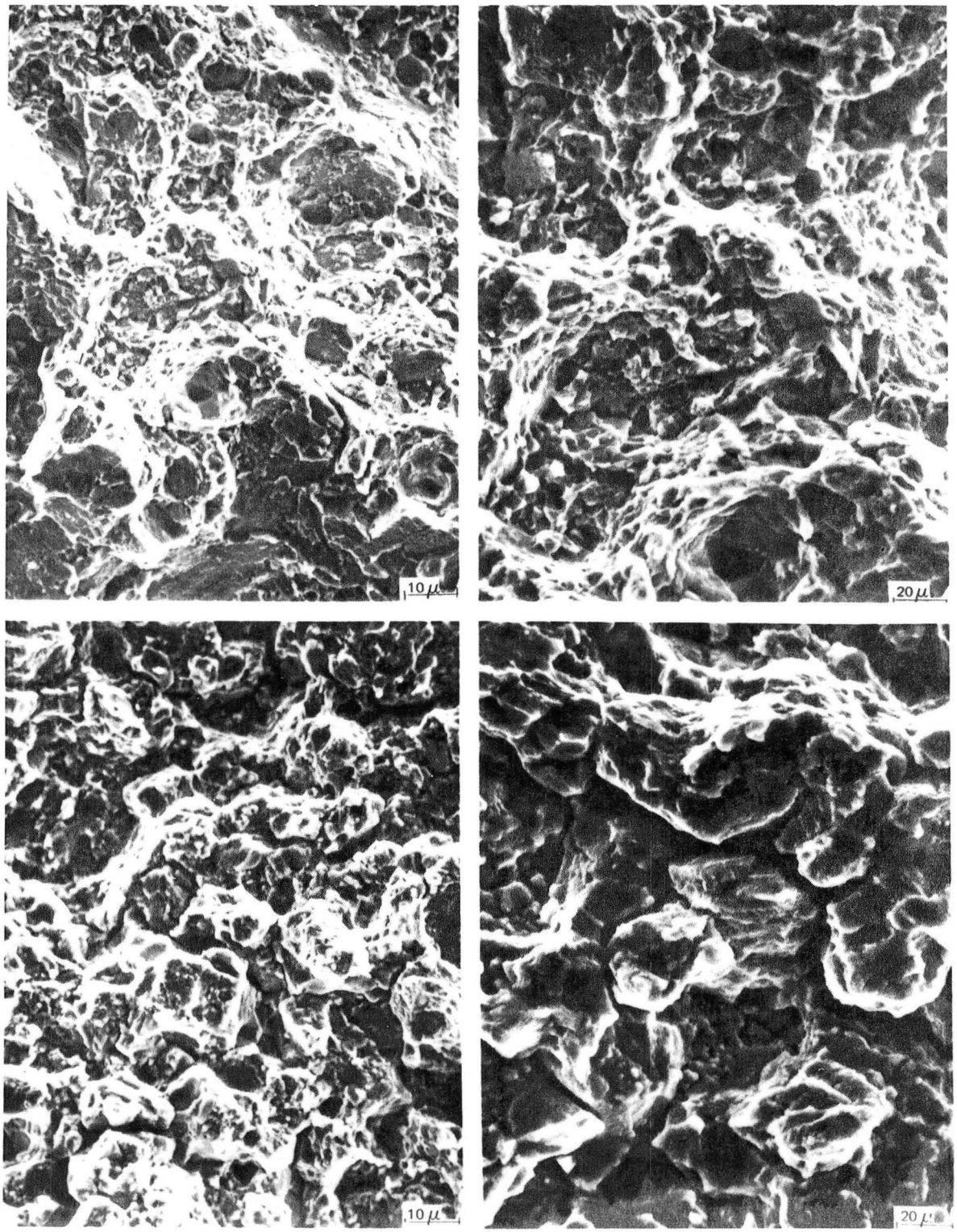

Figure 56 *Scanning Electron Micrographs Showing Predominant Failure Modes for MERL 76 Tensile Specimens Tested as Follows: Top: 621°C (1150°F) - Mixed Mode but Predominately Transgranular; Bottom: 704°C (1300°F) - Intergranular Mode*

Stress-Rupture

Approximately thirty-six specimens were stress-rupture tested in the temperature range of 649°C (1200°F) - 760°C (1400°F) to determine lower limit design data. A Larson-Miller plot of these data is shown in Figure 57. A detailed compilation of the test results are given in Appendix I.

Two test specimens exhibited abnormally low lives (1.5 and 1.7 hours) when compared to other specimens tested at these same conditions. Scanning electron microscopy of these fracture surfaces did not reveal any abnormal microstructural features. Prior data has shown that rupture strengths of high strength alloys such as MERL 76, can be sensitive to loading rate effect[3]. It is probable that these two specimens were loaded at a high loading rate and thus displayed low lives.

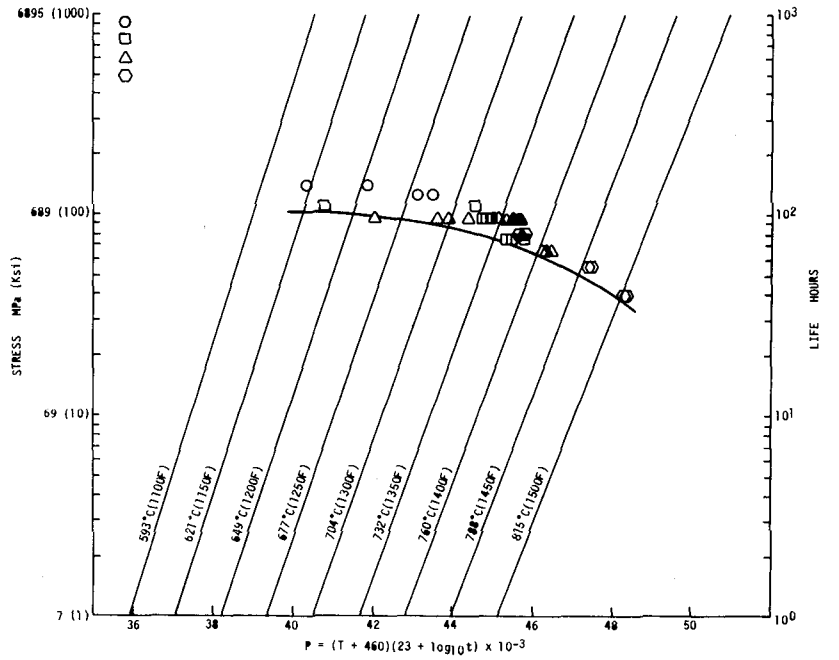

Figure 57 Stress-Rupture Design Data at 649°C (1200°F) -760°C (1400°F)

Fracture analysis of several of these ruptured specimens indicated an intergranular mode of failure. A typical fracture showing an intergranular mode of failure for a specimen tested at 704°C (1300°F)/758 MPa (110 ksi)/213 hrs is shown in Figure 58.

(3) Law, C. C.; "Plastic Flow in Fracture Processes in Powder Metallurgy Nickel Base Superalloy" Contract F49620-77-C-0083, June 1980 - Final Report.

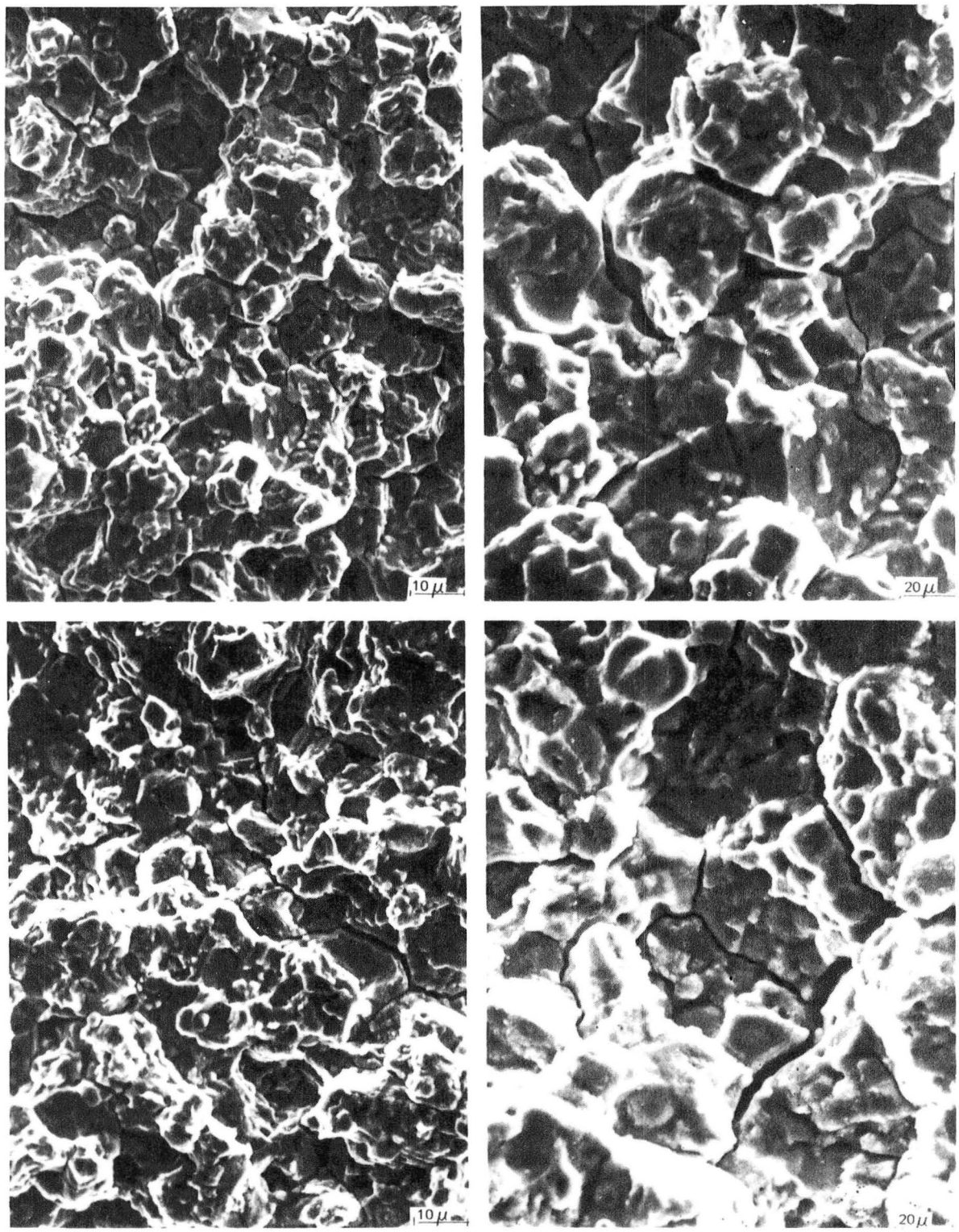

Figure 58 *Scanning Electron Micrographs of a Stress-Rupture Specimen Tested At 704°C (1300°F)/758 MPa (110 Ksi) for 213 Hours Showing An Integranular Mode of Failure*

Creep

Thirty-two specimens were tested in the temperature range of 593°C (1100°F) through 760°C (1400°F) to establish lower limit allowable curves. A Larson-Miller plot of time to 0.2% creep is given in Figure 59. The data for all specimens tested are given in Appendix J.

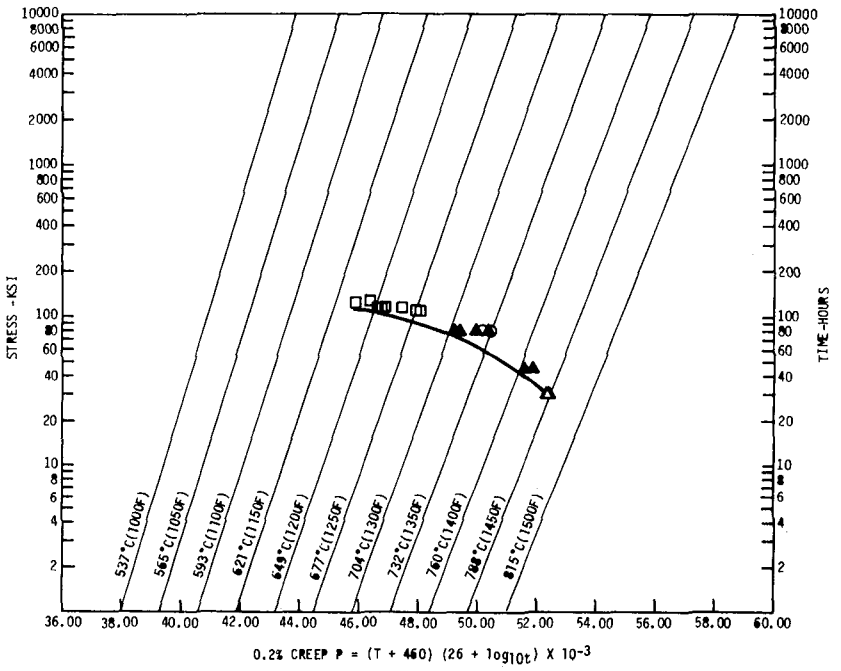

Figure 59 Creep Data

Low Cycle Fatigue Tests

o Sonntag Low Cycle Fatigue

Sonntag LCF testing was conducted in the temperature range of 427°C (800°F) - 635°C (1175°F) for both smooth and notched (K_t=2, 3) specimens. The effect of lowered life with increasing notch factor is shown in Figures 60-62. A comparison of these three figures will also reveal that given the same notch factor, the fatigue strength decreases with increasing temperature. A detailed compilation of results of these tests is given in Appendix K. The scatter observed in these test results is typical for Sonntag-type tests. A typical fracture surface showing three origins are shown in Figure 63. The fracture initiation site appears to be featureless with initiation occurring at a relatively slight machine mark.

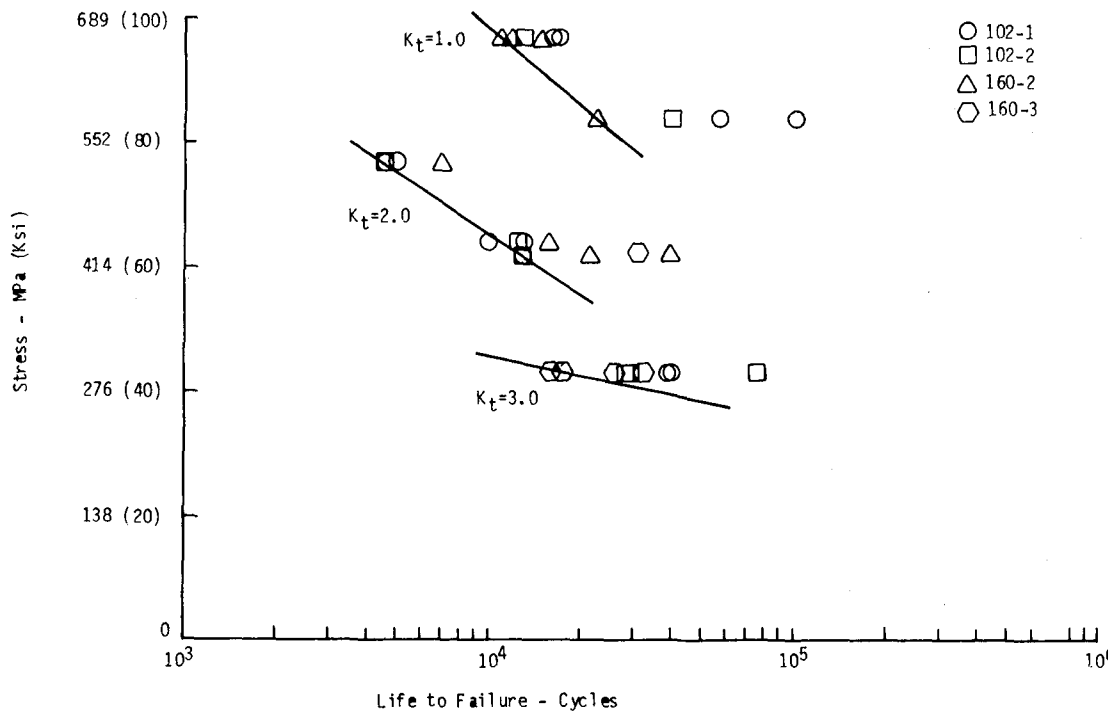

Figure 60 *427°C (800°F) Sonntag Low Cycle Fatigue Data*

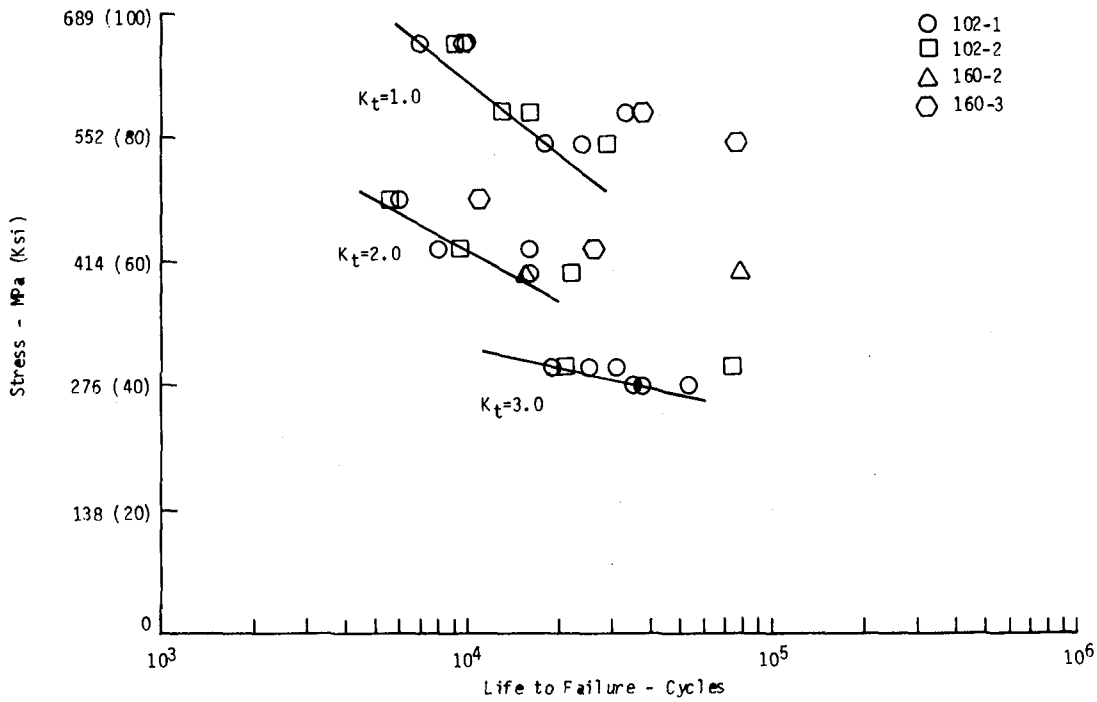

Figure 61 *538°C (1000°F) Sonntag Low Cycle Fatigue Data*

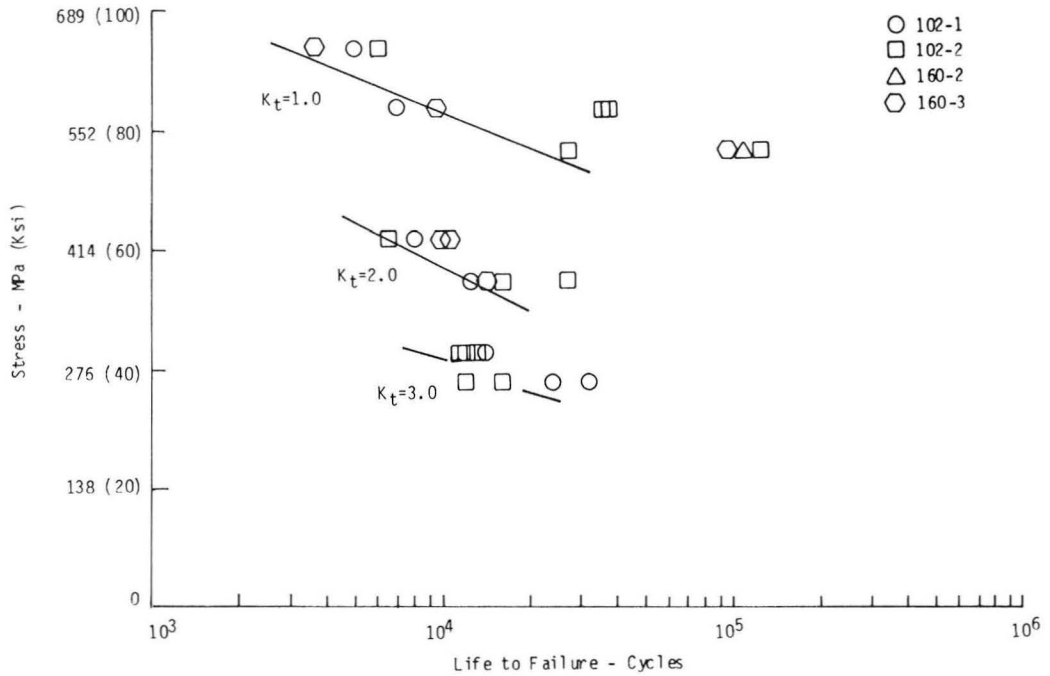

Figure 62 *635°C (1175°F) Sonntag Low Cycle Fatigue Data*

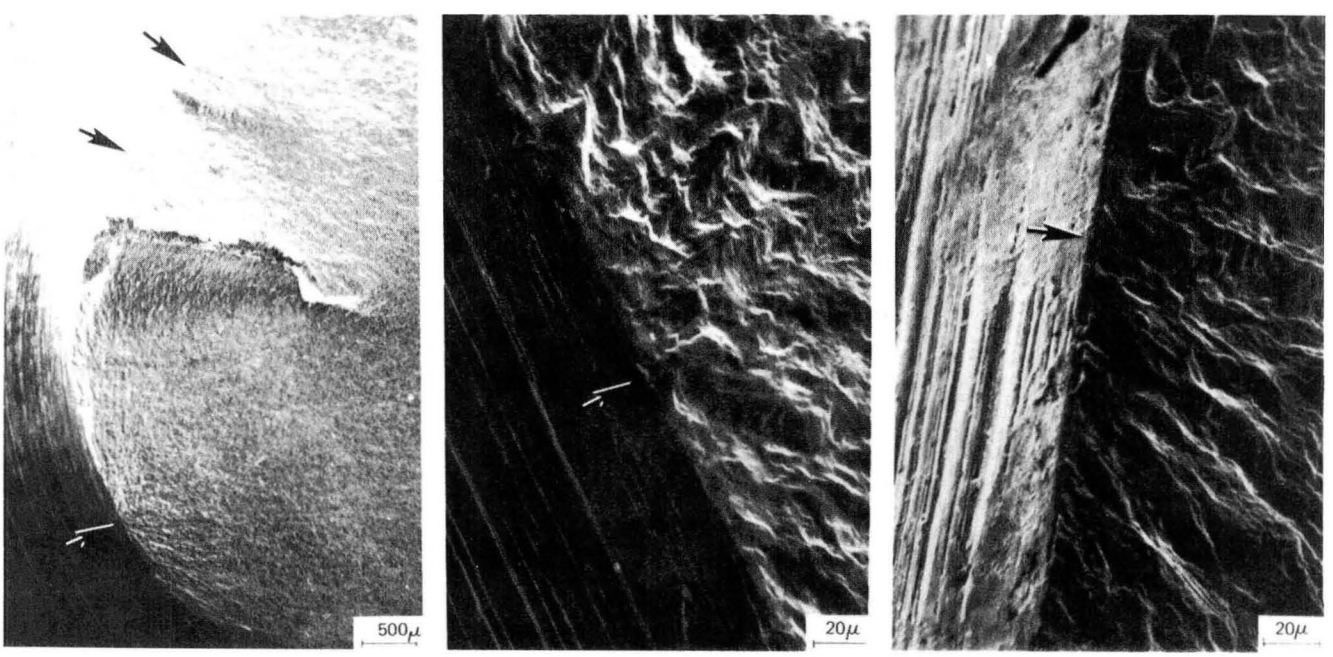

Figure 63 *Typical Fracture Origins for LCF Sonntag Specimens Showing Multiple Origins and Featureless Initiation*

o Bolt Hole Low-Cycle Fatigue

Notched (K_t=2.5) LCF testing was conducted in the temperature range of 427°C (800°F) - 649°C (1200°F) at a 55C°(100F°)interval using a bolt hole specimen. Fatigue life as dependent upon stress level for each temperature is given in Figures 64-68. A decrease in notch life with increasing temperature was not observed until 649°C (1200°F) as shown in Figure 69. A detailed presentation of the data and fracture analysis for several of the specimens is given in Appendix L.

The location of the crack initiation site was carefully identified so that scanning electron microscopy could be performed on the fracture surface. Mating surfaces were examined to obtain a complete characterization of the crack initiation site.

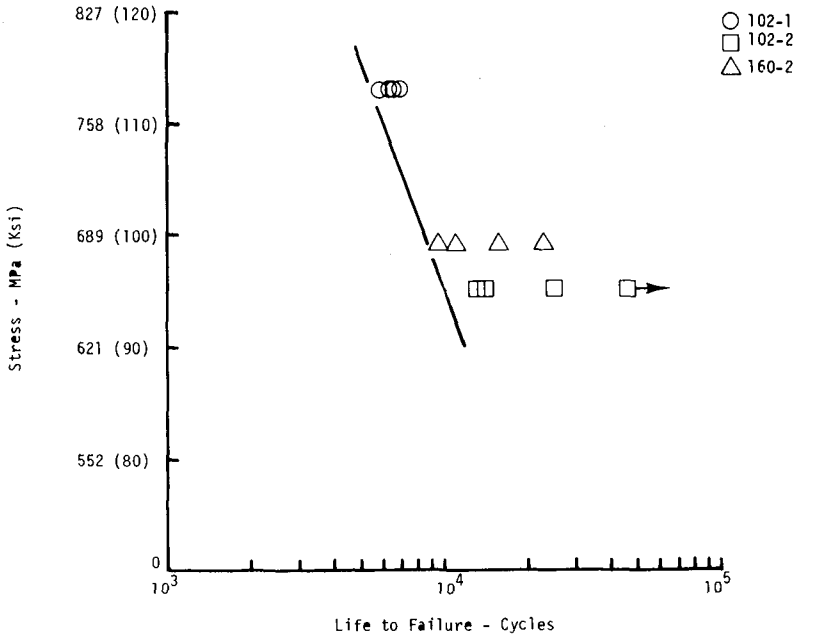

Figure 64 427°C (800°F) Notched (K = 2.5) Bolthole LCF Data

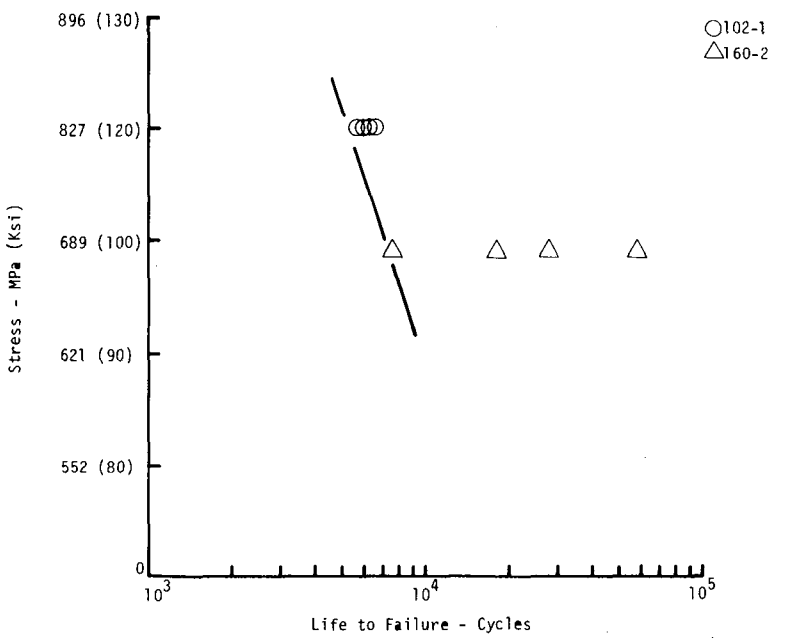

Figure 65 *482°C (900°F) Notched (K_t = 2.5) Bolthole LCF Data*

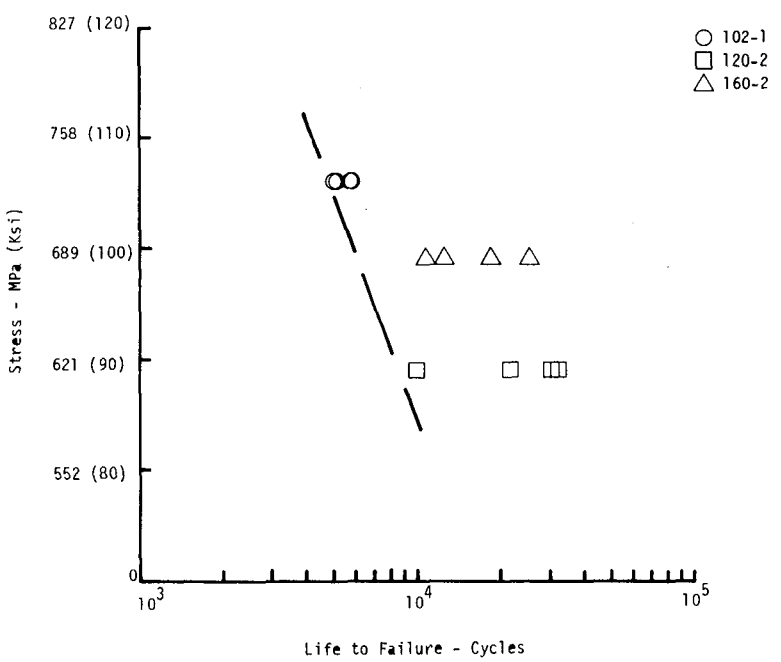

Figure 66 *538°C (1000°F) Notched (K_t = 2.5) Bolthole LCF Data*

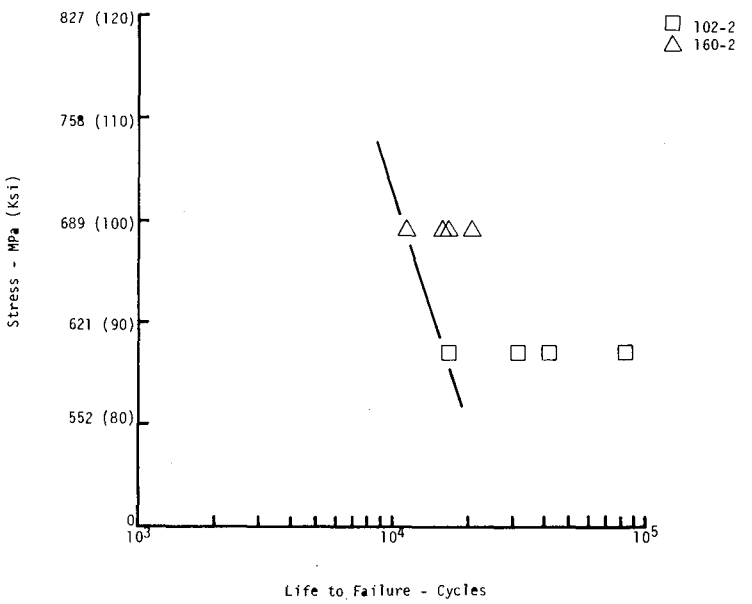

Figure 67 *593°C (1100°F) Notched (K_t = 2.5) Bolthole LCF Data*

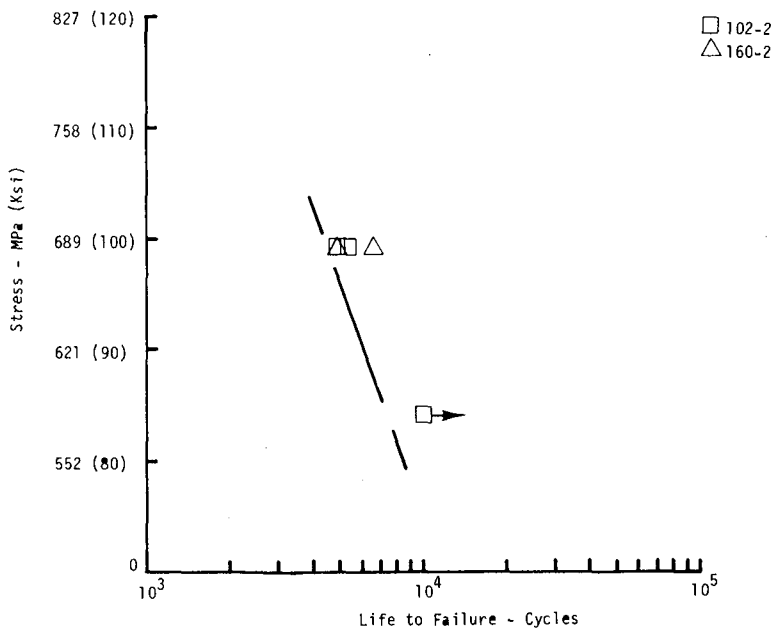

Figure 68 *649°C (1200°F) Notched (K_t = 2.5) Bolthole LCF Data*

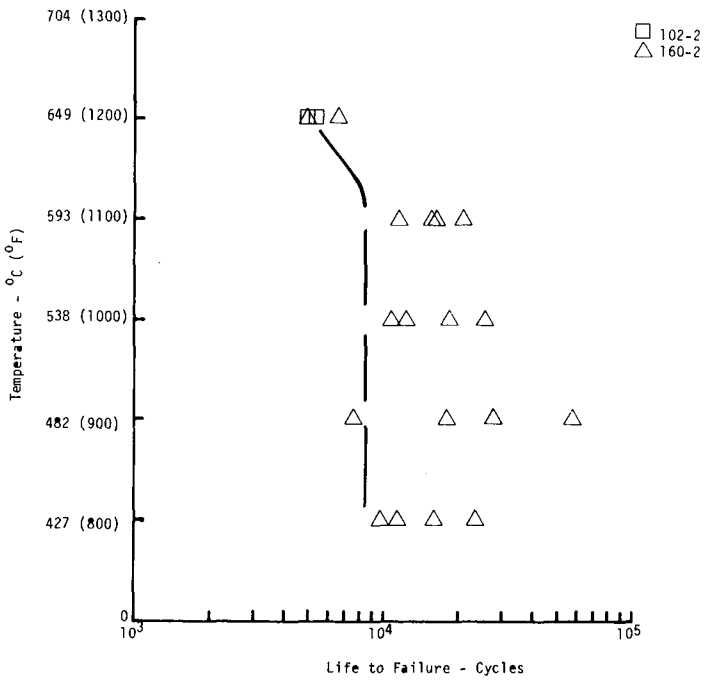

Figure 69 683 MPa (99 K_{si})Notched (K_t = 2.5) Bolthole LCF Data

For the specimens that were examined, porosity (~1 mil) was the primary origin of failure. A typical initiation site containing a pore is shown in Figure 70. In the same specimen, a secondary initiation site was observed. This secondary initiation site contained a 0.7 mil hafnium-rich inclusion presumably a hafnium oxide. One sample contained an aluminum-hafnium rich inclusion at the bolt hole surface as shown in Figure 71.

Threshold Stress Intensity

For the design system for disk components, it is essential to determine the stress intensity level below which crack growth does not occur. Accordingly, the threshold stress intensity level was established for the temperature range of 427°C (800°F) - 649°C (1200°F) and an R-ratio (σmin/σmax) of 0.1 to 0.8. The results indicate that an increase in R-ratio (0.1 to 0.8) lowered the fatigue crack threshold while, for the same R-ratio, an increase in temperature from 427°C (800°F) - 649°C (1200°F) appears to have not significantly altered the threshold intensity level (Table X).

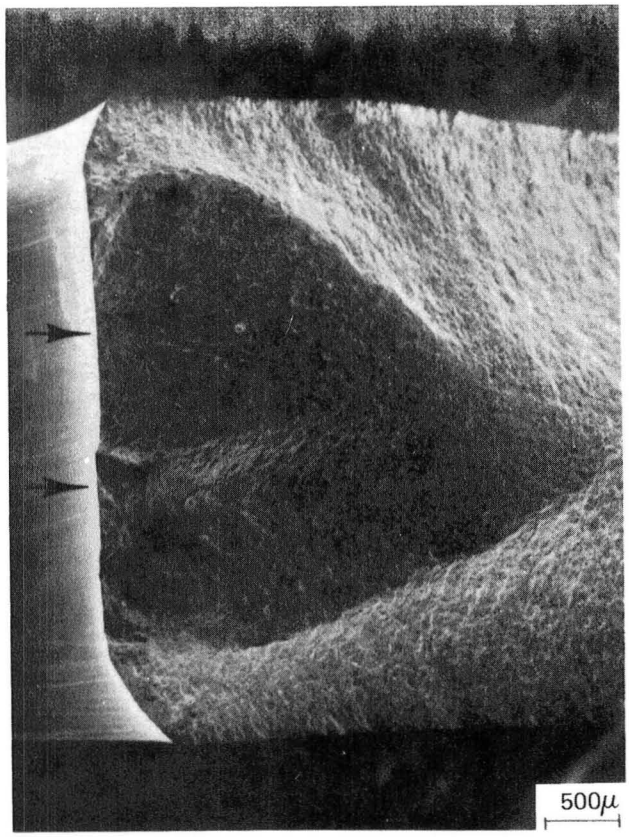

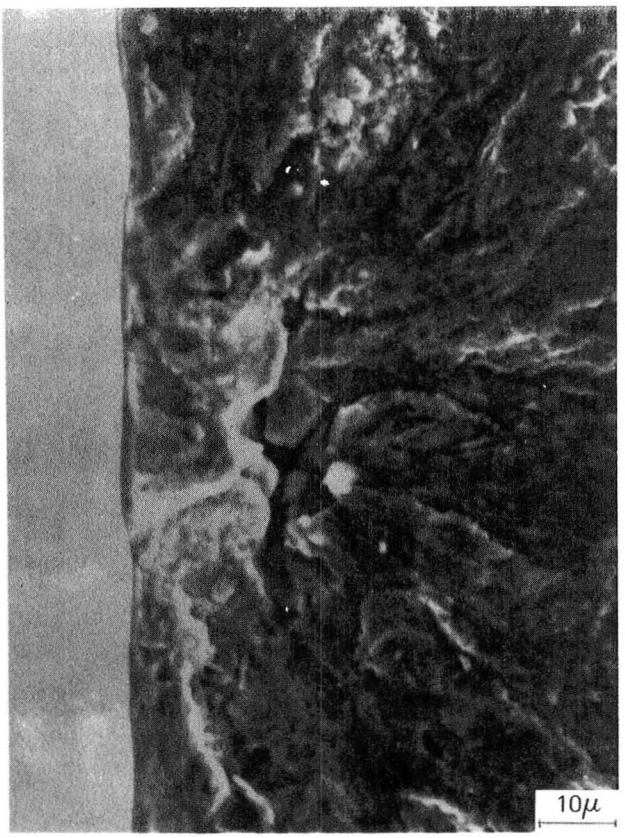

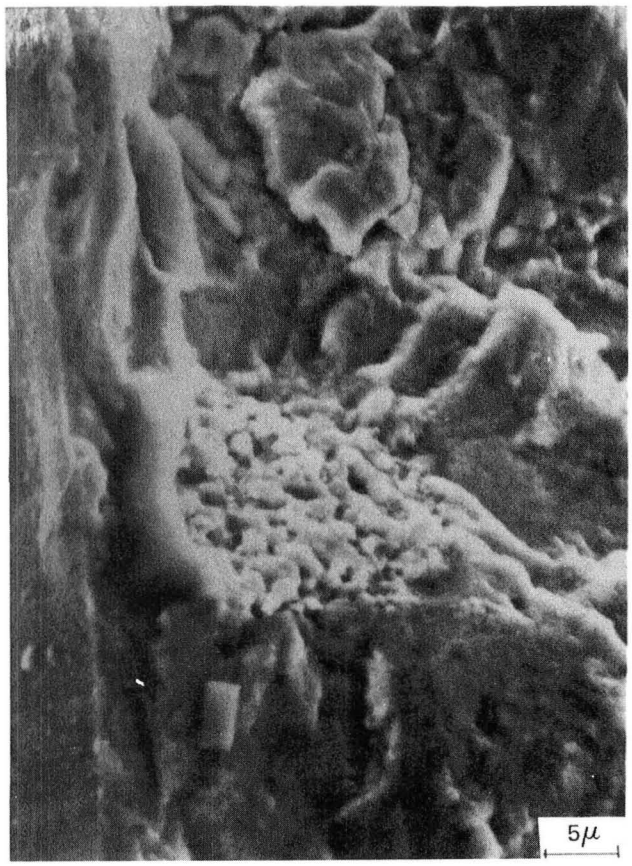

Figure 70 Typical Crack Initiation Site of a Bolt-Hole Specimen. While the primary origin contained a pore, a secondary origin displayed an aluminum-hafnium rich inclusion.

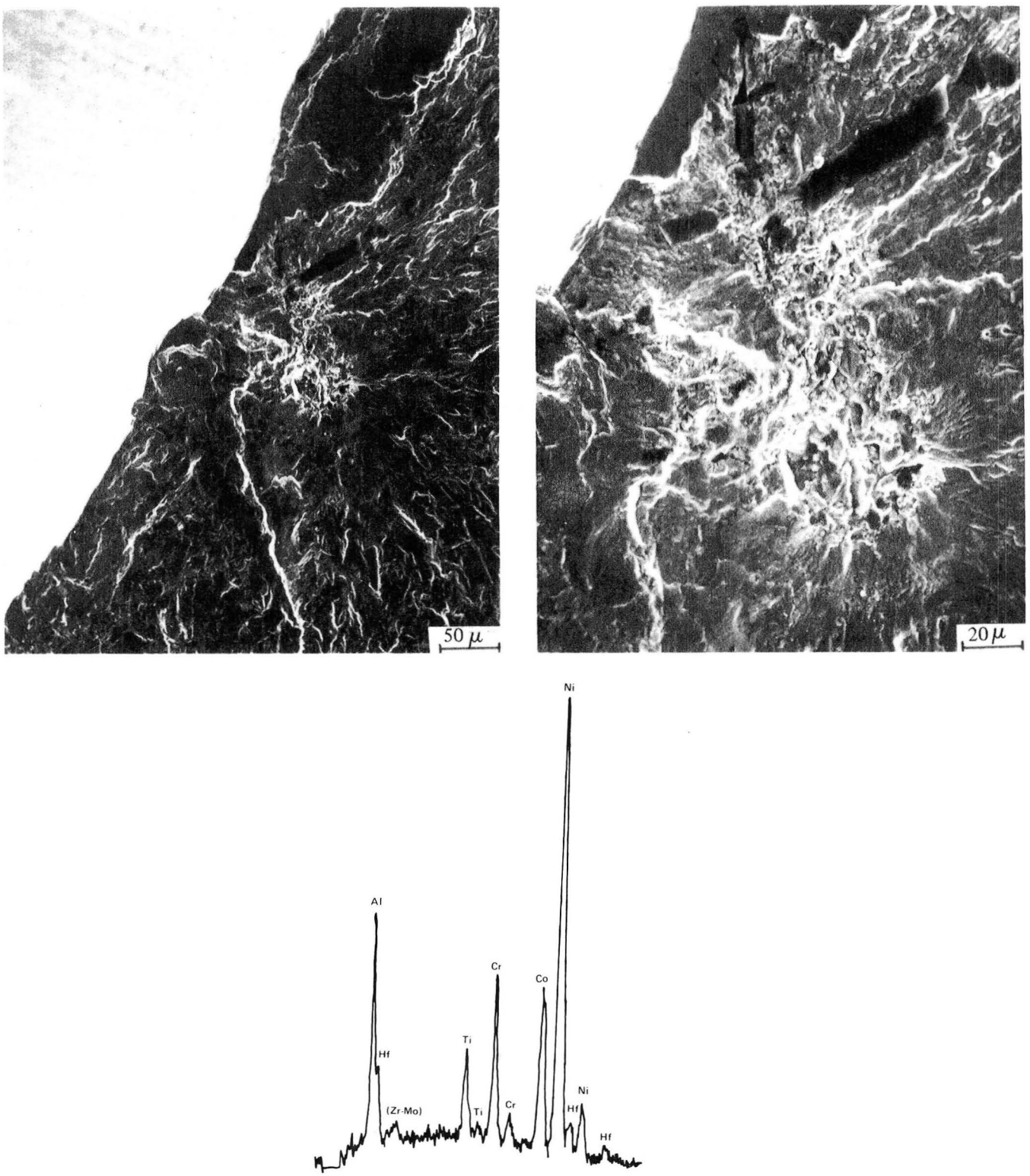

Figure 71 *Scanning Electron Micrographs of a .005 cm (0.002 in) x .015 cm (0.006 in) Inclusion Identified as Aluminum-Rich at the Fracture Origin of S/N 102-2-13 Tested at 593°C (1100°F)/ 0-599 MPa (87 Ksi) for 16,800 Cycles*

TABLE X

FATIGUE CRACK GROWTH THRESHOLD DATA FOR MERL 76

Heat Code	Temperature °C	Temperature (°F)	$R = \frac{min}{max}$	K MN $m^{-3/2}$	K (ksi $in^{1/2}$)
160-3	427	(800)	0.1	6.4	(5.8)
	427	(800)	0.1	6.6	(6.0)
	427	(800)	0.8	3.8	(3.5)
	538	(1000)	0.1	7.7	(7.0)
	538	(1000)	0.1	7.1	(6.5)
	649	(1200)	0.1	7.7	(7.0)
	649	(1200)	0.1	7.7	(7.0)

Fatigue Crack Growth

Crack growth rate of initiated cracks is an important consideration in the design of disk components. Consequently low-cycle fatigue crack propagation tests were conducted in the temperature range of 427°C (800°F) - 538°C (1000°F) and R-ratios (σmin/σmax) of 0.1 - 0.8. At 427°C (800°F) and 538°C (1000°F), the crack propagation rate became faster as the R-ratio was increased from 0.1 to 0.8 as shown in Figures 72 and 73. For an R-ratio of 0.1, an increase in temperature from 420°C (800°F) to 538°C (1000°F) increased the crack propagation rate while for R = 0.8, the crack propagation rate did not appear to be significantly altered (Figures 74 and 75).

Prior Particle Boundary Failures

During the course of measuring the mechanical properties of disks 102-1 and 102-2, in the design data phase of Task I, it was determined that these HIP consolidations exhibited marginal rupture life and ductility as shown in Table XI. Scanning electron microscopy of these fracture surfaces revealed considerable prior particle boundary separation (Figure 76) which probably contributed to the low notch rupture life and rupture ductility.

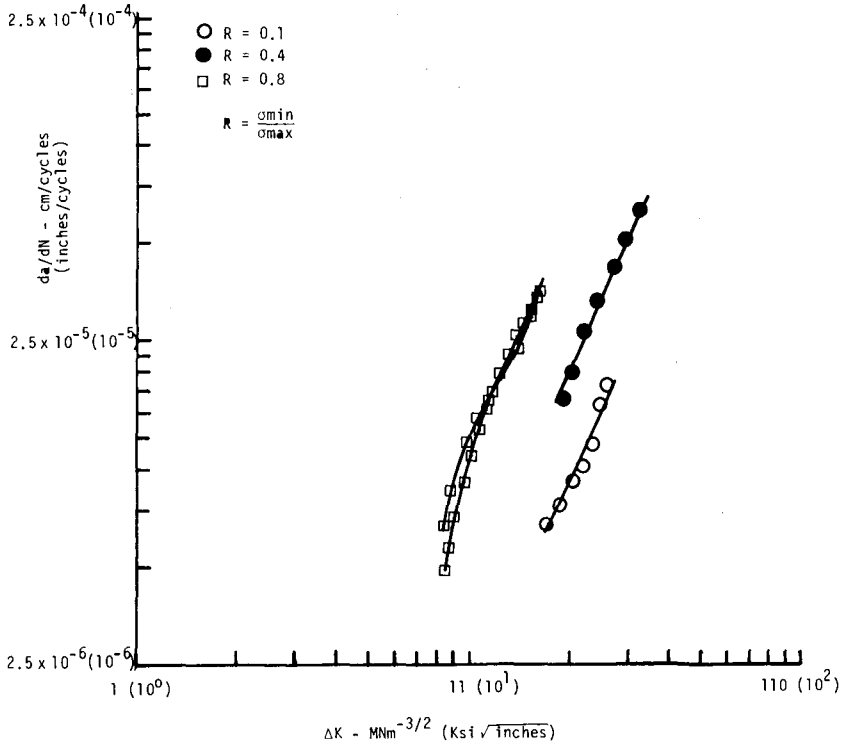

Figure 72 427°C (800°F) Crack Growth Rate

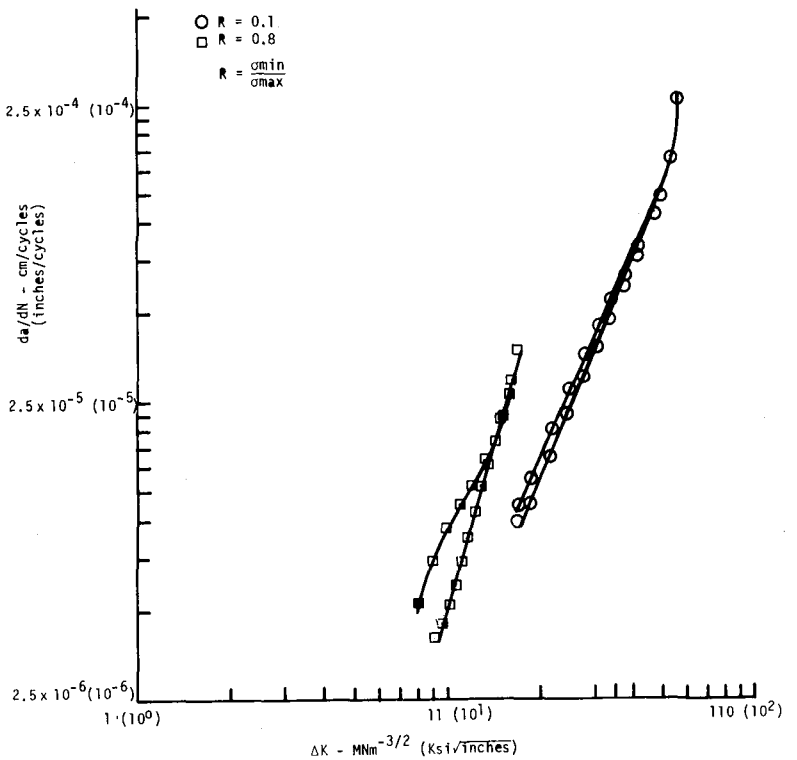

Figure 73 538°C (1000°F) Crack Growth Rate

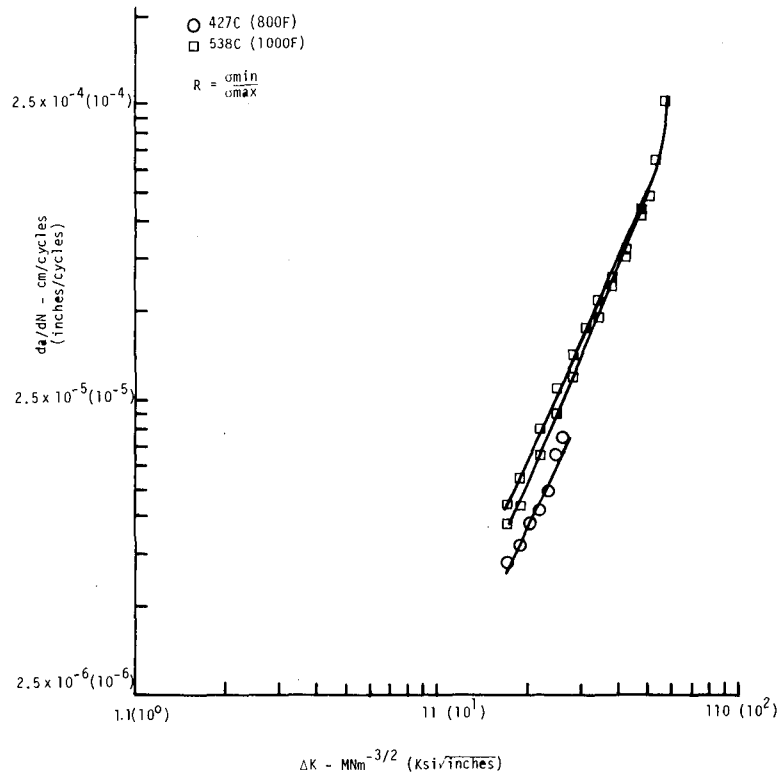

Figure 74 *R = 0.1 Crack Growth Rate*

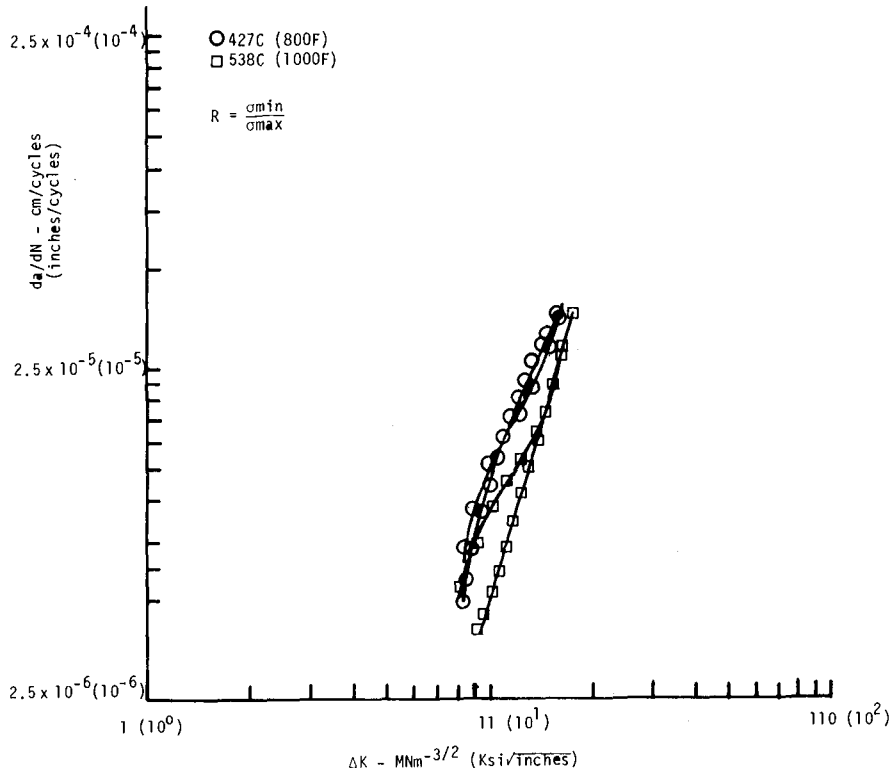

Figure 75 *R = 0.8 Crack Growth Rate*

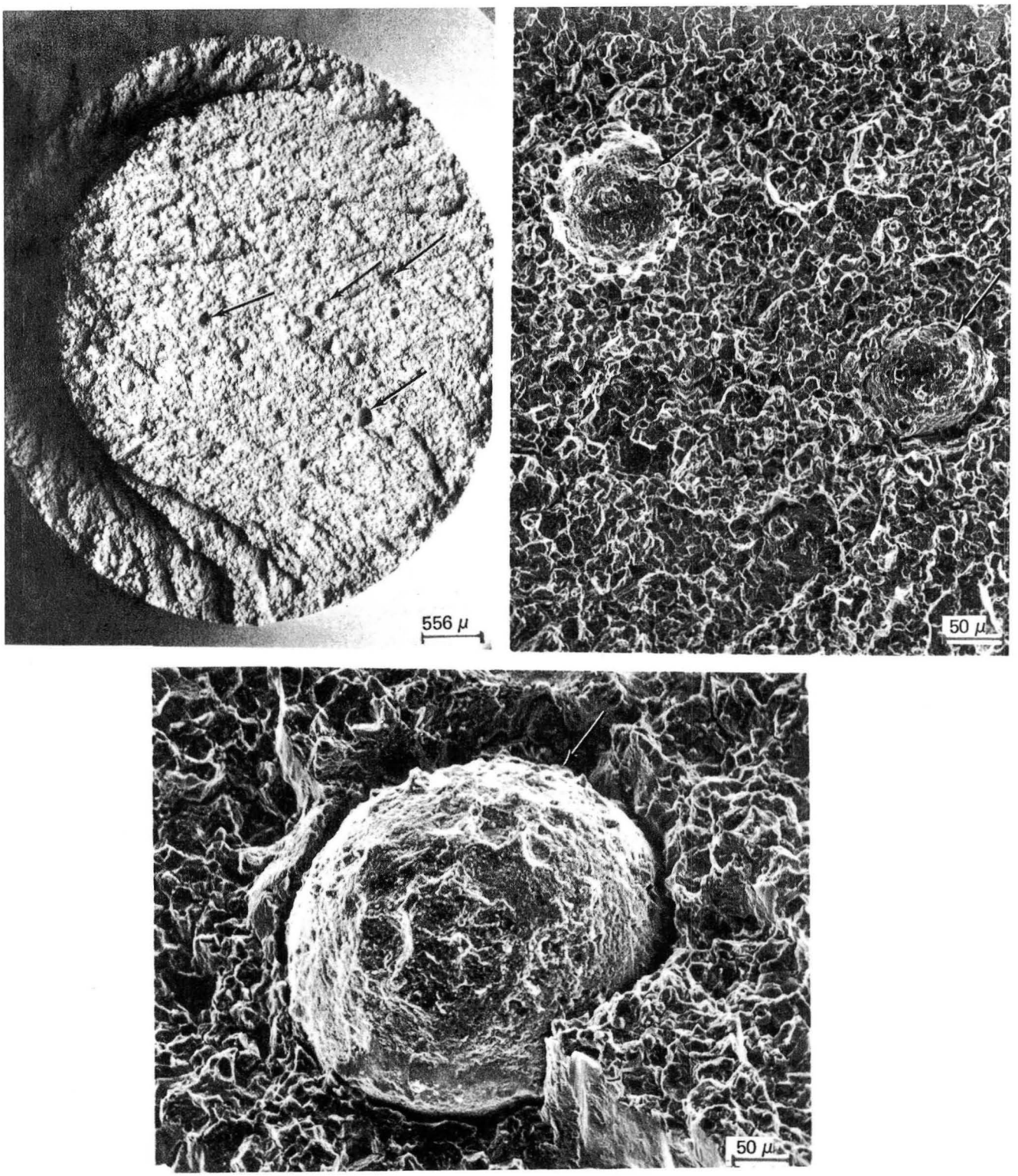

Figure 76 *Scanning Electron Micrographs of Fracture Surface of Stress-Rupture Specimen Tested At 732°C (1350°F)/655 MPa (95 KSI) for 16.7 Hours Showing Fracture Prevalent Along Prior Particle Boundaries (Arrows).*

TABLE XI

STRESS RUPTURE RESULTS
732°(1350°F/655 MPa(95.0 Ksi)

Powder Blend	Disk	Location	Life, Hrs.	El %
BN79003	102-1	Rim, Tangential	11.8	N
	Retest (1)		30.0	3.6
			19.1	N
		Test Ring	16.7	N
			9.8	N
	Retest (1)		27.8	2.9
		Rim, Radial	24.5	Notch Test
			10.5	Notch Test
	102-2	Test Ring	20.3	5.14
			15.0	N
		Rim Tangential	18.2	N
			11.2	N
		Rim Radial	19.6	Notch Test
			13.2	Notch Test
BN79003	Pipe #U-1	UDIMET-Filled	14.0	Notch Test
BN79007	Pipe #435	MERL-Filled	23.8	Notch Test
Target at 732°C (1350°F) 638 MPa (92.5 Ksi)			23.0	5%

(1) Combination bar remachined after notch failure after smooth stress-rupture testing. Life reported is of smooth bar only.

N = Notch failure in combo bar.

To further analyze this phenomena, a piece of untested material was removed from disk 102-1 consolidation and fractured at room temperature to eliminate the complication of an oxidized fracture surface of a specimen which had been tested at elevated temperature. X-ray energy spectroscopy detected hafnium-rich particles, probably hafnia, that decorated the prior particle boundaries as shown in Figure 77. These observations suggested that the prior particle boundary separation may have been related to the handling of powder during container filling, since the composition of the powder had met target goals. Individual heats as well as blends of the powder were examined using low power, binocular microscope which revealed that some of the particles displayed a golden color. Figure 78 is a photograph showing some of the golden particles. These golden particles apparently contain a very thin oxide which is not detectable by electron microprobe analysis.

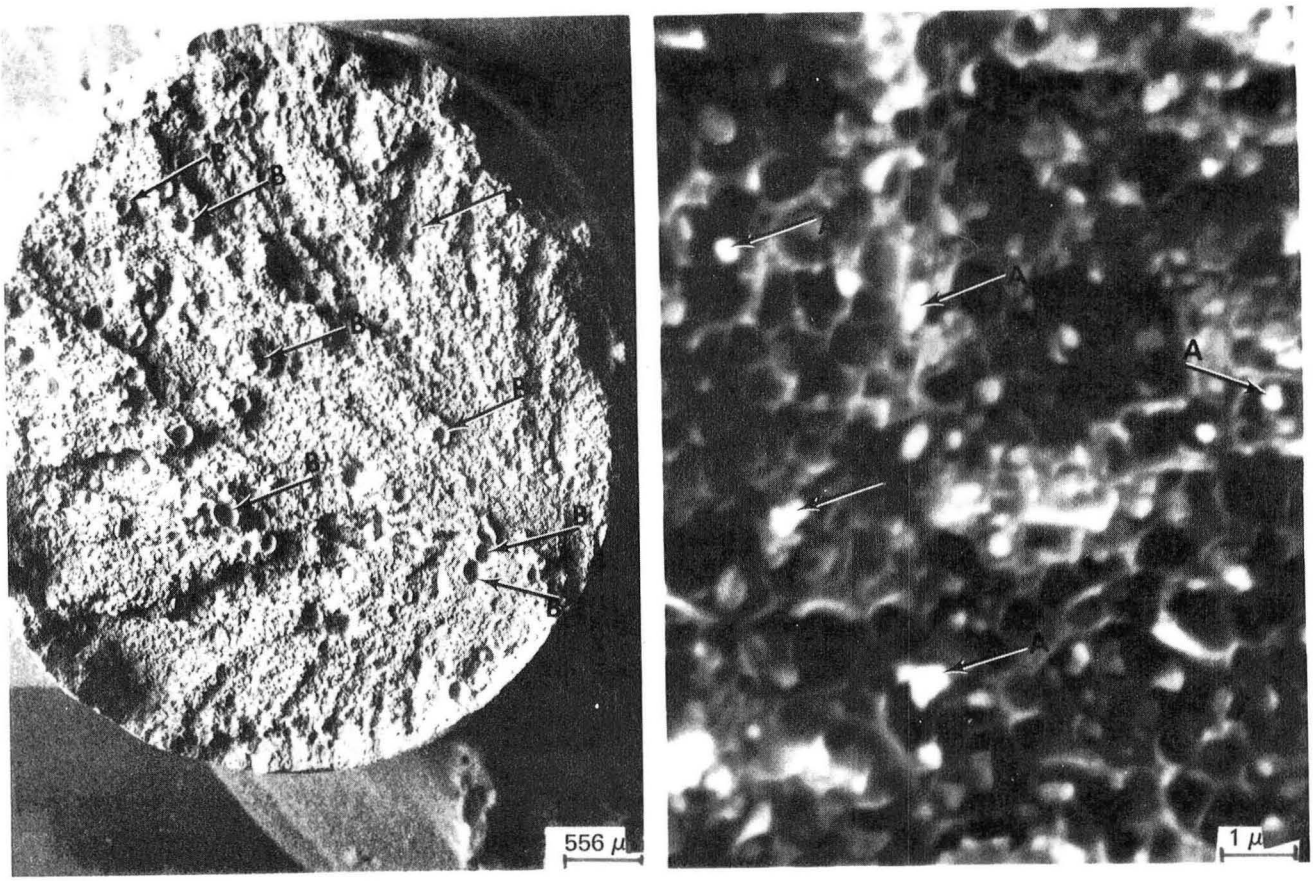

Figure 77 *X-Ray Energy Spectroscopy Determined That Discrete Particles (A) (Right) Which Are Hafnium Rich, Probably Hafnium Oxide, Decorate the Prior Particle boundaries (B) (Left) of material Fractured At Room Temperature.*

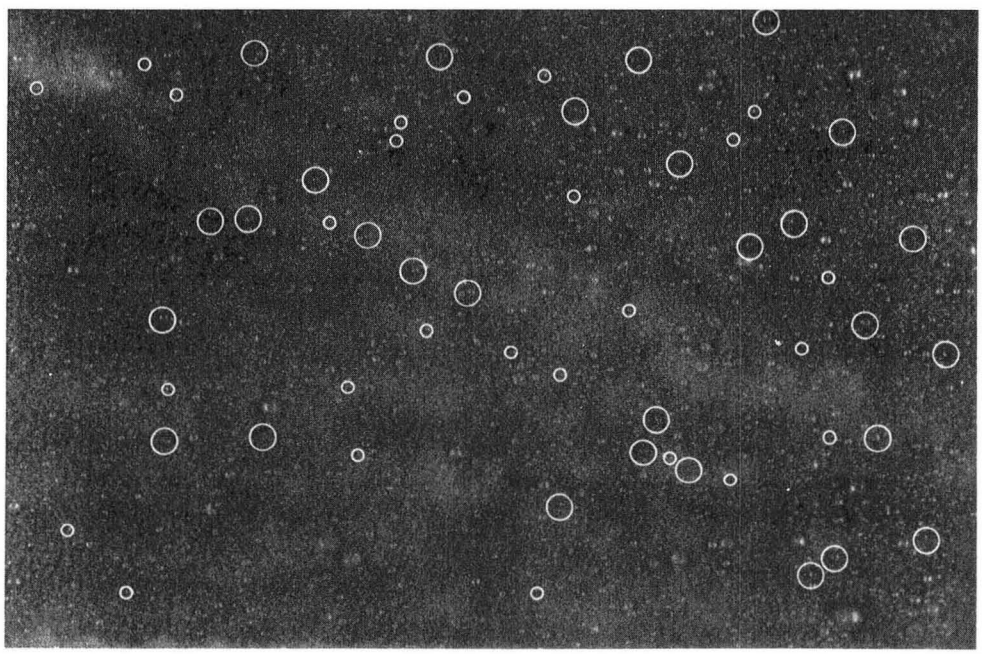

Figure 78 *Optical Micrograph of As-Received -80 Mesh Powder Containing "Golden" Particles (Circled).*

In an attempt to determine the point of introduction of the contaminated particles, the processing records for VIM ingot casting and powder atomization were examined next. A review of the processing records indicated that all target processing specifications were met. Vacuum leak-up rates and vacuum levels achieved during VIM ingot casting and atomization were within process specification. In addition, the vacuum levels and leak-up rates achieved during container filling (Appendix C), were also within specification and therefore should not have introduced any further significant contamination.

On the basis of this exhaustive analysis, prior particle boundary separation can be attributed to the presence of "golden" particles, presumably covered by hafnium oxide, in the as-received powder. The point of introduction of the golden particles has not been unequivocably established. It is assumed that oxygen was inadvertently introduced during the atomization cycle, either in the atomization chamber or collection chamber while the powder was hot, resulting in oxidation of some of the powder particles. Apparently, such a leak was so slight that it was undetectable by instrumentation.

Since the "golden" paricles were readily observable via binocular examination at 30X, this inspection prior to blending was included in powder sampling procedure prior to blending of the Process Control Plan (Appendix N).

Physical Properties

An integral part of the evaluation of alloys for disk application is the determination of physical properties to establish the design capabilities of the alloy. These properties included modulus of elasticity, thermal expansion, thermal conductivity and specific heat properties which are shown in Figures 79 through 82.

Other tests were conducted to fully characterize the physical properties of MERL 76. The density was determined to be 7.95 g/cc (0.287 lbs/in) and hardness ranged from R_C 39-43 as measured by the Reichert microhardness tester. The gamma prime solvus and incipient melt temperature were also determined to be 1190°C (2175°F) and 1196°C (2185°F), respectively as shown in Figure 83.

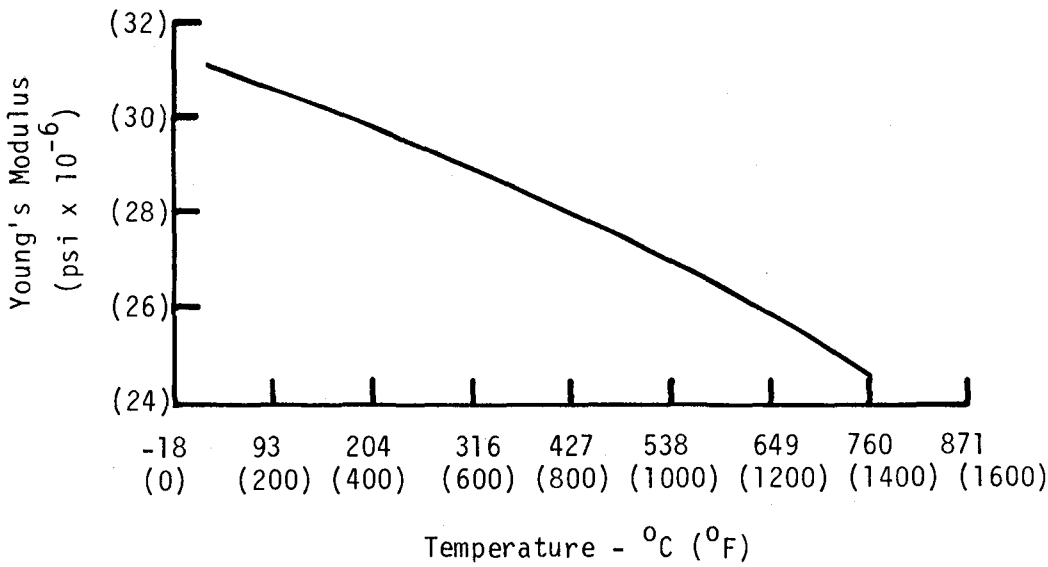

Figure 79 *Modulus Properties of MERL 76*

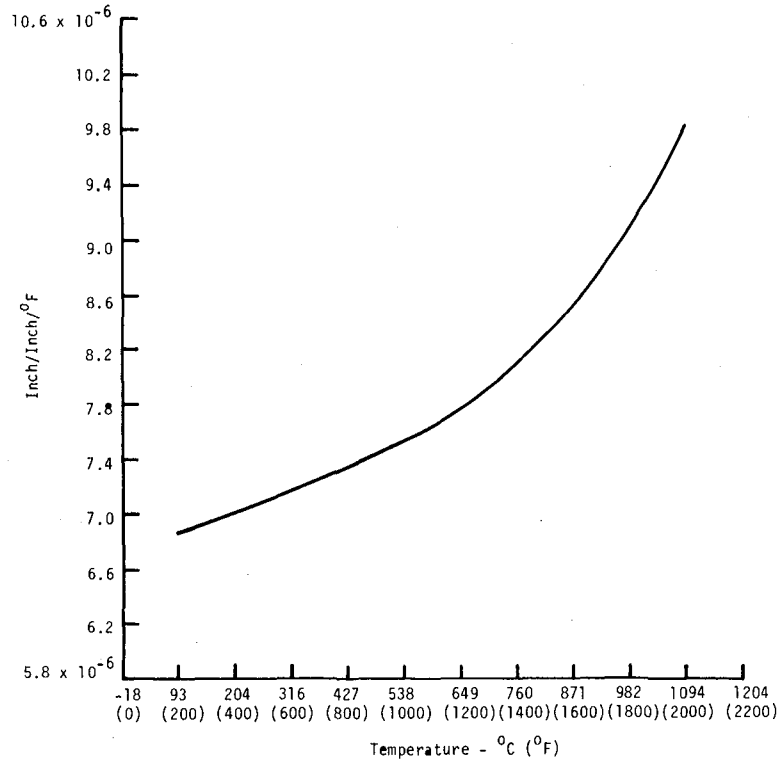

Figure 80 *Thermal Expansion Properties of MERL 76*

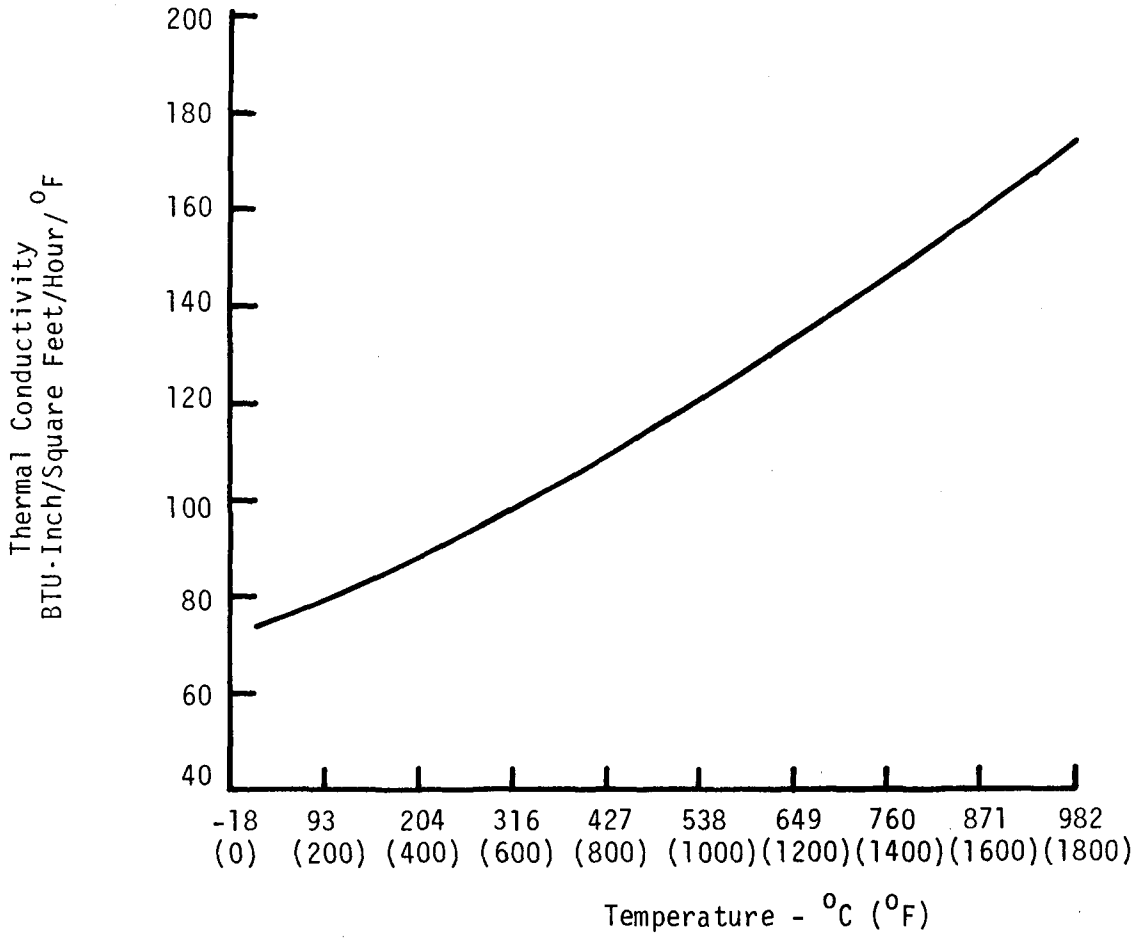

Figure 81 Thermal Conductivity Properties of MERL 76

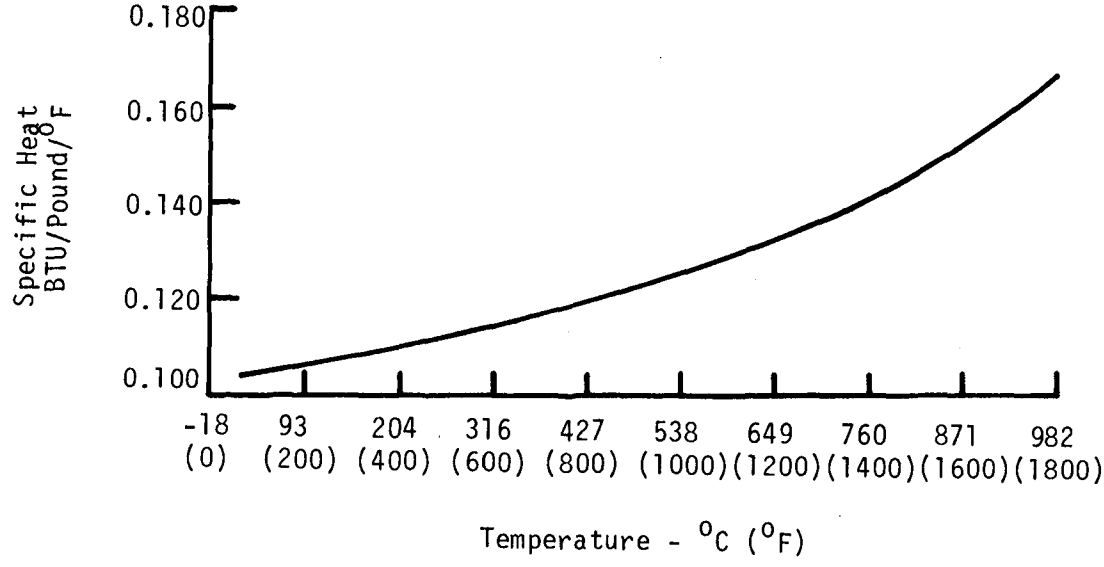

Figure 82 Specific Heat Properties of MERL /6

(a)

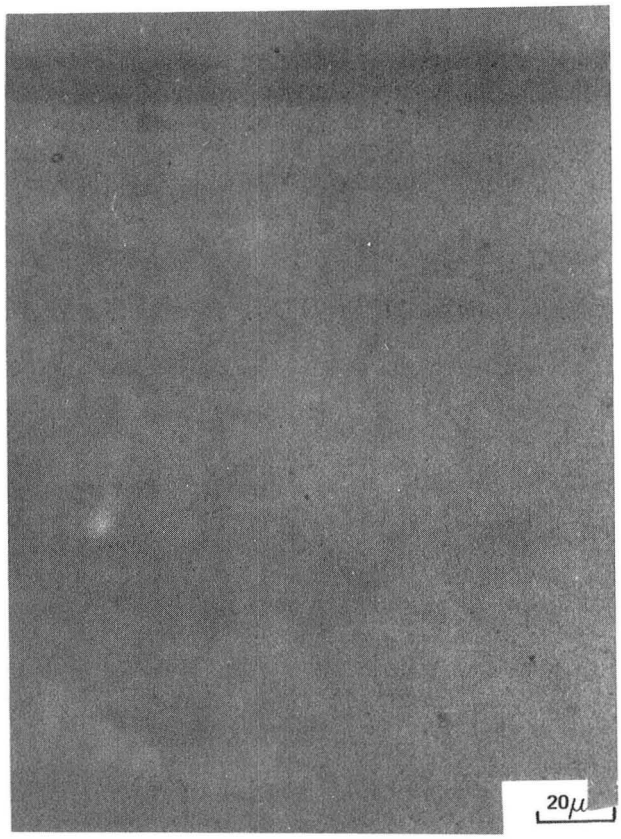

(b)

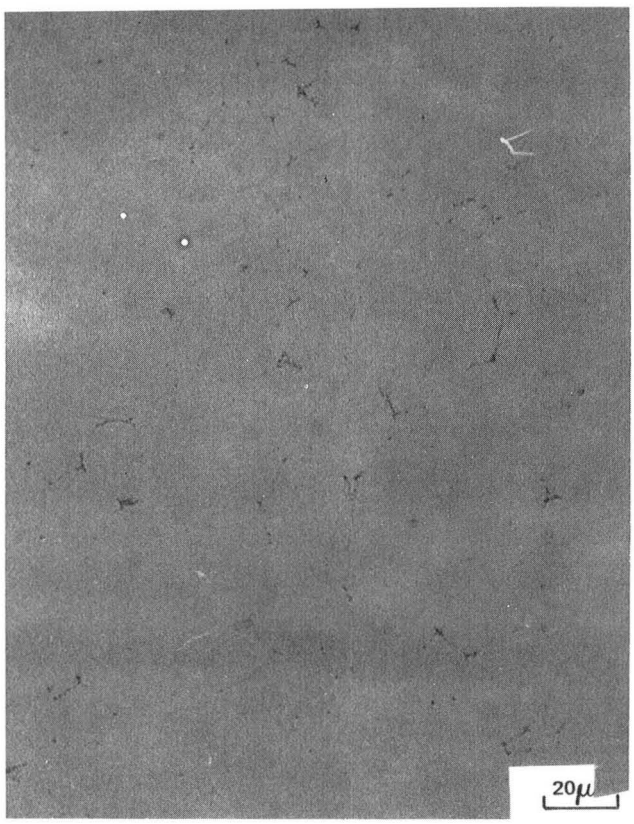

(c)

Figure 83 Photomicrographs of MERL 76 Showing Gamma Prime Solvus and Incipient Melt Temperatures to be 1190°C (2175°F) and 1196°C (2185°), Respectively

(a) 1185°C (2165°F)/4 hrs/WQ
(b) 1190°C (2175°F)/4 hrs/WQ
(c) 1196°C (2185°F)/4 hrs/WQ

Chemical Analysis

To successfully demonstrate acceptable quality HIP consolidations, a full chemistry analysis was performed on the integral test ring located on the bore inner diameter in addition to a comprehensive oxygen and nitrogen survey at six locations across a radial cross section of a disk.

The composition as determined for the integral test ring removed from a JT9D disk 160-2 is given in Table XII. Additional interstitial oxygen and nitrogen gas analysis indicated that the gas content was independent of location for a JT9D disk (160-2) and met target value as shown in Figure 84. These chemistry results coupled with the integral test ring properties demonstrated that acceptable quality consolidations were manufactured.

TABLE XII

COMPOSITION OF MERL 76 DISK 160-2

	w/o		ppm
Cr	12.2	Fe	36
Co	18.2	Cu	<10
Al	4.9	Mn	<10
Ti	4.3	N	24
Hf	0.43	O	95
Nb	1.29	Pb	< 1
Mo	3.2	Bi	<0.3
B	0.026	P	<20
Si	0.010		
C	0.022		
S	<0.002		
Zr	0.06		

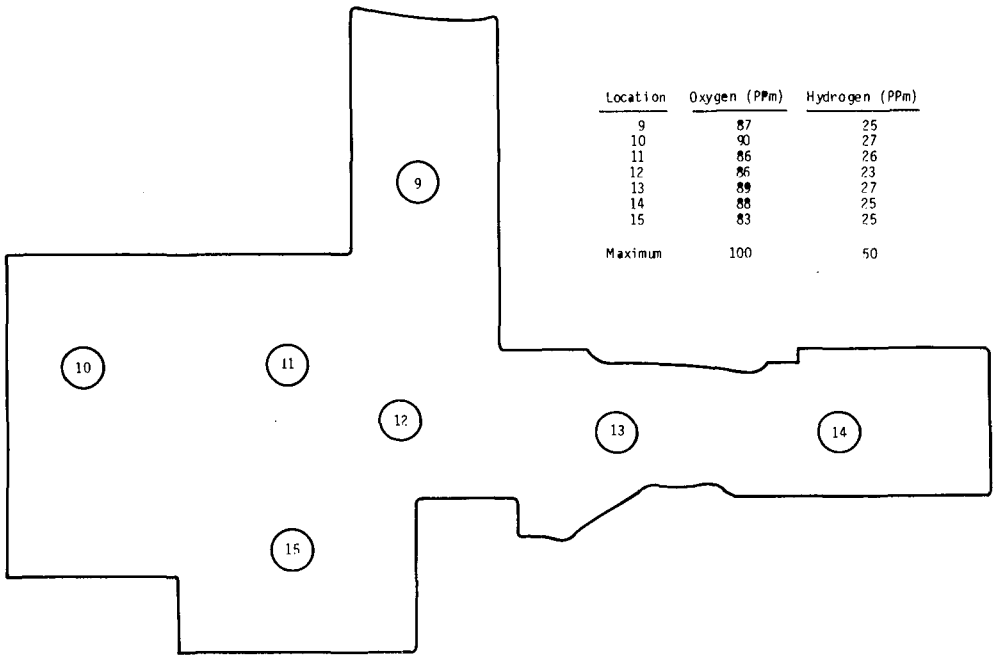

Figure 84 *Interstitial Gas Content of Integral Test Ring Removed From Disk 160-2*

Microstructural Analysis

Since the strength of MERL 76 is dependent upon section size due to the microstructural response to the cooling rate from the solution heat treat temperature, the microstructure of typical components in the fully heat treated condition was evaluated. A detailed characterization of the microstructure of the JT9D disk at various locations is described in the following section. Metallographic samples were prepared with Kalling's Etchant for 100X photos and AG21* etchant for 1000X photos.

A radial section of a JT9D disk (160-3) was examined at six locations representing different cooling rate from the solution heat treat temperature as a result of various section size. Optical microscopy did not reveal any significant differences in microstructure from one location to another. However, the use of replication electron microscopy enabled a closer examination of the microstructural constituents at a higher magnification. Figure 85 are electron micrographs showing the microstructure of MERL 76 to include three distinct size of gamma prime as follows:

(A) Large, globular, primary gamma prime (1.5-5 μm) and elongated gamma prime (0.2-1 μm) coarsened during HIP consolidation and solution temperature.

(B) Finer blocky matrix gamma prime (0.25 μm) precipitated during cooling from solution temperature.

(C) Extremely fine gamma prime (0.05 μm) precipitated during aging.

A comparison of a thin section area (bolt flange) with a thick section area (bore/center) indicated that the thin section displayed more fine "aging" gamma prime ($<0.05\,\mu$m) as shown in the higher magnification ($\sim$22,000X) micrographs in Figure 85.

---

*AG21 mixture: 50 lactic acid - 30 HNO_3 - 2Hf

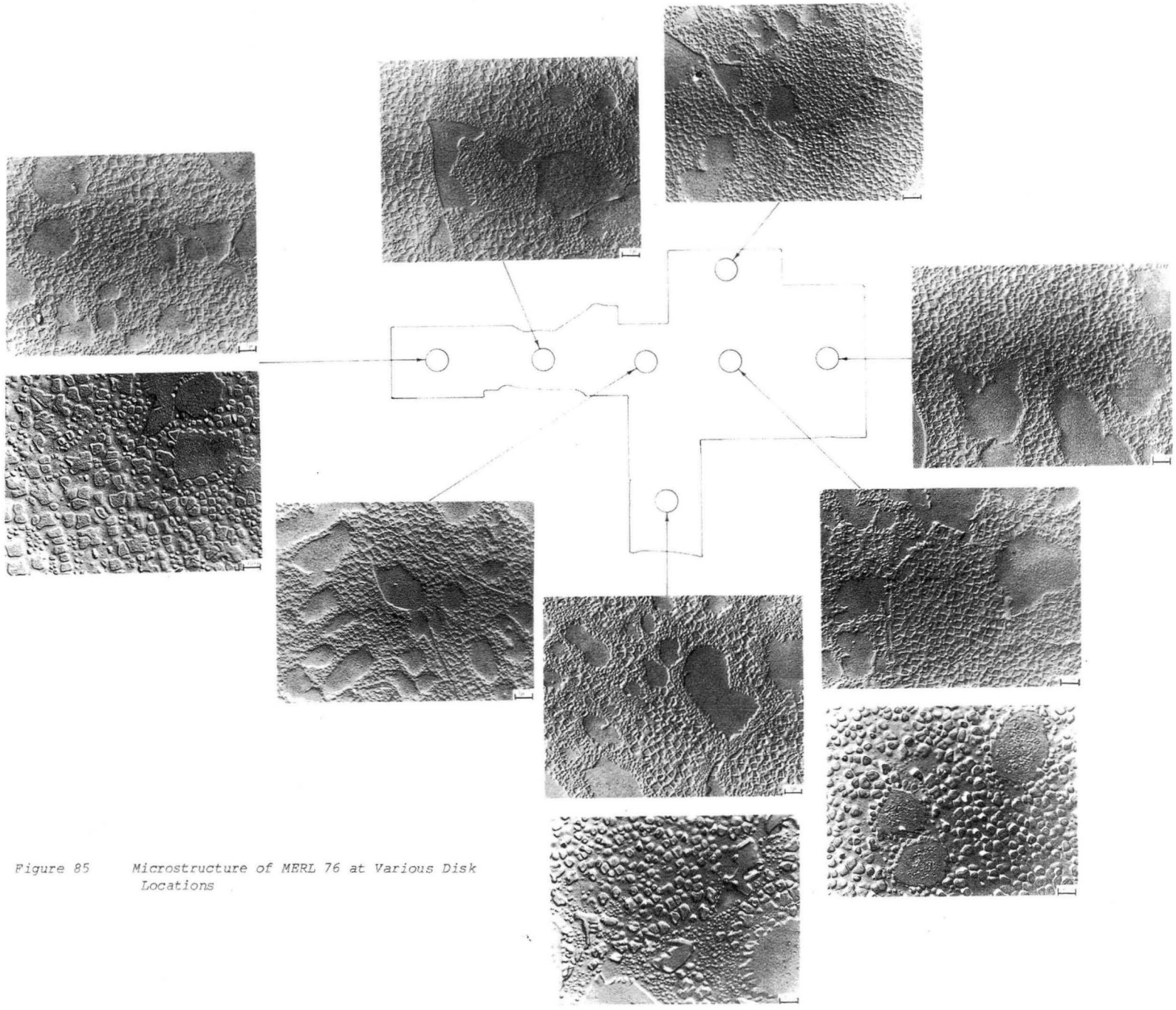

Figure 85 *Microstructure of MERL 76 at Various Disk Locations*

To fully characterize the microstructure of MERL 76, it is important to analyze any factors that might alter the normal MERL 76 microstructure which might result in unexpected processing problems. For this reason, the interaction region between the base metal MERL 76 and stainless steel containers was analyzed since the container remains in intimate contact with the MERL 76 during both the HIP consolidation and heat treat cycle. The microstructure of this interaction region is shown in Figure 86. To identify any regions of high hardness which could lead to processing difficulties (e.g., quench cracking, machining problems), a microhardness traverse was taken across the container/MERL 76 base metal interaction zone. The hardness increased progressively from the relatively soft steel (Rc 15) to the harder MERL 76 (Rc 42.5). There was no undesirable interaction zone that exhibited high hardness.

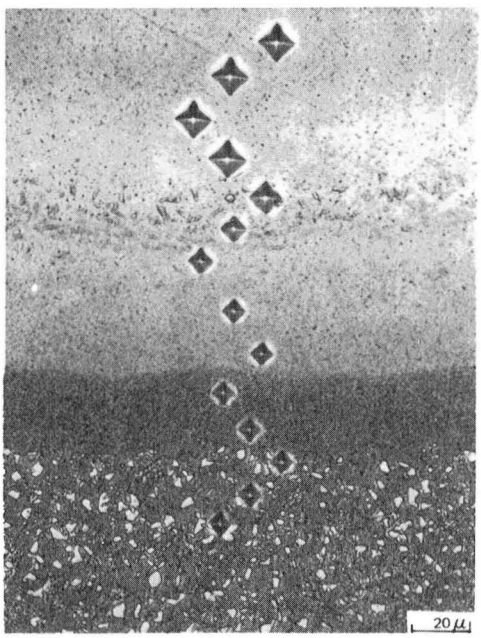

	R_C
174 DPH	<15
174 DPH	<15
174 DPH	<15
196 DPH	<15
196 DPH	15
289 DPH	28
315 DPH	31.5
356 DPH	36
368 DPH	37.5
380 DPH	38.5
380 DPH	38.5
303 DPH	30
380 DPH	38.5
421 DPH	42.5

Figure 86 Microhardness Values Across Interaction Zone of Disk 160-2

Process Control and Acceptance Criteria

To establish process control and acceptance criteria specifications, the manufacturing procedures which were used in this project must be carefully examined from the standpoint of not only the process itself but also the various tests that measure the integrity and properties of the hot isostatic pressed (HIP) consolidated component. Based upon an evaluation and review of the manufacturing procedures and control methods which were used in this

project, a detailed process control and acceptance criteria reflecting results of Task I were produced as presented in Appendices M and N, respectively.

TASK II - TEST COMPONENT MANUFACTURE AND SPIN/BURST RIG TESTING

Utilizing the process parameters established in Task I, one JT9D disk was manufactured for spin/burst rig test. A flow diagram of this task is shown in Figure 87.

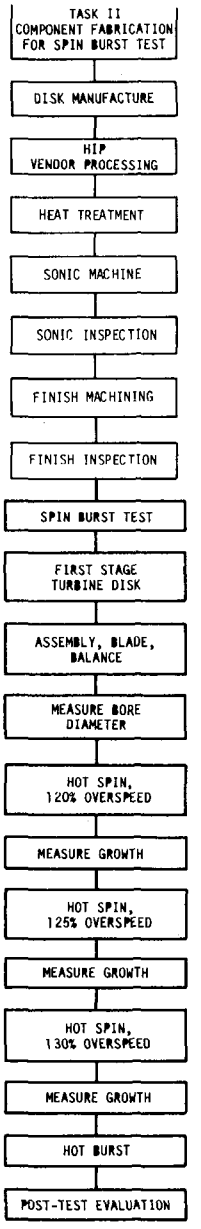

Figure 87 Task II Flow Diagram

Although the As-HIP consolidation (160-1) did not yield a sonic shape, sufficient material existed to yield a finish machined part as shown in Figure 88. To verify mechanical property response of the HIP component, an integral test coupon was provided within the design of the HIP container. The integral test coupon ring was located at the bore inner diameter - front face. Testing of the integral test coupon ring included tensile, stress rupture, interstitial oxygen and nitrogen tests and microstructural analysis as specified in the Acceptance Criteria. Results of the testing showed that tensile and rupture levels all exceeded target levels indicating that the consolidation was sound as given in Table XIII.

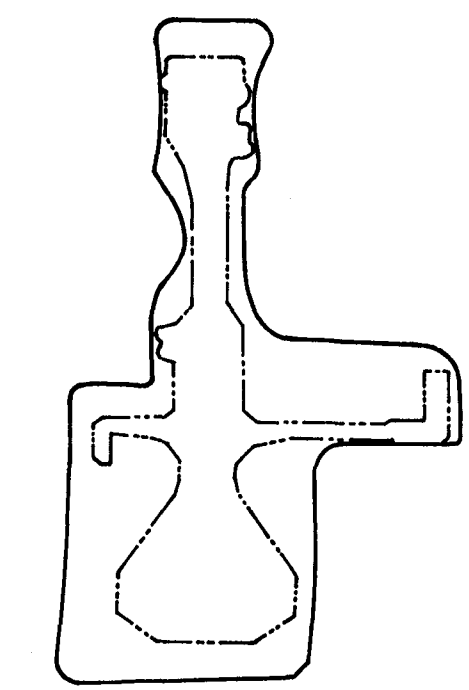

Figure 88 *Comparison of Outline of As-HIP Consolidation of Disk 160-1 with Machined Disk*

TABLE XIII

INTEGRAL TEST RING PROPERTIES OF JT9D DISK (160-1)

Tensile Results

Heat Code	Temperature °C (°F)	0.2% YS MPa (ksi)	UTS MPa (ksi)	EL %	RA %
160-1	RT	1023.9 (148.5)	1562.4 (226.6)	24.0	22.6
	RT	1027.3 (149.0)	1556.8 (225.8)	24.5	23.4
	621 (1150)	1044.6 (151.5)	1396.2 (202.5)	19.0	19.7
	621 (1150)	1041.1 (151.0)	1401.7 (203.3)	17.8	22.1
Target	RT	965 (140.0)	1481.0 (215.0)	15.0	15.0
		965 (140.0)	1337 (194.0)	12.0	12.0

Combined (Smooth/Notch) Stress Rupture Properties

Heat Code	Temperature °C (°F)	Stress MPa (ksi)	Hours to Failure	Type of Failure	EL %	RA %
160-1	732 (1350)	655 (95)	35.1	-N-		
	732 (1350)	655 (95)	53.2	-N-		

INTERSTITIAL GAS ANALYSIS

	Oxygen (ppm)	Nitrogen (ppm)
160-1	119	28

Because there was insufficient material in the as-HIP consolidation to yield a sonic shape, a proof-spin test, which was included in the manufacturing operation process to further confirm the consolidation's structural integrity, was not conducted. However, results of the qualification tests including integral test ring properties as well as sonic and fluorescent penetrant inspection tests demonstrated the acceptability of the component for test.

After sonic inspection, the disk was machined per blueprint P/N 812901, the principal dimensions of which are shown in Figure 89. The sonic shape was initially lathe-turned using carbide tools. Hole-drilling, slot-milling and broaching were next performed as shown in Figures 90, 91, and 92, respectively. Because some of the finish-machined surfaces were relatively close to the steel container, the disk was given a light anodic etch to ensure that there was no residual container on the surface. As a final evaluation, the disk was again fluorescent penetrant inspected. This revealed no cracks. Final dimensions were taken showing that the disk met blueprint requirements. The finish-machined disk is shown in Figure 93.

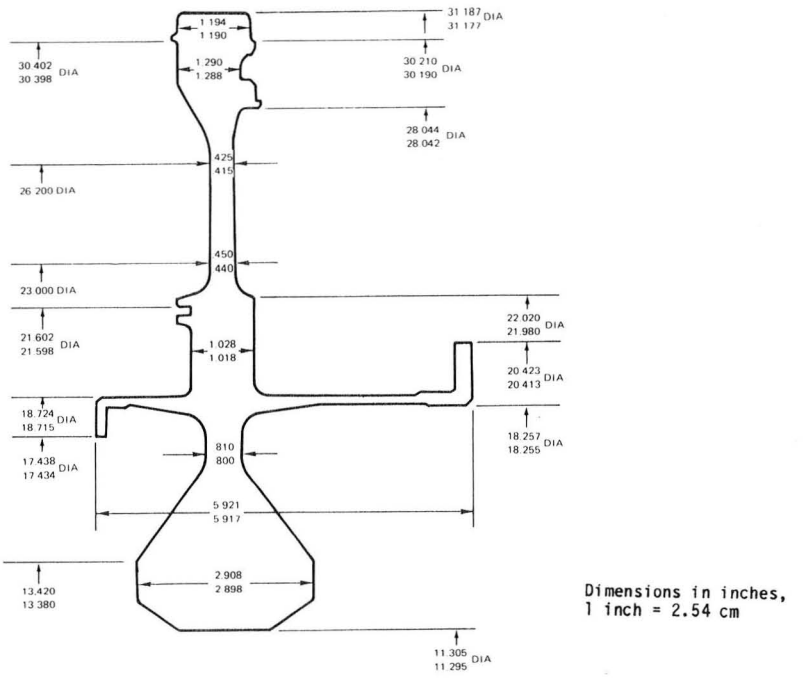

Figure 89 Principal Dimensions of JT9D First Turbine Disk P/N 812901

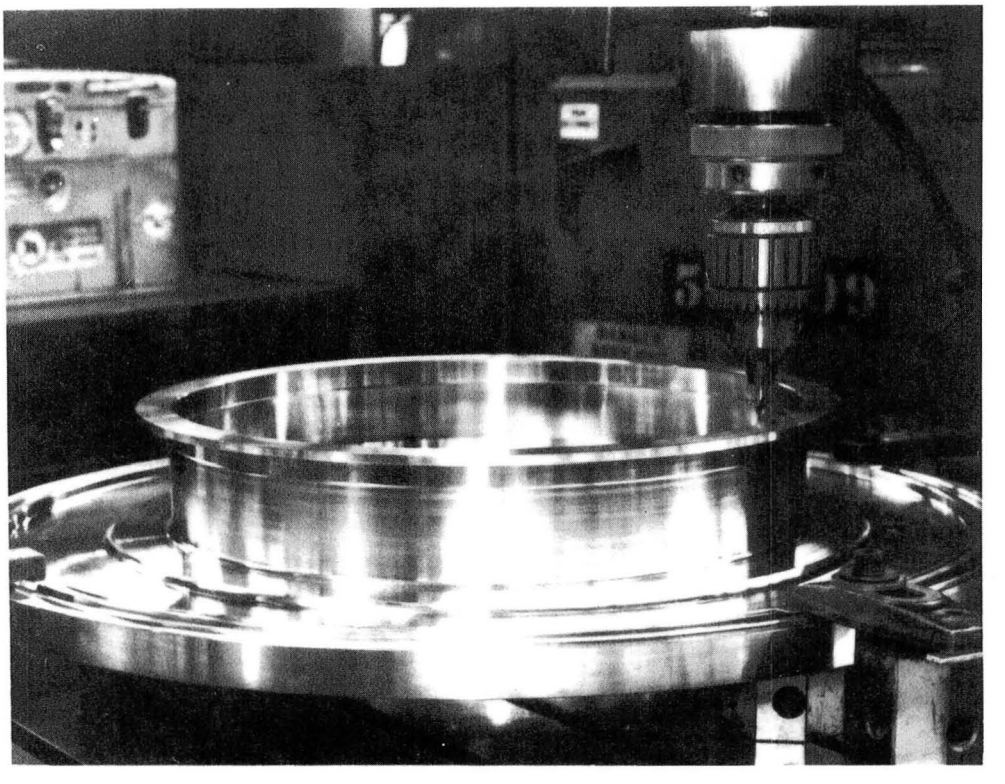

Figure 90 Hole Drilling Operation Being Performed on Disk 160-3

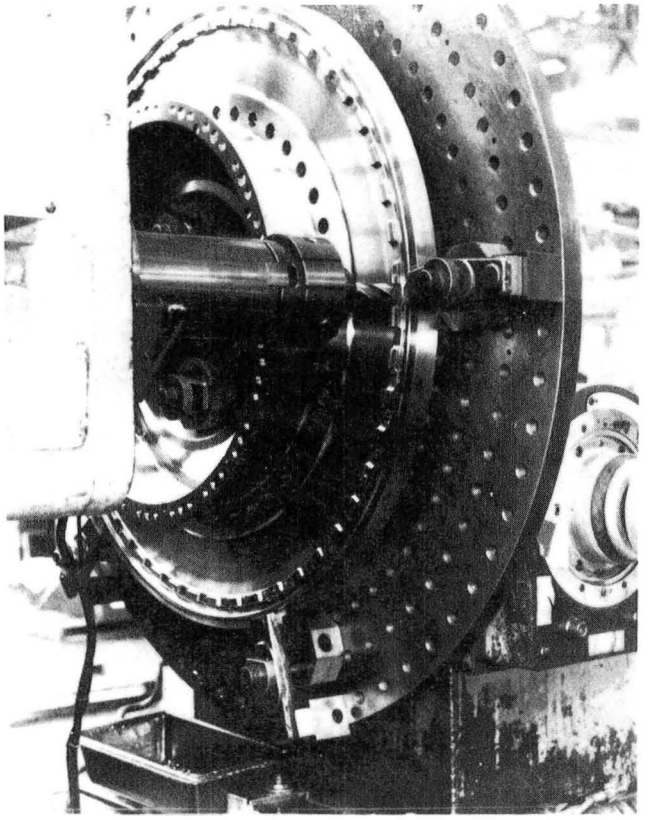

Figure 91 *Milling Operation Being Performed on Disk 160-3*

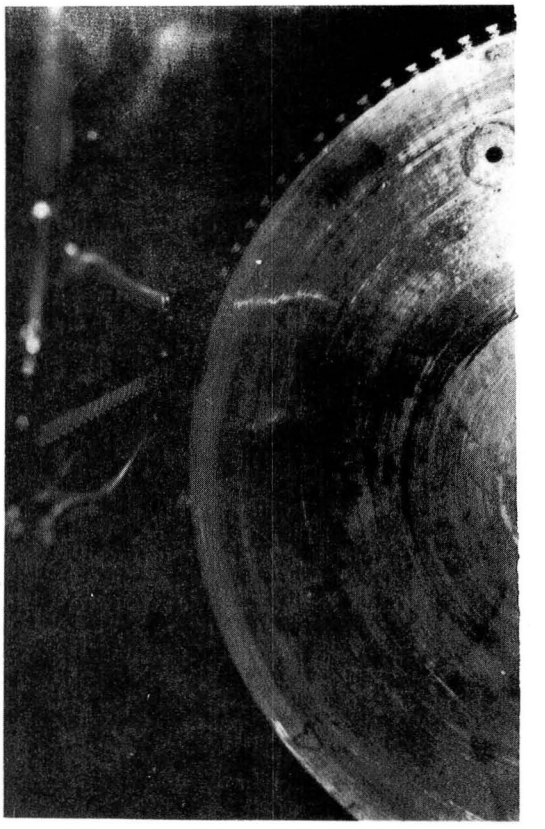

Figure 92 *Broaching Operation Being Performed on Disk 160-3*

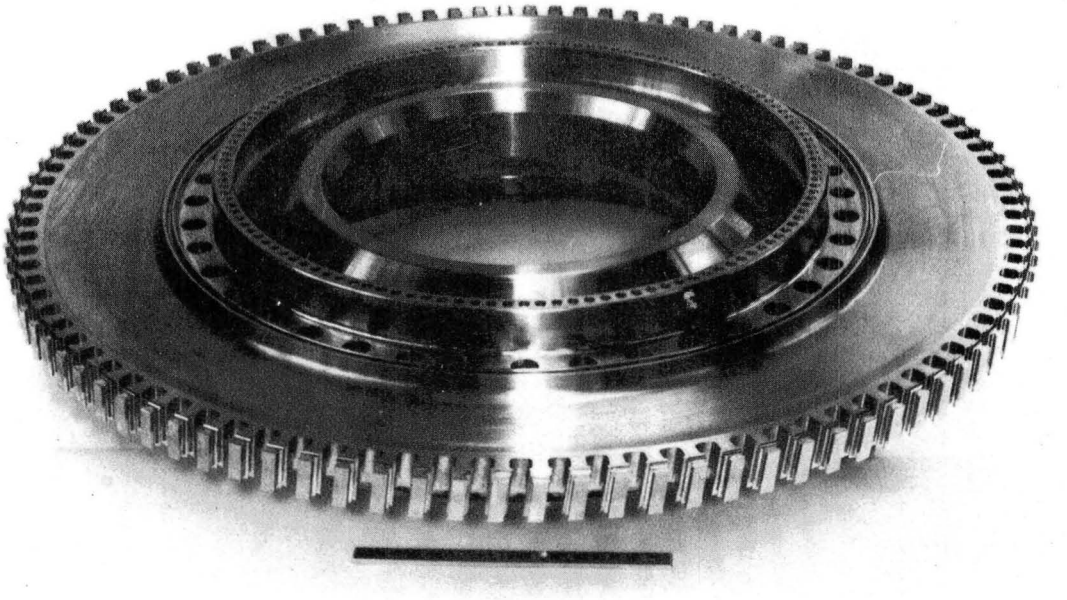

Figure 93 *Front View of Finish Machined MERL 76 JT9D-70 First Stage Turbine Disk*

In order to establish the burst (overspeed) capability for MERL 76 in disk applications, a spin test was conducted at 621°C (1150°F). Disk 160-1 was bladed, thermocoupled and assembled in a rig shown in Figures 94 and 95. Approximately twenty thermocouples were installed at such locations of the disk as shown in Figure 94. The disk assembly was mounted to a steam-drive turbine and inserted into a pit which contained a resistance heated furnace. The pit was evacuated to approximately 5 mm Hg and this pressure was dynamically maintained during the test; a vacuum was necessary to facilitate rotation of the rig. At an idle speed of 1000 rpm, the disk assembly was heated to a 621°C (1150°F) average temperature. After holding at 621°C (1150°F) for at least 15 minutes, the disk assembly was accelerated to the desired speed and held for five minutes. After each speed increment, the spin pit was opened and growth measurements were taken at four locations on the disk as shown in the inset of Figure 96.

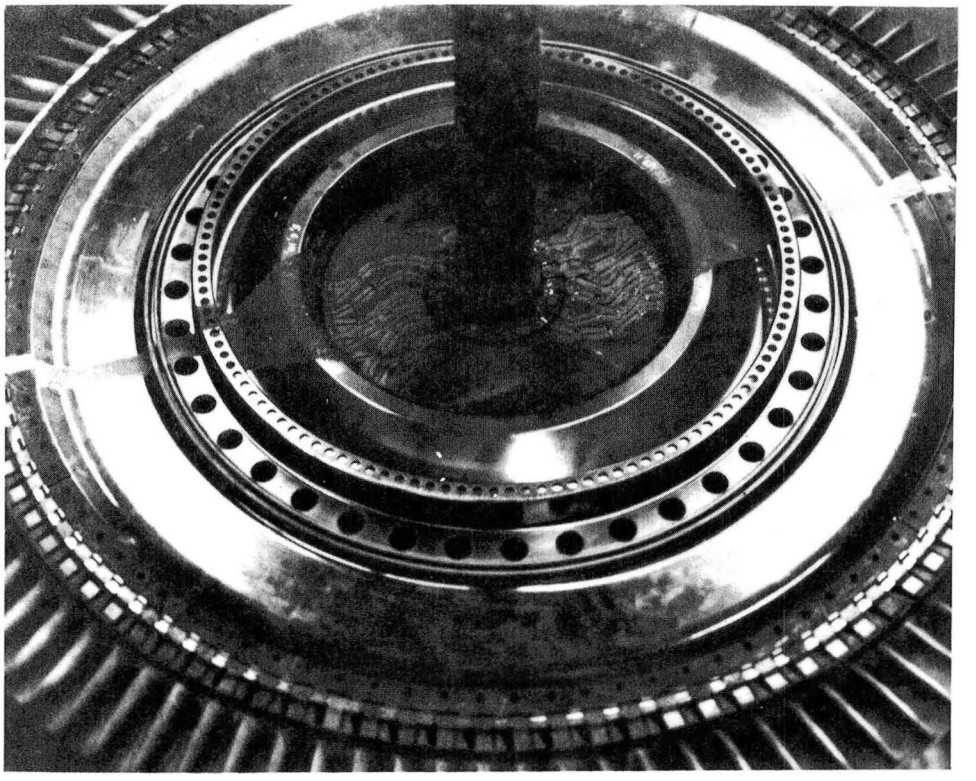

Figure 94 Location of Thermocouples Installed for Hot Spin Test

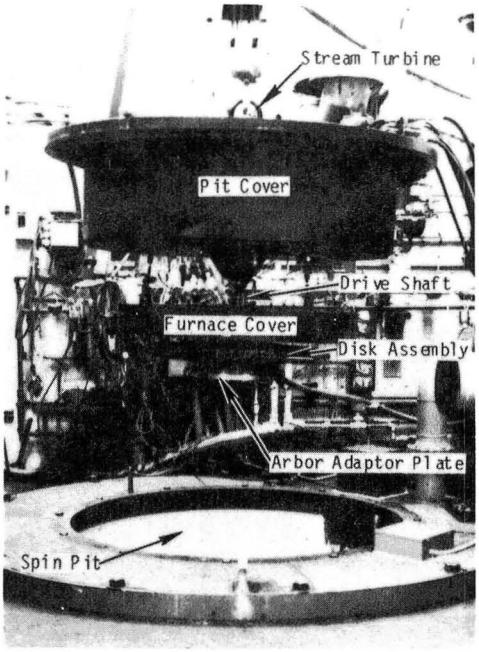

Figure 95 Spin Test Pit

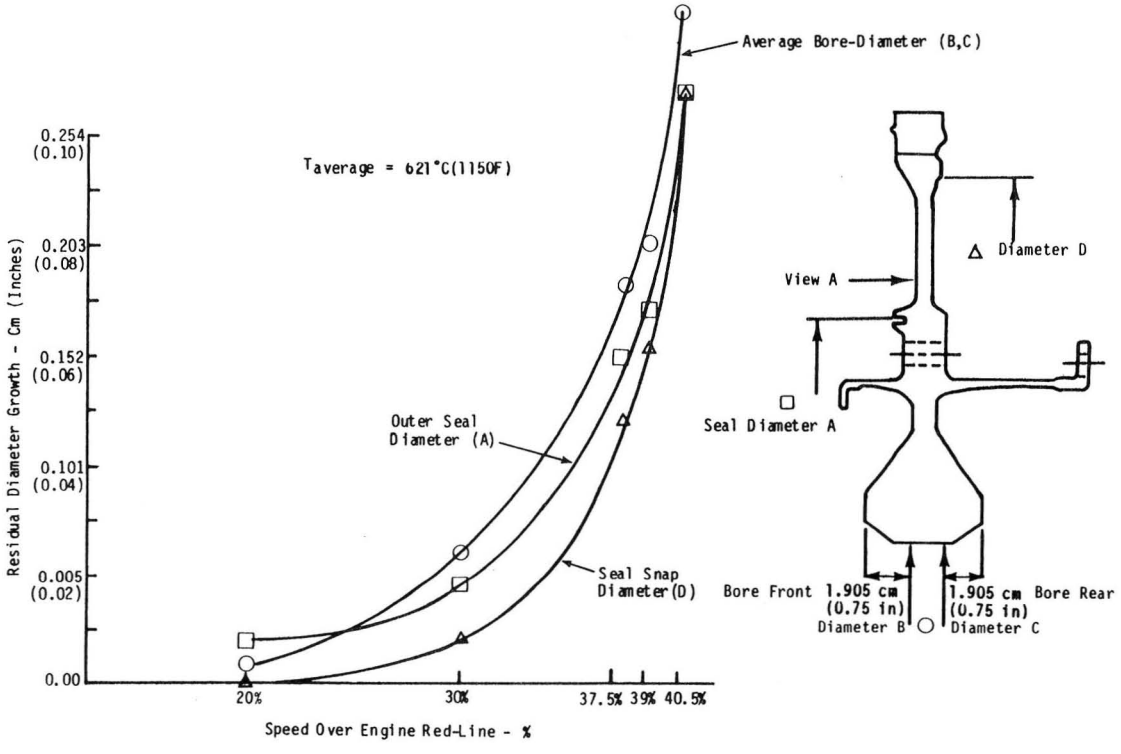

Figure 96 Growth Measurements of Disk at Different Speed Increments

Based upon the engine redline speed, the disk assembly was subjected to a 20%, 30% and 37.5% overspeed with growth measurements (Figure 96) taken after each increment. At an overspeed increment of 39% an oil seal in the steam turbine assembly failed, shutting down the rig. An additional set of growth measurements were taken at this point. Before the disk burst, the rig failed catastrophically at 40.5% overspeed.

The rig failure involved separation of the drive shaft allowing the rotor assembly to fall to the bottom of the pit. The damage to the disk assembly included impact damage on the rear face which rubbed against the bottom of the pit and sheared off the bolt flange approximately 0.64 cm (0.250 in) above the web face (Figure 97).

Figure 97 Damage of Disk Assembly After Rig Failure

A failure analysis traced the failure origin to the side plate (Figure 98) which retained the blades on the disk. This failure caused a primary imbalance in the disk assembly which then resulted in the failure of the rig arbor.

Although the disk did not burst, sufficient growth data was collected prior to rig failure to demonstrate that MERL 76 is capable of safe operation in a JT9D engine.

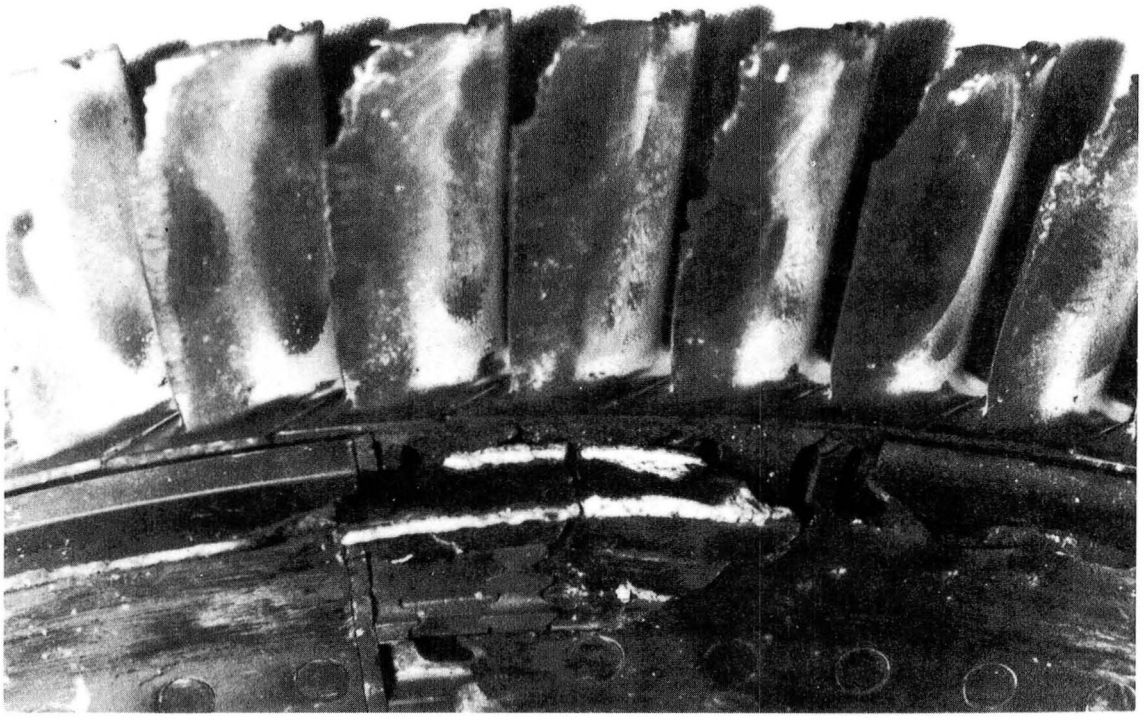

Figure 98 Failure Origin of Rig

Task III - COMPONENT MANUFACTURE FOR EXPERIMENTAL ENGINE TEST

A flow diagram of this task is shown in Figure 99.

Manufacturing procedures, as established in Task I and used for machining the spin disk 160-1 in Task II, were also used for disk 160-3 which is to be tested in a land-based experimental engine. As in the case for disk 160-1, disk 160-3 did not have sufficient material in the as-HIP consolidation shape configuration to completely yield a sonic shape. Consequently, a proof-spin test was not conducted. As in Task II, integral test coupons were provided for

JT9D disk 160-3 to verify the mechanical property response of the HIP component. Locations of the test coupons were the same as disk 160-1 and test conditions were as specified in the acceptance criteria which was also followed for disk 160-3. For these consolidations tensile and rupture properties all exceeded target levels as shown in Table XIV indicating that these consolidations were sound.

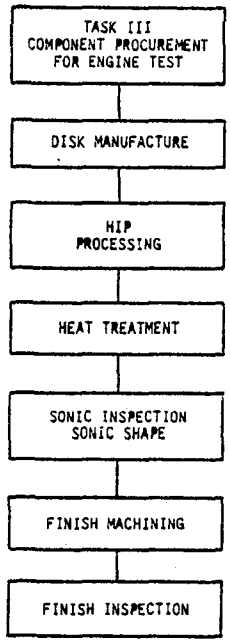

Figure 99 Task III Flow Diagram

TABLE XIV

INTEGRAL TEST RING PROPERTIES OF JT9D DISK (160-3)

Tensile Results

Heat Code	Temperature °C (°F)	0.2% YS MPa (ksi)	UTS MPa (ksi)	EL %	RA %
160-3	RT	1056.3 (153.2)	1587.2 (230.3)	23.9	21.6
	RT	1053.5 (152.8)	1599.6 (232.0)	22.7	20.6
	621 (1150)	1042.5 (151.2)	1423.8 (206.5)	21.9	21.6
	621 (1150)	1041.1 (151.0)	1432.7 (207.8)	22.8	25.0
Target	RT	964.6 (140)	1481.3 (215)	15.0	15.0
	1150	964.6 (140)	1336.6 (194)	12.0	12.0

Combined (Smooth/Notch) Stress Rupture Properties

Heat Code	Temperature °C (°F)	Stress MPa (ksi)	Hours to Failure	Type of Failure	EL %	RA %
160-3	732 (1350)	655 (95)	47.1/60.5*	-N/S-	5.0*	7.3*
	732 (1350)	655 (95)	49.8/56.9*	-N/S-	6.9*	8.0*

*Ater notch failure, specimens were remachined and tested as smooth bar.

INTERSTITIAL GAS ANALYSIS

	Oxygen (ppm)	Nitrogen (ppm)
160-3	87	22

Based on the results of the acceptance tests (e.g., integral ring properties, Table XIV, sonic inspection, fluorescent penetrant inspection), which exceeded minimum requirements and indicated a component of acceptable quality, disk 160-3 was designated for engine demonstration testing. As in the case for disk 160-1, an anodic etch to assure that no residual container material was left on the disk was applied to the finish machined disk and was followed by fluorescent penetrant inspection, which revealed no indications.

During finish machining of disk 160-3 per P/N 812901 (see Figure 88), it was determined that residual container material (approximately 0.05 cm/0.020" thick) was observed over a 20° arc segment on the rear face of the bolt-hole flange as shown in Figure 100. After the residual can material was removed by milling, this area was shot peened. Both Pratt & Whitney Aircraft's Engine Design Engineering and National Aeronautics and Space Administration's Program Manager granted approval of this slight design modification of the disk. A macrograph of this finish machined disk showing the milled-flange is shown in Figure 101. This slight taper in the flange required re-balancing of the disk.

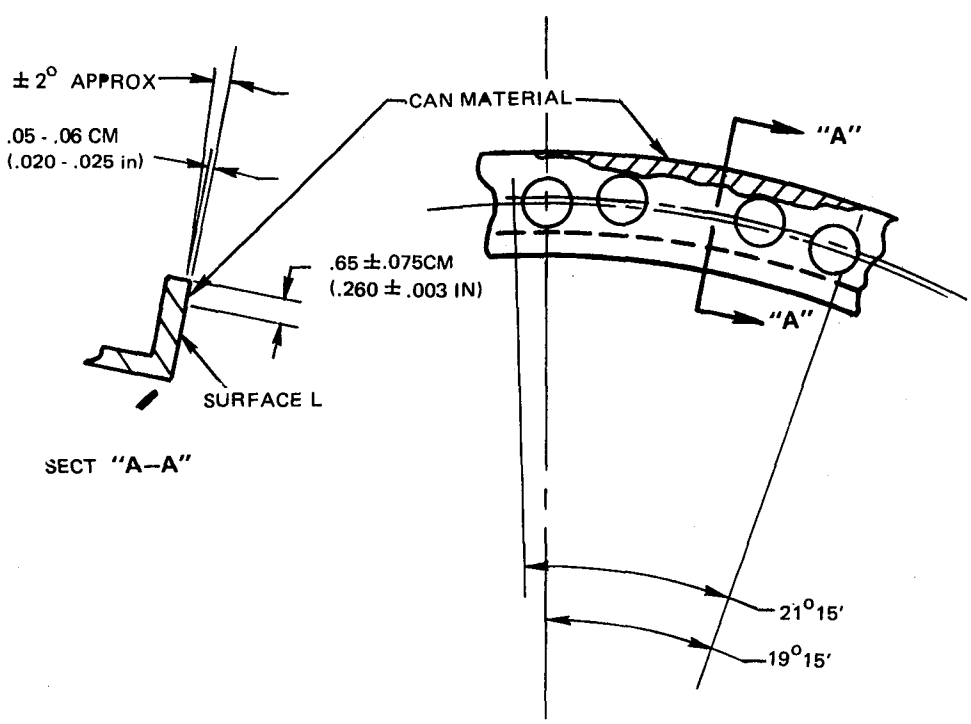

Figure 100 Bolt Flange-Face Modification of Disk 160-3

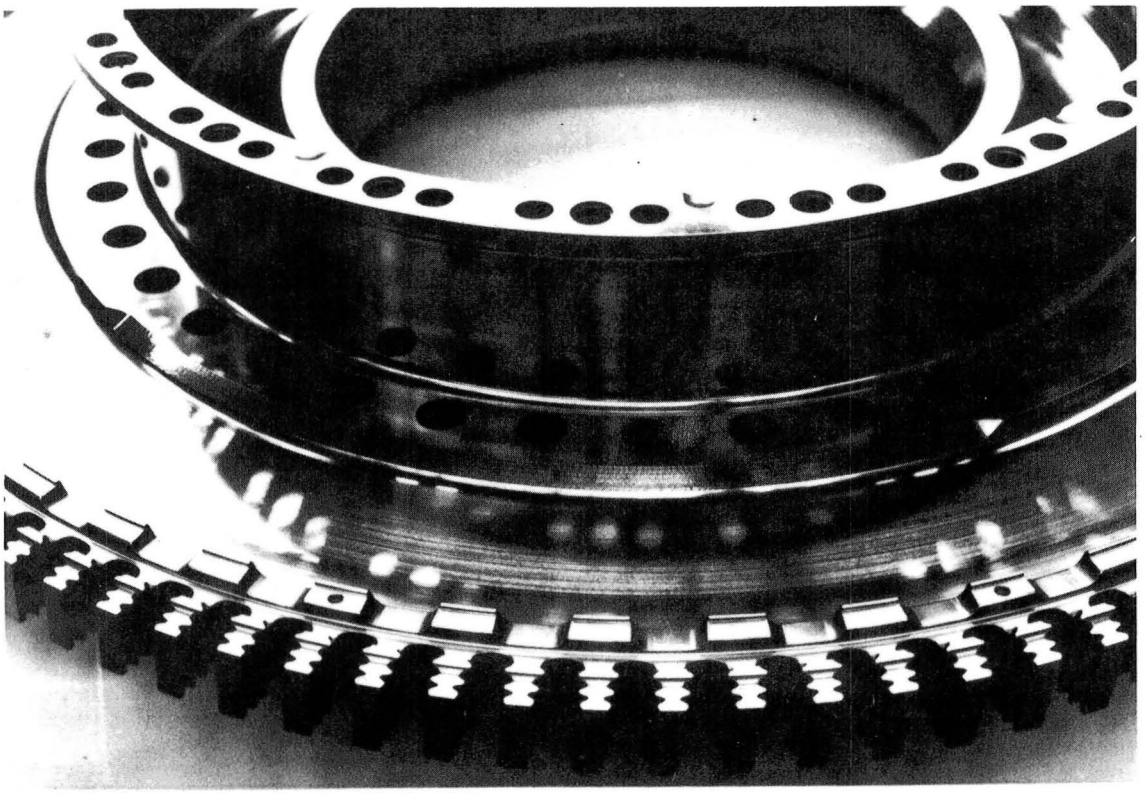

Figure 101 Finish Machined Disk Showing Tapered Bolt-Flange Face

TASK IV - ENGINE DEMONSTRATION TESTING

The objective of this task is to demonstrate the performance capability of a finish-machined MERL 76 disk in an experimental JT9D ground-based engine for at least 150 hours of endurance testing. On the date of this writing, the engine test has not been conducted but is planned for December 1981 through January 1982. The details of this engine test are classified as category 2 - F.E.D.D. and will be reported in a separate document - Volume II (CR-165550).

TASK V - POST TEST ANALYSIS

Post-Engine Test Analysis

The results of a post-test evaluation of the experimental engine tested HIP MERL 76 disk are classified as category 2 - F.E.D.D. data. Accordingly, the

analysis of this engine test including dimensional inspection results of the disk before and after the engine test will be reported in Volume II of this project (CR-165550).

Analysis of Results

This program established manufacturing procedures for the production of acceptable quality direct HIP consolidated MERL 76 disk components. These procedures included powder manufacture, container design, powder handling technique, HIP consolidation cycle, and non-destructive inspection techniques. Based upon the evaluation of the manufacturing procedures, a process control plan and acceptance criteria were established as presented in Appendices M and N, respectively.

Three disks were characterized by more comprehensive testing which led to a proposed material specification. Lower limit design curves were established for tensile, stress-rupture, creep to 0.2%, and notched low cycle fatigue (Kt = 2.5) fatigue properties, in addition to generating low cycle fatigue crack propagation and low cycle fatigue crack threshold data. Design lower limits which established the material capability are given in Appendix O.

A fourth disk was subjected to a component spin/burst rig test at 621°C (1150°F). Although the disk did not burst because of rig failure, sufficient growth measurements up to 40% over red-line speed demonstrated that MERL 76 meets or exceeds the speed margin required for operation in an advanced JT9D commercial engine.

The objectives of this program were all met. These objectives were to increase the rim temperature capability by 22C°(40F°), reduce component weights by 77-88 kg (35-40 lbs), and reduce material cost by 30% as compared to bill-of-material Superwaspaloy®. When compared to Superwaspaloy®, MERL 76 exhibited at least a 22C°(40F°) advantage at 732°C (1350°F) and as much as 56C°(100F°) at 621°C (1150°F), as shown in Figure 102. By taking advantage of the superior strength and lower density of the MERL 76 alloy as compared to Superwaspaloy®, the JT9D first and second stage turbine disk can be designed thinner and lighter by 77-88 kg (35-40 lbs)(Figure 103). Based on 1980 costs to supply sonic JT9D disk shape forgings, the usage of direct HIP MERL 76 components cost at least 30% less than that for Superwaspaloy® (Figure 104).

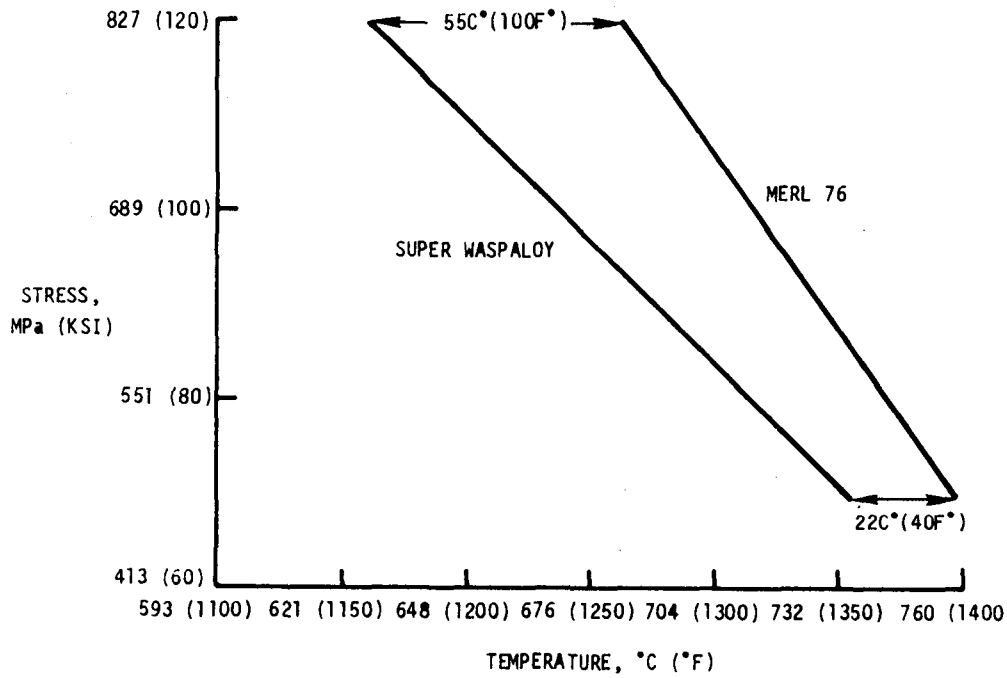

Figure 102 Increased Rim Temperature Capability of MERL 76 Over Superwaspaloy

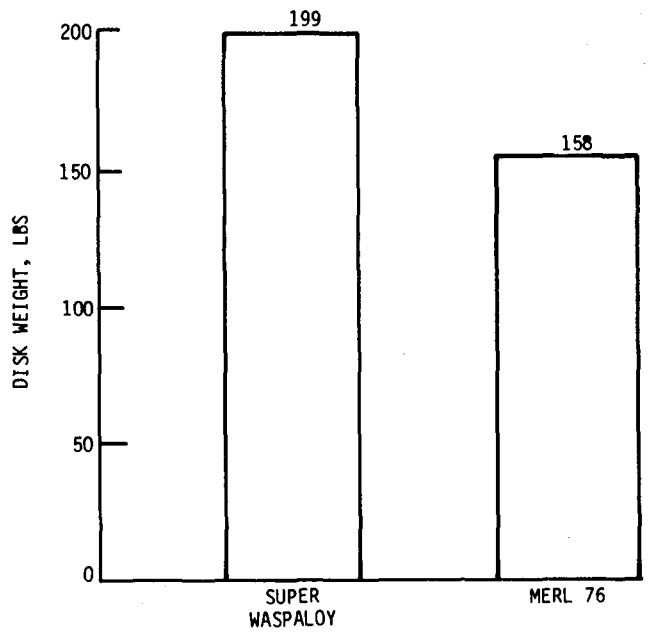

Figure 103 MERL 76 Reduces Component Weight When Compared to Waspaloy

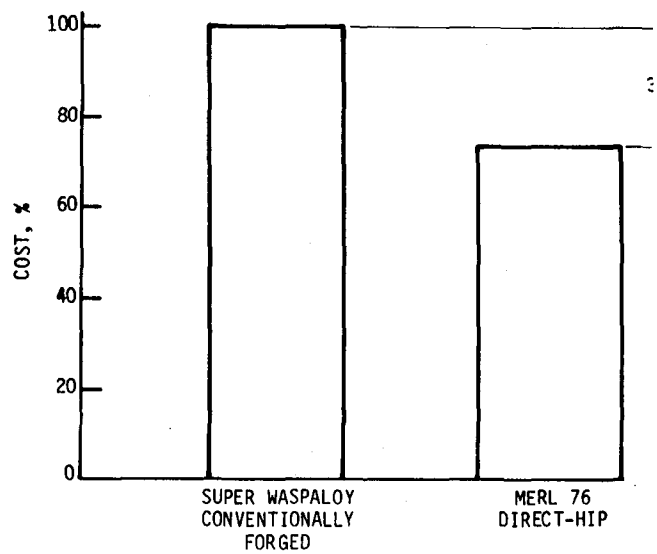

Figure 104 MERL 76 Reduces Cost Base Purchase of JT9D Turbine Shapes in 1980

FINAL RECOMMENDATIONS

Based on the results of this program and related P&WA experience, direct HIP MERL 76 disks are suitable for incorporation in a commercial engine.

CONCLUSIONS

Based upon metallographic, ultrasonic, dimensional, chemical, and mechanical property analyses of direct HIP consolidated MERL 76 disks, conclusions are made as follows:

1) Suitable manufacturing methods were established for direct-HIP consolidated MERL 76 disks. Based upon the evaluation of these manufacturing methods, a process control plan and acceptance criteria were established. A heat treatment (1163°C(2125°F)/2 hrs./OQ + 871°C(1600°F)/0.67 hrs./AC + 982°C(1800°F)/16 hrs.AC+649°C(1200°F)/24 hrs/AC+760°C(1400°F)/16 hrs/ AC) was selected that gave the best mechanical properties.

2) Comprehensive mechanical property testing of three full-size disk consolidations were utilized to establish design-allowable curves for tensile, creep to 0.2%, stress-rupture, and notched (K_t = 2.5) low cycle fatigue properties. Additional data were generated for low cycle fatigue crack propagation and low cycle fatigue crack threshold properties. To further characterize MERL 76, physical properties including linear expansion, thermal conductivity, and dynamic modulus were also measured.

3) Component spin test demonstrated adequate spin margin for MERL 76 to be used as rotating component in gas turbine engines.

4) Direct HIP MERL 76 material increased stress-rupture capability by 22C° (40F°), reduced component weight by 77-88 kg (35-40 lbs) and reduced material cost by at least 30% when compared to conventionally forged Superwaspaloy®.

APPENDIX A

CHEMICAL ANALYSES OF SPECIAL METALS INGOT, POWDER AND CONSOLIDATIONS

			Consolidation Designations 34D-1, 35D-2, 35D-3, 35S-2, 51S-4, 51S-5						102-1, 102-2					160-1, -2, -3					
	Target		VIM Ingot			Powder Blend		Con. # **	VIM Ingot		Powder Blend		HIP*** Con. #	VIM Ingot				Powder Blend	Con. # **
Element	Minimum	Maximum	711058	711059	711060	BN77070	BN77071	34D-1	711802	711861	BN79003	BN79007	102-2	8091	8092	8261	8262	01680	160-2
Ni	R		R	R	R	R	R	R	R	R	R	R	R	R	R	R	R	R	R
Cr	11.9	12.9	12.6	12.5	12.6	12.56	12.53	12.6	12.5	12.4	12.51	12.54	12.0	12.61	12.67	12.45	12.54	11.9	12.2
Co	18.0	19.0	18.7	18.8	18.8	18.81	18.61	18.0	18.6	18.3	18.50	18.22	18.4	18.51	18.27	18.30	18.48	17.9	18.2
Mo	2.8	3.6	3.30	3.20	3.20	3.32	3.33	3.3	3.15	3.2	3.29	3.30	3.3	3.17	3.25	3.26	3.21	3.2	3.2
Al	4.85	5.15	4.98	5.00	5.10	4.97	4.90	4.8	5.06	5.0	4.93	4.88	5.1	4.94	4.99	4.94	5.02	4.9	4.9
Ti	4.15	4.50	4.40	4.35	4.29	4.43	4.49	4.2	4.35	4.30	4.20	4.32	4.2	4.27	4.23	4.33	4.38	4.3	4.3
Nb	1.50(3)	1.80	1.68	1.70	1.69	1.65	1.80	1.6 (3)	1.42	1.46	1.46	1.57	1.41	0.01	0.01	N.D.	N.D.	1.32	1.29
Hf	0.60(4)	0.90	0.74	0.79	0.78	0.65	0.69	0.69(4)	0.39	0.40	0.39	0.44	0.48	0.01	0.01	N.D.	N.D.	0.42	0.43
B	0.016	0.024	0.021	0.022	0.020	0.021	0.019	0.020	0.019	0.019	0.02	N.D.	0.02	0.019	0.019	0.018	0.019	0.018	0.026
Zr	0.04	0.08	0.06	0.06	0.06	0.05	0.05	0.05	0.06	0.06	0.05	0.06	0.045	0.05	0.06	0.06	0.06	0.07	0.06
C	0.015	0.030	0.02	0.03	0.025	0.026	0.026	0.024	0.022	0.021	0.026	0.024	0.023	0.024	0.03	0.026	0.027	0.024	0.022
Mn	0.02		0.02	0.02	0.02	0.007	0.007	0.0012	0.01	0.02	0.008	0.008	N.D	0.01	0.01	0.01	0.01	N.D.	10
S	0.01		0.003	0.003	0.003	0.006	0.006	0.0034	0.002	0.002	N.D.	0.01	N.D.	0.003	0.002	0.002	0.002	N.D.	0.002
P	0.01		0.01	0.01	0.01	0.004	0.004	0.002	N.D.	N.D.	0.004	0.004	N.D.	0.002	0.001	0.001	0.002	N.D.	0.002
Si	0.10		0.10	0.10	0.01	0.09	0.07	0.05	0.03	0.1	0.01	0.01	N.D.	0.02	0.02	0.01	0.02	N.D.	0.10
Fe	0.30		0.14	0.11	0.11	0.06	0.07	0.048	0.11	0.11	0.05	0.05	N.D.	0.06	0.07	0.04	0.04	N.D.	0.0036
Cu	0.07		0.07	0.07	0.07	0.03	0.03	0.001	N.D.	N.D.	0.03	0.03	N.D.	0.01	0.02	0.01	0.01	N.D.	0.0010
Bi ppm	0.05		0.05	0.05	0.05	0.5	0.5	0.2	N.D.	N.D.	0.02	0.3	N.D.	0.1	0.1	0.1	0.1	N.D.	0.3
Pb ppm	2.0		2.0	2.0	2.0	2.0	2.0	0.0008	N.D.	N.D.	1.	1.	N.D.	1.	1.	1.	1.	N.D.	1
O ppm	100.0		7.0	7.0	10.0	108.	103.	88.0	8.	9.	92.	106.0	89.	6.	6.	7.	8.	180*	95
N ppm	50.0		11.0	11.0	9.0	22.	21.	15.0	19.	21.	18.	28.0	20.	14.	7.	7.	13.	25.	24.

Target MERL 76 Composition Modified as Follows:
(3) 1.20 - 1.60 Nb
(4) 0.30 - 0.50 Hf

* Repeat analysis indicated that oxygen level ranges from 105 - 118 ppm.
** Consolidation Number
*** HIP Consolidation Number

APPENDIX B

POWDER SIEVE ANALYSES

Mesh Size Range		BN77070	BN77071	BN79003	BN79007	010680
	+60	ND	ND		0	ND
-60	+80	0	0		0	ND
-80	+100	1.2	1.0		1.0	0.13
-100	+120	3.6	3.6		3.3	ND
-120	+140	5.0	5.3		4.8	ND
-140	+170	6.0	6.3		5.5	ND
-170	+200	9.1	9.8		7.7	ND
-200	+230	6.9	7.1		5.1	14.0
-230	+270	8.9	9.3		6.1	15.0
-270	+325	6.3	10.4		11.8	6.4
-325	+400	19.4	13.9		6.4	8.7
-400	+500	15.2	15.4		25.1	55.8
-500		18.4	17.9		23.1	ND

ND = Not Determined

APPENDIX C

COMPONENT PROCESSING HISTORY

Consolidation #	Configuration	Ingot No.	Powder Blend	Weight Kg (lbs.)	Temp. °C (oF)	Dynamic Pressure Torr	Leak Rate Microns/3 min
34S-1	JT10D-4 Seal	7-11058 7-11059 7-11060	BN 77070	55 (121)	316 (600)	10^{-5}	3
35S-2	JT10D-4 Seal	7-11058 7-11059 7-11060	BN 77070	55 (121.5)			5
35S-3	JT10D-4 Seal	7-11058 7-11059 7-11060	BN 77070	54.5 (120)			4
51S-4	JT10D-4 Seal	7-11058 7-11059 7-1060	BN 77070	56.8 (125			2
51S-5	JT10D-4 Seal	7-11058 7-11059 7-11060	BN 77070	58.6 (129)			2
34D-1	JT10D-4 Disk	7-11058 7-11059 7-11060	BN 77070	313.6 (690)			2
35D-2	JT10D-4 Disk	7-11058 7-11059 7-11060	BN 77070	318.2 (700)			2
35D-3	JT10D-4 Disk	7-11058 7-11059 7-11060	BN 77070	304.5 (670)			2
102-1	JT10D-132 Modified Disk	7-11802, 7-11861+ Revert B/N 77071	BN 79003	253.6 (558)		4×10^{-5}	11.5
102-2	JT10D-132 Modified Disk	7-11802, 7-11861+ Revert B/N 77071	BN 79003	250 (550)		4×10^{-5}	4.5
MC101-1	JT9D-70 Disk First Iteration	7-11802, 7-11861+ Revert B/N 77071	BN 79007				
MC102-2	JT9D-70 Disk First Iteration	7-11802 7-11861+ Revert B/N 77071	BN 79007				
160-1	JT9D-70 Disk Second Iteration (P/N 812901) SKT 65672	8262 8091 8092 8261	010680	280 (618)		1.5×10^{-5}	5
160-2	JT9D-70 Disk Second Iteration (P/N 812901) SKT 65672	8262 8091 8092 8261	010680	273 (599.5)			2
160-3	JT9D-70 Disk Second Iteration (P/N 812901) SKT 65672	8262 8091 8092 8261	010680	284 (625)			2

APPENDIX D

COMPONENT PROCESSING HISTORY

Consolidation	HIP Parameters	Grain Size	Heat Treatment	Use
34S-1	1169°C-1177°C (2135°F-2150°F)/ 103 MPa (15ksi)/3 hours	9-11		Compaction Leaked
35S-2	1169°C-1177°C (2135°F-2150°F)/ 103 MPa (15ksi)/3 hours	9-11	1163°C (2125°F)/2hours/Furnace cool at 38°C (100°F) per hour to 1121°C (2050°F)/0.5 hour/OQ + 649°C (1200°F)/24 hours/ AC + 760°C (1400°F)/16 hours/AC	
35S-3	1169°C-1177°C (2135°F-2150°F)/ 103 MPa (15ksi)/3 hours	9-11		Compaction leaked
51S-4	1182°C (2160°F)/103 MPa (15ksi)/ 3 hours	9-11		
51S-5	1182°C (2160°F)/103 MPa (15ksi)/ 3 hours	9-11	1163°C (2125°F)/2 hours/Rapid Air Cool + various (b, h, i)	Heat Treat Study
34D-1	1169°C-1177°C (2135°F-2150°F)/ 103 MPa (15ksi)/3 hours + re-HIP	9-11	Various	Quench HT studies Thin/Thick
35D-2	1169°F (2135°F)-1177°F (2150°F)/103 MPa (15ksi)/3 hours	4-6	1163°C (2125°F)/2 hours/OQ + various (b, k, l)	Heat Treat Study
35D-3	1169-1177°C (2135°F-2150°F)/ 103 MPa (15ksi)/3 hours	9-11	1163°C (2125°F)/2 hours/OQ + various	Heat Treat Study
102-1	1182°F (2160°F)/103 MPa (15ksi)/3 hours	8-10	1163°C (2125°F)/2 hours/OQ + 871°C (1600°F)/40 minutes/ AC + 982°C (1800°F)/45 minutes/AC + 649°C (1200°F)/ 24 hours/AC + 760°C (1400°F)/16 hours/AC	Design Data
102-2	1182°F (2160°F)/103 MPa (15ksi)/3 hours	8-10	1163°C (2125°F)/2 hours/OQ + 871°C (1600°F)/40 minutes/ AC + 982°C (1800°F)/45 minutes/AC + 649°C (1200°F)/ 24 hours/AC + 760°C (1400°F)/16 hours/AC	Design Data
MC101-1	1182°F (2160°F)/103 MPa (15ksi)/3 hours	8-10	1163°C (2125°F)/2 hours/OQ + 871°C (1600°F)/40 minutes/ AC + 982°C (1800°F)/45 minutes/AC + 649°C (1200°F)/ 24 hours/AC + 760°C (1400°F)/16 hours/AC	
MC101-2	1182°F (2160°F)/103 MPa (15ksi)/3 hours	8-10	1163°C (2125°F)/2 hours/OQ + 871°C (1600°F)/40 minutes/ AC + 982°C (1800°F)/45 minutes/AC + 649°C (1200°F)/ 24 hours/AC + 760°C (1400°F)/16 hours/AC	
160-1	1182°C (2160°F)/103 MPa (15ksi)/3 hours	8-10	1163°C (2125°F)/2 hours/OQ + 871°C (1600°F)/40 minutes/ AC + 982°C (1800°F)/45 minutes/AC + 649°C (1200°F)/ 24 hours/AC + 760°C (1400°F)/16 hours/AC	Spin Burst
160-2	1182°C (2160°F)/103 MPa (15ksi)/3 hours	8-10	1163°C (2125°F)/2 hours/OQ + 871°C (1600°F)/40 minutes/ AC + 982°C (1800°F)/45 minutes/AC + 649°C (1200°F)/ 24 hours/AC + 760°C (1400°F)/16 hours/AC	Design Data
160-3	1182°C (2160°F)/103 MPa (15ksi)/3 hours	8-10	1163°C (2125°F)/2 hours/OQ + 871°C (1600°F)/40 minutes/ AC + 982°C (1800°F)/45 minutes/AC + 649°C (1200°F)/ 24 hours/AC + 760°C (1400°F)/16 hours/AC	Engine Test

APPENDIX E

TENSILE AND SMOOTH/NOTCH STRESS RUPTURE PROPERTIES OF DISK 34D-1

Location	Heat Treatment (Quench Medium)	Test Temp.	Tensile 0.2% Y.S MPa(ksi)	Tensile UTS MPa(ksi)	Tensile % El	Tensile % RA	Stress-Rupture 732°C(1350°F) 655 MPa (95.0 ksi) Life-Hrs.		Stress-Rupture % El
Hub (Thin Section)	(oil)	RT	1055(153)	1607(233)	20.7	22.6	28.4	Notch	
			1076(156)	1607(233)	19.2	22.6	28.7	Notch	
	(350°F salt)		1034(150)	1579(229)	21.7	24.4	31.9	Notch	
			1027(149)	1586(230)	22.1	23.6	23.3	Notch	
	(650°F salt)		1020(148)	1579(229)	20.0	23.5	32.7	Notch	
			1000(145)	1517(220)	16.3	16.8	32.2	Notch	
	(Air)(1)		1069(155)	1600(232)	20.0	21.7	32.7	Notch	
			1089(158)	1613(234)	18.4	19.1	32.2	Notch	
Bore (Thick Section)	(Oil)		1034(150)	1593(231)	19.4	21.4	14.1	Notch	
			1020(148)	1600(232)	20.4	22.1	31.7	Notch	
	(350°F salt)		1007(146)	1579(229)	19.6	21.5	35.8	Notch	
			1055(153)	1613(234)	22.2	25.5	17.8	Notch	
	(650°F salt)		993(144)	1579(229)	23.1	24.3	12.3	Notch	
			1000(145)	1558(226)	19.3	21.6	12.1	Notch	
	(Air)		979(142)	1551(225)	20.5	22.6	24.0	Notch	
			986(143)	1572(228)	21.2	19.8	28.1	11.2	16.1
TARGET MINIMUM		RT	1034(150)	1482(215)	15.0	15.0	23.0	5.0@732°C (1350°F)/638 MPa (92.5 ksi)	

(1) Material Removed From Near The Surface Rather Than At The Center Of Section. This Location Would Give Unexpected Higher Strengths.

APPENDIX E (Cont'd)

Location	Heat Treatment (Quench Medium)	Test Temp.	Tensile 0.2% Y.S MPa(ksi)	Tensile UTS MPa(ksi)	% El	% RA
Hub (Thin Section)	(Oil)	621°C (1150°F)	1062(154)	1482(215)	21.8	29.5
			1041(151)	1475(214)	20.0	27.5
	(350°F salt)		972(141)	1434(208)	21.8	29.8
			1014(147)	1434(208)	25.1	31.3
	(650°F salt)		979(142)	1434(208)	24.4	34.1
			1007(146)	1455(211)	21.0	27.9
	(Air)		1007(146)	1441(209)	21.8	31.9
			1000(145)	1462(212)	18.7	31.4
Bore (Thick Section)	(Oil)	621°C (1150°F)	1014(147)	1141(209)	22.8	27.9
			1041(151)	1482(215)	19.8	27.3
	(350°F salt)		1020(148)	1427(207)	22.5	31.7
			1020(148)	1434(208)	21.9	30.9
	(650°F salt)		1020(148)	1427(207)	23.2	31.0
			1000(145)	1427(207)	25.0	32.4
	(Air)		931(135)	1379(200)	26.7	34.7
			945(137)	1379(200)	23.7	31.9
TARGET MINIMUM		621°C 1150°F	(150)	(194)	15.0	15.0
Hub (Thin Section)	(Oil)	704°C (1300°F)	1048(152)	1310(191)	16.1	22.9
	(350°F salt)		1014(147)	1282(186)	19.0	29.6
	(650°F salt)		1020(148)	1262(183)	20.4	33.1
	(Air)		1027(149)	1324(192)	20.0	33.5
Bore (Thick Section)	(Oil)		1007(146)	1262(183)	21.5	27.3
	(350°F salt)		993(144)	1255(182)	17.6	30.5
	(650°F salt)		965(140)	1248(181)	21.5	34.8

Location	Heat Treatment (Quench Medium)	Test Temp.	Tensile 0.2% Y.S MPa(ksi)	Tensile UTS MPa(ksi)	% El	% RA
	(Air)		924(134)	1207(175)	25.0	39.0
TARGET MINIMUM		704°C (1300°F)	1014(147)	1172(170)	12.0	12.0

Soln @ 1160°C(2125F)/2 hrs, age @ 649°C(1200°F)/24 hrs + 760°C(1400°F)/16 hrs

TENSILE PROPERTIES OF SEAL 35S-2

Test Temp.	0.2% Yield Strength MPa (Ksi)	Ultimate Tensile Strength MPa (Ksi)	Elongation %	Reduction In Area %
RT	1103(160.1)	1636(237.4)	21.2	18.7
RT	1102(160.0)	1654(240.0)	20.6	18.5
RT - TARGET	1034(150.0)	1482(215.0)	15.0	15.0
621°C(1150°F)	1132(164.3)	1522(220.9)	22.2	22.0
621°C(1150°F)	1107(160.7)	1501(217.9)	23.6	26.4
704°C(1300°F)	1094(158.8)	1316(191.0)	18.9	23.1
704°C(1300°F) - TARGET	1014(147.0)	1172(170)	12.0	12.0

COMBINED SMOOTH/NOTCH STRESS-RUPTURE PROPERTIES OF SEAL 35S-2

Test Conditions	Life Hours	Elongation - %
732°C(1350°F)/655 MPa(95Ksi)	16.7	(Notch)
732°C(1350°F)/638 MPa(92.5 Ksi)- TARGET	23.0	5.0

APPENDIX E (Cont'd)

TENSILE PROPERTIES OF TOBI SEAL 51S-5

Ident.	Test Temp. °C (°F)	0.2% YS MPa*	0.2% YS Ksi	UTS MPa*	UTS Ksi	% EL	% RA
b-31	21	1056	153.2	1557	225.8	24.6	25.3
b-32	(70)	1057	153.3	1541	223.5	23.9	26.5
h-40		1120	162.5	1566	227.2	20.2	22.8
h-41		1082	156.9	1549	224.7	22.7	24.0
i-49		1057	153.3	1555	225.5	21.6	21.9
i-50		1098	159.3	1578	228.9	20.9	22.0
	Target	1034	150.0	1482	215	15.0	15.0
b-34	621	1025	148.7	1419	205.8	23.5	30.7
b-35	(1150)	1011	146.7	1398	202.8	25.2	30.2
h-43		1025	148.6	1389	201.4	24.5	30.4
h-44		1020	148.0	1390	201.6	26.1	32.7
i-51		1000	145.1	1405	203.8	22.0	32.2
i-52		994	144.1	1394	202.2	22.7	28.3
b-37	704	1004	145.6	1256	182.2	25.7	33.2
h-45	(1300)	1039	150.7	1294	187.7	15.2	21.4
h-46		1011	146.6	1257	182.3	19.3	24.1
i-53		1043	151.3	1298	188.3	24.2	35.2
i-54		1006	145.9	1268	183.9	22.5	34.1
	Target	1014	147.0	1172	170.0	12.0	12.0

HIP at 1182°C (2160°F)/103.5 MPa (15 ksi)/3 hrs, and heat treated at 1171°C (2140°F)/2 hrs/RAC + Age*

*Age Heat Treatments

b. 649°C (1200°F)/24 hrs + 760°C (1400°F)/16 hrs

h. 871°C (1600°F)/0.67 hr + 982°C (1800°F)/0.75 hr + 649°C (1200°F)/24 hrs + 760°C (1400°F)/16 hrs

i. 871°C (1600°F)/1 + 649°C (1200°F)/24 + 760°C (1400°F)/16

APPENDIX F

TENSILE PROPERTIES OF DISK 35D-3 SOLUTION HEAT TREATED AT 1163°C (2125°F)/2 HRS/OQ + AGED AT VARIOUS CYCLES

Ident.	HIP Temp °C (°F)	Specimen Location	Test Temp °C (°F)	0.2% YS MPa (Ksi)	UTS MPa (Ksi)	% El	% RA
a-49	1177 (2150)	Bore-Center	21 (70)	1030.7 (149.6)	1544.7 (224.2)	20.2	23.4
a-50				1025.9 (148.9)	1504.1 (218.3)	18.5	23.4
b-13				1032.8 (149.9)	1528.2 (221.8)	18.2	22.5
b-14				1032.8 (149.9)	1535.8 (222.9)	19.8	19.9
c-5				1069.3 (155.2)	1519.9 (220.6)	15.6	19.0
c-6				1013.5 (147.1)	1479.3 (214.7)	15.8	18.8
e-18				997.0 (144.7)	1491.0 (216.4)	19.3	20.0
e-19				992.2 (144.0)	1501.3 (217.9)	19.0	22.5
f-23				980.4 (142.3)	1473.1 (213.8)	19.3	20.5
f-24				999.1 (145.0)	1465.5 (212.7)	16.2	19.5
g-30				1051.4 (152.6)	1480.0 (214.8)	13.9	16.1
h-35				1070.0 (155.3)	1530.3 (222.1)	19.0	20.2
h-36				1069.3 (155.2)	1476.5 (214.3)	15.6	19.0
h-55				1056.9 (153.4)	1462.1 (212.2)	13.3	16.3
i-43				1112.0 (161.4)	1463.4 (212.4)	11.6	13.7
i-44				1130.6 (164.1)	1470.3 (213.4)	11.3	12.6
i-58				1040.4 (151.0)	1447.6 (210.1)	12.0	15.8
j-10				941.9 (136.7)	1460.0 (211.9)	19.3	20.3
j-11				982.5 (142.6)	1477.9 (214.5)	17.8	22.3
b-61		Bore-ID	21 (70)	1109.3 (161.0)	1559.2 (226.3)	14.9	19.2
b-62				1104.5 (160.3)	1541.3 (223.7)	15.8	18.6
b-64				1030.7 (149.6)	1517.9 (220.3)	19.4	20.9
g-33				1116.2 (162.0)	1540.6 (223.6)	13.7	16.8
h-66				1041.8 (151.2)	1470.3 (213.4)	15.0	17.8
h-67				991.5 (143.9)	1434.5 (208.2)	14.5	16.0
h-71				1041.8 (151.2)	1468.9 (213.2)	15.2	16.7
i-74				1087.9 (157.9)	1477.2 (214.4)	11.5	16.5
i-75				1097.6 (159.3)	1466.2 (212.8)	9.8	12.5
h-79		Rim	21 (70)	1046.6 (151.9)	1470.3 (213.4)	15.2	17.3
h-80				1062.4 (154.2)	1496.5 (217.2)	14.8	17.8
i-83				1070.7 (155.4)	1486.2 (215.7)	12.4	15.0
i-84				1083.8 (157.3)	1453.1 (210.9)	11.1	13.9
	Target Minimum		21 (70)	1033.5 (150.0)	1481.4 (215.0)	15.0	15.0

APPENDIX F (Cont'd)

Ident.	HIP Temp °C (°F)	Specimen Location	Test Temp °C (°F)	0.2% YS MPa (Ksi)	UTS MPa (Ksi)	% El	% RA
a-51	1177 (2150)	Bore-Center	621 (1150)	995.6 (144.5)	1418.0 (205.8)	30.7	32.9
a-52				998.4 (144.9)	1409.0 (204.5)	24.3	28.2
b-3				1011.5 (146.8)	1431.7 (207.8)	26.4	28.7
b-4				1005.3 (145.9)	1429.7 (207.5)	27.5	30.2
b-15				1001.8 (145.4)	1426.9 (207.1)	28.6	31.0
b-16				995.0 (138.6)	1433.8 (208.1)	21.1	29.0
c-7				1005.9 (146.0)	1432.4 (207.9)	29.4	33.1
c-8				981.1 (142.4)	1385.6 (201.1)	35.7	33.9
d-28				1001.8 (145.4)	1420.7 (206.2)	30.7	32.5
e-20				970.8 (140.9)	1361.5 (197.6)	31.7	33.8
e-21				912.2 (132.4)	1378.7 (200.1)	32.4	31.7
f-25				908.8 (131.9)	1375.2 (199.6)	29.9	31.7
f-26				974.9 (141.5)	1377.3 (199.9)	27.8	26.1
g-32				963.9 (139.9)	1391.8 (202.0)	32.5	34.4
h-37				1043.8 (151.5)	1486.9 (215.8)	20.9	25.9
h-38				1051.4 (152.6)	1475.1 (214.1)	24.5	28.5
h-56				999.1 (145.0)	1373.9 (199.4)	29.5	32.0
h-57				986.6 (143.2)	1385.6 (201.1)	26.0	28.9
i-47				1028.7 (149.3)	1446.9 (210.0)	27.9	30.8
i-48				1032.8 (149.9)	1466.9 (212.9)	22.6	27.5
i-59				987.3 (143.3)	1426.9 (207.1)	28.6	33.2
i-60				1005.9 (146.0)	1437.3 (208.6)	24.9	26.3
j-12				853.7 (123.9)	1303.6 (189.2)	31.2	33.4
j-31				942.6 (136.8)	1338.0 (194.2)	29.8	33.2
b-63		Bore-ID	621 (1150)	1002.5 (145.5)	1428.3 (207.3)	27.5	30.2
g-34				1011.5 (146.8)	1486.9 (215.8)	24.2	27.5
h-68				1024.5 (148.7)	1421.4 (206.3)	27.0	30.0
h-69				1008.7 (146.4)	1420.7 (206.2)	24.2	26.1
h-72				980.4 (142.3)	1413.1 (205.1)	22.5	28.1
h-73				1051.4 (152.6)	1453.8 (211.0)	19.6	25.7
i-76				1033.5 (150.0)	1485.5 (215.6)	19.8	22.3
i-77				1088.6 (158.0)	1523.4 (221.1)	19.0	20.7
h-81		Rim	621 (1150)	1039.0 (150.8)	1417.3 (205.7)	20.7	23.6
h-82				1044.5 (151.6)	1420.0 (206.1)	26.2	28.0
i-85				1010.8 (146.7)	1430.4 (207.6)	27.1	21.7
i-86				986.6 (143.2)	1430.4 (207.6)	23.9	27.4

APPENDIX F (Cont'd)

TENSILE PROPERTIES OF DISK 35D-3 SOLUTION HEAT TREATED AT 1163°C (2125°F)/2 HRS/OQ + AGED AT VARIOUS CYCLES

Ident.	HIP Temp °C (°F)	Specimen Location	Test Temp °C (°F)	0.2% YS MPa (Ksi)	UTS MPa (Ksi)	% El	% RA
a-53	1177 (2150)	Bore-Center	704 (1300)	1012.8 (147.0)	1276.0 (185.2)	31.2	34.4
a-54				989.4 (143.6)	1268.4 (184.1)	32.7	32.7
b-17				1003.9 (145.7)	1287.1 (186.8)	29.8	37.1
c-9				988.0 (143.4)	1255.4 (182.2)	39.8	42.2
e-22				962.5 (139.7)	1230.6 (178.6)	41.5	45.5
f-27				1007.3 (146.2)	1285.7 (186.6)	35.9	37.6
h-39				1021.8 (148.3)	1274.0 (184.9)	27.4	28.4
h-40				1002.5 (145.5)	1242.3 (180.3)	25.9	29.8
b-65		Bore-ID	704 (1300)	1012.8 (147.0)	1278.1 (185.5)	31.5	37.9
h-70				1015.6 (147.4)	1245.7 (180.8)	27.1	32.1
i-78				1035.6 (150.3)	1310.5 (190.2)	16.2	23.1
		Target	704 (1300)	1012.8 (147.0)	1171.3 (170.0)	12.0	12.0

a. 649°C (1200°F)/24 hrs + 760°C (1400°F)/8 hrs

b. 649°C (1200°F)/24 hrs + 760°C (1400°F)/16 hrs

c. 649°C (1200°F)/24 hrs + 760°C (1400°F)/48 hrs

d. 649°C (1200°F)/8 hrs + 760°C (1400°F)/16 hrs

e. 649°C (1200°F)/24 hrs + 788°C (1450°F)/8 hrs

f. 649°C (1200°F)/24 hrs + 816°C (1500°F)/8 hrs

g. 760°C (1400°F)/48 hrs

h. 871°C (1600°F)/0.67 hr + 982°C (1800°F)/0.75 hr + 649°C (1200°F)/24 hrs + 760°C (1400°F)/16 hrs

i. 871°C (1600°F)/1 hr + 649°C (1200°F)/24 hrs + 760°C (1400°F)/16 hrs

j. 649°C (1200°F)/24 hrs + 760°C (1400°F)/16 hrs + 871°C (1600°F)/1hr

APPENDIX G

TENSILE PROPERTIES OF TOBI SEAL 51S-5

Ident.	Test Temp °C (°F)	0.2% YS MPa (Ksi)	UTS MPa (Ksi)	% El	% RA
b-31	21	1056 (153.2)	1557 (225.8)	24.6	25.3
b-32	(70)	1057 (153.3)	1541 (223.5)	23.9	26.5
h-40		1120 (162.5)	1566 (227.2)	20.2	22.8
h-41		1082 (156.9)	1549 (224.7)	22.7	24.0
i-49		1057 (153.3)	1555 (355.5)	21.6	21.9
i-50		1098 (159.3)	1578 (228.9)	20.9	22.0
	Target	1034 (150.0)	1482 (215.0)	15.0	15.0
b-34	621	1025 (148.7)	1419 (205.8)	23.5	30.7
b-35	(1150)	1011 (146.7)	1398 (202.8)	25.2	30.2
h-43		1025 (148.6)	1389 (201.4)	24.5	30.4
h-44		1020 (148.0)	1390 (201.6)	26.1	32.7
i-51		1000 (145.1)	1405 (203.8)	22.0	32.2
i-52		994 (144.1)	1394 (202.2)	22.7	28.3
b-37	704	1004 (145.6)	1256 (182.2)	25.7	33.2
h-45	(1300)	1039 (150.7)	1294 (187.7)	15.2	21.4
h-46		1011 (146.6)	1257 (182.3)	19.3	24.1
i-53		1043 (151.3)	1298 (188.3)	24.2	35.2
i-54		1006 (145.9)	1268 (183.9)	22.5	34.1
	Target	1014 (147.0)	1172 (170.0)	12.0	12.0

HIP at 1182°C (2160°F)/103.5 MPa (15 ksi)/3 hrs, and heat treated at 1171°C (2140°F)/2 hrs/RAC + Age*

*Age Heat Treatments

b. 649°C (1200°F)/24 hrs + 760°C (1400°F)/16 hrs

h. 871°C (1600°F)/0.67 hr + 982°C (1800°F)/0.75 hr + 649°C (1200°F)/24 hrs +760°C (1400°F)/16 hrs

i. 871°C (1600°F)/1 hr + 649°C (1200°F)/24 hrs + 760°C (1400°F)/16 hrs

APPENDIX H

TENSILE DESIGN DATA FOR DISKS 102-1, 102-2, 160-2

Temp °C (°F)	Specimen Location	Disk No.	0.2% YS MPa (Ksi)	UTS MPa (Ksi)	EL %	RA %
RT	BTNS	102-1	1090.1 (158.1)	1605.1 (232.8)	17.6	20.0
			1090.1 (158.1)	1597.5 (231.7)	19.0	20.0
		102-2	1106.6 (160.5)	1649.9 (239.3)	22.4	19.1
			- -	1629.9 (236.4)	21.1	18.2
	BTC	160-2	1014.9 (147.2)	1545.1 (224.1)	24.1	27.6
			1020.4 (148.0)	1545.1 (224.1)	26.4	24.8
			1028.0 (149.1)	1555.5 (225.6)	24.8	24.4
			995.6 (144.4)	1527.9 (221.6)	23.9	24.3
			991.5 (143.8)	1525.8 (221.3)	23.8	25.7
	WR	160-2	1018.4 (147.7)	1536.8 (222.9)	29.0	26.0
			1010.1 (146.5)	1535.5 (222.7)	29.1	27.5
	RTNS	102-1	1075.6 (156.0)	1573.4 (228.2)	17.2	18.1
			1065.2 (154.5)	1553.4 (225.3)	15.5	13.1
		102-2	1103.2 (160.0)	1614.8 (234.2)	19.1	17.2
			1093.5 (158.6)	1622.3 (235.3)	18.3	16.2
	RTC	160-2	1019.1 (147.8)	1536.8 (222.9)	24.3	24.4
			1008.7 (146.3)	1527.2 (221.5)	25.6	30.0
			1019.7 (147.9)	1538.9 (223.2)	25.1	25.3
			1019.1 (147.8)	1542.4 (222.7)	25.8	25.8
			1019.7 (147.9)	1534.8 (222.6)	29.5	28.5
260(500)	BTC	160-2	979.1 (142.0)	1467.9 (212.9)	17.1	16.0
			979.1 (142.0)	1492.7 (216.5)	21.9	22.6
	RTC	160-2	992.9 (144.0)	1483.1 (215.1)	20.4	19.3
			987.3 (143.2)	1469.3 (213.1)	23.9	23.9
482(900)	BTC	160-2	962.5 (139.6)	1438.9 (208.7)	25.3	29.6
			999.7 (145.0)	1468.6 (213.0)	23.4	26.2
	RTC	160-2	1014.9 (147.2)	1476.2 (214.1)	25.3	27.7
			1008.0 (146.2)	1451.4 (210.5)	26.4	27.0

APPENDIX H (Cont'd)

Temp °C (°F)	Specimen Location	Disk No.	0.2% YS MPa (Ksi)	UTS MPa (Ksi)	EL %	RA %
621(1150)	BTNS	102-1	1088.7 (157.9)	1622.3 (235.3)	21.0	21.9
			1057.0 (153.3)	1489.3 (216.0)	19.5	23.7
		102-2	1063.2 (154.2)	1438.9 (208.7)	23.6	26.6
			1057.0 (153.3)	1407.2 (204.1)	22.0	23.7
	BTC	160-2	969.4 (140.6)	1363.8 (197.8)	24.4	34.0
			952.2 (138.1)	1337.6 (194.0)	29.3	37.4
			961.1 (139.4)	1368.6 (198.5)	23.7	35.6
			1010.1 (146.5)	1387.9 (201.3)	28.6	28.8
			982.5 (142.5)	1377.6 (199.8)	30.1	34.3
	WR	160-2	982.5 (142.5)	1353.4 (196.3)	34.7	33.4
			959.6 (139.2)	1399.2 (195.5)	30.7	29.7
	RTNS	102-1	1074.2 (155.8)	1499.6 (217.5)	17.7	20.9
			1090.1 (158.1)	1467.2 (212.8)	19.0	21.8
		102-2	1085.2 (157.5)	1461.0 (211.9)	22.3	26.6
			1083.2 (157.1)	1465.8 (212.6)	22.1	24.8
	RTC	160-2	985.0 (142.9)	1387.9 (201.3)	27.6	28.2
			1001.1 (145.2)	1366.5 (198.2)	32.7	33.7
			1008.0 (146.2)	1387.9 (201.3)	27.7	26.2
			989.4 (143.5)	1366.5 (198.2)	31.7	31.6
			985.0 (142.9)	1362.4 (197.6)	27.7	26.0
704(1300)	BTC	160-2	997.0 (144.6)	1217.6 (176.6)	29.3	32.9
			994.2 (144.2)	1214.2 (176.1)	27.1	27.6
	RTC	160-2	998.4 (144.8)	1214.2 (176.1)	21.3	19.9
			948.7 (137.6)	1204.5 (174.7)	22.7	26.2
760(1400)	BTC	160-2	888.7 (128.9)	1059.0 (153.6)	28.8	27.0
			867.4 (125.8)	1065.9 (154.6)	30.2	29.7
	RTC	160-2	919.1 (133.3)	1102.5 (159.9)	14.0	17.7
			927.3 (134.5)	1097.7 (159.2)	15.5	19.5

Legend:
- BTNS — Bore Tangential Near Surface
- BTC — Bore Tangential Center
- WR — Web Radial
- RTNS — Rim Tangential Near Surface
- RTC — Rim Tangential Center

APPENDIX I

COMBINATION SMOOTH-NOTCH STRESS-RUPTURE DESIGN DATA
FOR DISKS 102-1, 102-2, 160-2

Specimen Location	Disk No.	Temperature °C (°F)	Stress MPa (Ksi)	Hours To Failure	El (%)	RA (%)	Type of Failure
WR	160-2	649 (1200)	965 (140)	169.3	11.3	7.8	-S-
RT	160-2	649 (1200)	965 (140)	21.1	-	-	-N-
WR	160-2	649 (1200)	862 (125)	1041.3	16.0	18.3	-S-
RT	160-2	649 (1200)	862 (125)	1717.1	11.4	10.6	-S-
RT	160-2	704 (1300)	758 (110)	213.0	-	-	-N-
RT	160-2	704 (1300)	758 (110)	1.5	-	-	-N-
WR	160-2	704 (1300)	655 (95)	318.6	-	-	-N-
RT	160-2	704 (1300)	655 (95)	327.6	-	-	-N-
RT	160-2	704 (1300)	655 (95)	296.2	-	-	-N-
WR	160-2	704 (1300)	517 (75)	604.3	-	-	-N-
RT	160-2	704 (1300)	517 (75)	1095.0	-	-	-N-
RT	160-2	704 (1300)	517 (75)	736.1	-	-	-N-
WR	160-2	732 (1350)	655 (95)	89.4	14.0	10.8	-S-
WR	160-2	732 (1350)	448 (65)	384.0	-	-	-N-
RT	102-2	732 (1350)	655 (95)	18.2	-	-	-N-
RT	102-2	732 (1350)	655 (95)	11.2	-	-	-N-
RT	102-2	732 (1350)	655 (95)	34.0	-	-	-N-
RT	102-2	732 (1350)	655 (95)	59.5	-	-	-N-
RT	160-2	732 (1350)	655 (95)	139.4	-	-	-N-
RT	160-2	732 (1350)	655 (95)	1.7	-	-	-N-
BT	160-2	732 (1350)	638 (92.5)	114.6	-	-	-N-
BT	160-2	732 (1350)	638 (92.5)	150.8*	-	-	-N-
RT	160-2	732 (1350)	638 (92.5)	158.4	-	-	-N-
RT	160-2	732 (1350)	638 (92.5)	159.3	-	-	-N-
RT	160-2	732 (1350)	448 (65)	369.7	-	-	-N-
RT	160-2	732 (1350)	448 (65)	493.3	-	-	-N-
RT	160-2	760 (1400)	552 (80)	35.5	-	-	-N-
RT	160-2	760 (1400)	552 (80)	42.7	-	-	-N-
RT	160-2	760 (1400)	379 (55)	349.3	-	-	-N-
RT	160-2	760 (1400)	379 (55)	317.6	-	-	-N-
RT	160-2	760 (1400)	276 (40)	961.6	-	-	-N-
RT	160-2	760 (1400)	276 (40)	1390.9	-	-	-N-

*Rim tangential replaced bore tangential specimen due to mechanical problem.

APPENDIX J

CREEP DESIGN DATA FOR DISKS 102-1, 102-2, 160-2

Specimen Location	Disk No.	Temperature °C (°F)	Stress MPa (Ksi)	Hours To 0.1%	Hours To 0.2%	Comments
RTC	160-2	593 (1100)	758 (110)	-	-	Discontinued 1532 0.08%
RTC	160-2	593 (1100)	758 (110)	-	-	Discontinued 1452 0.01%
RTC	160-2	593 (1100)	689 (100)	-	-	Discontinued 1866 0.03%
RTC	160-2	593 (1100)	689 (100)	455	-	Discontinued 1387 0.13%
RTC	160-2	649 (1200)	862 (125)	18	90	
RTC	160-2	649 (1200)	862 (125)	10	45	
WR	160-2	649 (1200)	793 (115)	59	183	
WR	160-2	649 (1200)	793 (115)	46	158	
RTC	160-2	649 (1200)	793 (115)	63	129	
RTC	160-2	649 (1200)	793 (115)	191	399	
RTC	160-2	649 (1200)	758 (110)	280	888	
RTC	160-2	649 (1200)	758 (110)	265	749	
WR	160-2	704 (1300)	552 (80)	325	516	
R	102-1	704 (1300)	552 (80)	13	36	
R	102-1	704 (1300)	552 (80)	11	32	
R	160-2	704 (1300)	552 (80)	260	489	
R	160-2	704 (1300)	552 (80)	195	321	
WR	160-2	732 (1350)	552 (80)	8	21	
WR	160-2	732 (1350)	552 (80)	6	17	
RTC	160-2	732 (1350)	552 (80)	34	40	
RTC	160-2	732 (1350)	552 (80)	37	68	
RTC	160-2	732 (1350)	310 (45)	270	444	
RTC	160-2	732 (1350)	310 (45)	159	306	
RTC	160-2	732 (1350)	207 (30)	460	852	
RTC	160-2	732 (1350)	207 (30)	428	779	
RTC	160-2	760 (1400)	379 (55)	13	37	
RTC	160-2	760 (1400)	379 (55)	23	54	
RTC	160-2	760 (1400)	276 (40)	85	161	
RTC	160-2	760 (1400)	276 (40)	74	149	
RTC	160-2	760 (1400)	207 (30)	160	304	
RTC	160-2	760 (1400)	207 (30)	136	289	

APPENDIX K

AXIAL LOW CYCLE FATIGUE RESULTS
Smooth (Kt = 1.0)

Heat Code	Temperature °C (°F)	Stress MPa (Ksi)	Cycles X 10^3 to Failure
102-1	427 (800)	669 + 669 (97 + 97)	16.0
102-1	427 (800)	669 ∓ 669 (97 ∓ 97)	17.0
102-2	427 (800)	669 ∓ 669 (97 ∓ 97)	13.0
160-2	427 (800)	669 ∓ 669 (97 ∓ 97)	11.6
160-2	427 (800)	669 ∓ 669 (97 ∓ 97)	14.6
160-2	427 (800)	669 ∓ 669 (97 ∓ 97)	10.7
102-1	427 (800)	579 ∓ 579 (84 ∓ 84)	102.0
102-1	427 (800)	579 ∓ 579 (84 ∓ 84)	57.0
102-2	427 (800)	579 ∓ 579 (84 ∓ 84)	40.0
160-2	427 (800)	579 ∓ 579 (84 ∓ 84)	22.4
102-1	538 (1000)	655 + 655 (95 + 95)	10.0
102-1	538 (1000)	655 ∓ 655 (95 ∓ 95)	7.0
102-2	538 (1000)	655 ∓ 655 (95 ∓ 95)	9.0
160-3	538 (1000)	655 ∓ 655 (95 ∓ 95)	9.8
102-1	538 (1000)	579 ∓ 579 (84 ∓ 84)	33.0
102-2	538 (1000)	579 ∓ 579 (84 ∓ 84)	13.0
102-2	538 (1000)	579 ∓ 579 (84 ∓ 84)	16.0
160-3	538 (1000)	579 ∓ 579 (84 ∓ 84)	37.7
102-1	538 (1000)	545 ∓ 545 (79 ∓ 79)	24.0
102-1	538 (1000)	545 ∓ 545 (79 ∓ 79)	18.0
102-2	538 (1000)	545 ∓ 545 (79 ∓ 79)	29.0
160-3	538 (1000)	545 ∓ 545 (79 ∓ 79)	77.4
102-1	635 (1175)	648 + 648 (94 + 94)	5.0
102-2	635 (1175)	648 ∓ 648 (94 ∓ 94)	6.0
102-2	635 (1175)	648 ∓ 648 (94 ∓ 94)	6.0
160-3	635 (1175)	648 ∓ 648 (94 ∓ 94)	3.6
102-1	635 (1175)	579 ∓ 579 (84 ∓ 84)	7.0
102-2	635 (1175)	579 ∓ 579 (84 ∓ 84)	38.0
102-2	635 (1175)	579 ∓ 579 (84 ∓ 84)	35.0
160-2	635 (1175)	579 ∓ 579 (84 ∓ 84)	9.5
102-2	635 (1175)	531 ∓ 531 (77 ∓ 77)	124.0
102-2	635 (1175)	531 ∓ 531 (77 ∓ 77)	27.0
160-2	635 (1175)	531 ∓ 531 (77 ∓ 77)	108.3
160-3	635 (1175)	531 ∓ 531 (77 ∓ 77)	97.0

APPENDIX K (Cont'd)

Heat Code	Temperature °C (°F)	Stress MPa (Ksi)	Cycles X 10^{-3} to: 1/32"	Failure
102-1	427 (800)	531 + 531 (77 + 77)	4.0	5.0
102-1	427 (800)	531 ∓ 531 (77 ∓ 77)	4.0	4.5
102-2	427 (800)	531 ∓ 531 (77 ∓ 77)	4.0	4.5
160-2	427 (800)	531 ∓ 531 (77 ∓ 77)	-	7.0
102-1	427 (800)	441 ∓ 441 (64 ∓ 64)	10.0	13.0
102-1	427 (800)	441 ∓ 441 (64 ∓ 64)	8.0	10.0
102-2	427 (800)	441 ∓ 441 (64 ∓ 64)	12.0	12.5
160-2	427 (800)	441 ∓ 441 (64 ∓ 64)	-	15.9
102-1	427 (800)	427 ∓ 427 (62 ∓ 62)	8.0	13.0
102-1	427 (800)	427 ∓ 427 (62 ∓ 62)	11.0	13.0
102-2	427 (800)	427 ∓ 427 (62 ∓ 62)	11.0	13.0
160-2	427 (800)	427 ∓ 427 (62 ∓ 62)	20.0	21.5
160-2	427 (800)	427 ∓ 427 (62 ∓ 62)	-	39.6
160-3	427 (800)	427 ∓ 427 (62 ∓ 62)	-	31.1
102-1	538 (1000)	483 + 483 (70 + 70)	-	6.0
102-2	538 (1000)	483 ∓ 483 (70 ∓ 70)	4.5	5.5
102-2	538 (1000)	483 ∓ 483 (70 ∓ 70)	4.5	5.5
160-3	538 (1000)	483 ∓ 483 (70 ∓ 70)	-	11.0
102-1	538 (1000)	427 ∓ 427 (62 ∓ 62)	6.0	8.0
102-1	538 (1000)	427 ∓ 427 (62 ∓ 62)	14.0	16.0
102-2	538 (1000)	427 ∓ 427 (62 ∓ 62)	8.0	9.5
160-3	538 (1000)	427 ∓ 427 (62 ∓ 62)	-	26.4
102-1	538 (1000)	400 ∓ 400 (58 ∓ 58)	14.0	16.0
102-2	538 (1000)	400 ∓ 400 (58 ∓ 58)	20.0	22.0
160-2	538 (1000)	400 ∓ 400 (58 ∓ 58)	-	15.5
160-2	538 (1000)	400 ∓ 400 (58 ∓ 58)	72.0	80.2
102-1	635 (1175)	427 + 427 (62 + 62)	6.0	8.0
102-2	635 (1175)	427 ∓ 427 (62 ∓ 62)	4.0	6.5
160-3	635 (1175)	427 ∓ 427 (62 ∓ 62)	-	10.7
160-3	635 (1175)	427 ∓ 427 (62 ∓ 62)	-	9.1
102-1	635 (1175)	379 ∓ 379 (55 ∓ 55)	8.0	12.5
102-2	635 (1175)	379 ∓ 379 (55 ∓ 55)	15.0	16.0
102-2	635 (1175)	379 ∓ 379 (55 ∓ 55)	25.0	27.0
160-3	635 (1175)*	379 ∓ 379 (55 ∓ 55)	12.0	14.4

*1404 NNS-1020

APPENDIX K (Cont'd)

Heat Code	Temperature °C (°F)	Stress MPa (Ksi)	Cycles X 10^{-3} to: 1/32"	Failure
102-1	427 (800)	296 + 296 (43 + 43)	27.0	39.0
102-1	427 (800)	296 ∓ 296 (43 ∓ 43)	35.0	40.0
102-2	427 (800)	296 ∓ 296 (43 ∓ 43)	20.0	29.0
102-2	427 (800)	296 ∓ 296 (43 ∓ 43)	34.0	42.0
102-2	427 (800)	296 ∓ 296 (43 ∓ 43)	24.0	28.0
102-2	427 (800)	296 ∓ 296 (43 ∓ 43)	70.0	77.0
160-3	427 (800)	296 ∓ 296 (43 ∓ 43)	32.0	32.7
160-3	427 (800)	296 ∓ 296 (43 ∓ 43)	6.0	17.6
160-3	427 (800)	296 ∓ 296 (43 ∓ 43)	8.0	15.9
160-3	427 (800)	296 ∓ 296 (43 ∓ 43)	18.0	25.7
102-1	538 (1000)	296 + 296 (43 + 43)	14.0	19.0
102-1	538 (1000)	296 ∓ 296 (43 ∓ 43)	16.0	25.0
102-1	538 (1000)	296 ∓ 296 (43 ∓ 43)	16.0	31.0
102-2	538 (1000)	296 ∓ 296 (43 ∓ 43)	16.0	21.0
102-2	538 (1000)	296 ∓ 296 (43 ∓ 43)	70.0	74.0
102-1	538 (1000)	276 ∓ 276 (40 ∓ 40)	26.0	35.0
102-1	538 (1000)	276 ∓ 276 (40 ∓ 40)	30.0	38.0
102-1	538 (1000)	276 ∓ 276 (40 ∓ 40)	26.0	38.0
102-1	538 (1000)	276 ∓ 276 (40 ∓ 40)	44.0	54.0
102-1	635 (1175)	296 + 296 (43 + 43)	10.0	14.0
102-1	635 (1175)	296 ∓ 296 (43 ∓ 43)	8.0	11.5
102-2	635 (1175)	296 ∓ 296 (43 ∓ 43)	10.0	13.0
102-2	635 (1175)	296 ∓ 296 (43 ∓ 43)	8.0	12.0
102-1	635 (1175)	262 ∓ 262 (38 ∓ 38)	20.0	32.0
102-1	635 (1175)	262 ∓ 262 (38 ∓ 38)	16.0	24.0
102-2	635 (1175)	262 ∓ 262 (38 ∓ 38)	12.0	16.0
102-2	635 (1175)	262 ∓ 262 (38 ∓ 38)	10.0	12.0

APPENDIX L

BOLT HOLE TYPE LOW CYCLE FATIGUE DESIGN DATA
FOR DISKS 102-1, 102-2, 160-2

Temperature °C (°F)	Stress MPa (Ksi) Min	Max	Time at (Seconds) No Load	Load	Disk No.	Cycles X 10^{-3} To: 1/32"	Failure	Comments
427 (800)	0	779 (113)	10	10	102-1	6.0	7.1	
427 (800)	0	779 (113)	10	10	102-1	5.5	6.7	
427 (800)	0	779 (113)	10	10	102-1	4.0	6.5	
427 (800)	0	779 (113)	10	10	102-1	4.0	5.9	
427 (800)	0	683 (99)	10	10	160-2	8.0	11.3	
427 (800)	0	683 (99)	10	10	160-2	12.3	16.0	
427 (800)	0	683 (99)	10	10	160-2	7.6	9.7	1.5x0.6 mil pore
427 (800)	0	683 (99)	10	10	160-2	20.6	23.5	1.0x0.5 mil pore
427 (800)	0	655 (95)	10	10	102-2	8.0	13.1	
427 (800)	0	655 (95)	10	10	102-2	11.0	14.0	
427 (800)	0	655 (95)	10	10	102-2	21.0	25.2	
427 (800)	0	655 (95)	10	10	102-2	45.0	46.2	
482 (900)	0	758 (110)	10	10	102-1	5.0	5.9	
482 (900)	0	758 (110)	10	10	102-1	4.0	5.6	
482 (900)	0	758 (110)	10	10	102-1	5.0	6.2	
482 (900)	0	758 (110)	10	10	102-1	5.0	6.6	
482 (900)	0	683 (99)	10	10	160-2	24.5	28.0	
482 (900)	0	683 (99)	10	10	160-2	15.0	18.1	
482 (900)	0	683 (99)	10	10	160-2	5.0	7.6	0.75x0.5 mil pore
482 (900)	0	683 (99)	10	10	160-2	54.5	58.1	0.5x0.5 mil pore
538 (1000)	0	731 (106)	10	10	102-1	4.0	5.7	
538 (1000)	0	731 (106)	10	10	102-1	4.0	5.0	
538 (1000)	0	731 (106)	10	10	102-1	4.0	5.1	
538 (1000)	0	731 (106)	10	10	102-1	4.0	5.8	
538 (1000)	0	683 (99)	10	10	160-2	11.0	12.7	
538 (1000)	0	683 (99)	10	10	160-2	23.5	25.7	1.0x1.0 mil pore
538 (1000)	0	683 (99)	10	10	160-2	7.0	10.9	0.5 mil mil pore
538 (1000)	0	683 (99)	10	10	160-2	16.5	18.5	
538 (1000)	0	614 (89)	10	10	102-2	-	21.9	
538 (1000)	0	614 (89)	10	10	102-2	-	30.9	
538 (1000)	0	614 (89)	10	10	102-2	-	10.0	
538 (1000)	0	614 (89)	10	10	102-2	-	32.6	

APPENDIX L (Cont'd)

BOLT HOLE TYPE LOW CYCLE FATIGUE DESIGN DATA
FOR DISKS 102-1, 102-2, 160-2

Temperature °C (°F)	Stress MPa (Ksi) Min	Max	Time at (Seconds) No Load	Load	Cycles X 10^{-3} To: Disk No.	1/32"	Failure	Comments
593 (1100)	0	683 (99)	10	10	160-2	12.5	15.7	
593 (1100)	0	683 (99)	10	10	160-2	12.5	16.2	
593 (1100)	0	683 (99)	10	10	160-2	8.5	11.4	0.6x0.6 mil pore
593 (1100)	0	683 (99)	10	10	160-2	19.5	20.4	0.4x0.4 mil pore
593 (1100)	0	600 (87)	10	10	102-2	-	41.4	1 mil porosity
593 (1100)	0	600 (87)	10	10	102-2	13.0	16.8	2 x 6 mil Al-rich inclusion
593 (1100)	0	600 (87)	10	10	102-2	-	81.7	1.5 porosity
593 (1100)	0	600 (87)	10	10	102-2	29.2	31.5	1.5x1.5 mil pore
649 (1200)	0	683 (99)	10	10	102-2	4.0	5.4	
649 (1200)	0	683 (99)	10	10	102-2	4.0	4.9	
649 (1200)	0	683 (99)	10	10	160-2	3.5	4.9	
649 (1200)	0	683 (99)	10	10	160-2	5.7	6.6	0.7x0.4 mil pore
649 (1200)	0	579 (84)	10	10	102-2	-	10.0	
649 (1200)	0	579 (84)	10	10	102-2	-	10.0	
649 (1200)	0	579 (84)	10	10	102-2	-	10.0	
649 (1200)	0	579 (84)	10	10	102-2	-	10.0	

APPENDIX M

ACCEPTANCE CRITERIA FOR MERL 76 HIP CONSOLIDATIONS

1. SCOPE:

1.1 Form: Hot isostatically pressed powder metallurgy product.

1.2 Application: Primarily for rotor parts operating at temperatures up to 760°C (1400°F).

2. APPLICABLE DOCUMENTS: The following publications form a part of these criteria to the extent specified herein; the latest issue shall apply.

2.1 SAE Publications: Available from Society of Automotive Engineers, Inc., 400 Commonwealth Drive, Warrendale, PA 15096.

2.1.1 Aerospace Material Specifications:

AMS 2269 Chemical Check Analysis Limits, Wrought Nickel and Nickel Base Alloys
AMS 2350 Standards and Test Methods
AMS 2630 Ultrasonic Inspection

2.2 ASTM Publications: Available from American Society for Testing and Materials, 1916 Race Street, Philadelphia, PA 19103.

ASTM E112 Estimating Average Grain Size of Metals
ASTM E354 Chemical Analysis of High-Temperature, Electrical, Magnetic, and Other Similar Iron, Nickel, and Cobalt-Base Alloys

2.3 Government Publications: Available from Commanding Officer, Naval Publications and Forms Center, 5801 Tabor Avenue, Philadelphia, PA 19120.

2.3.1 Federal Standards:

Federal Test Method Standard No. 151 - Metals; Test Methods

3. Technical Requirements:

3.1 Composition: Shall conform to the following percentages by weight, determined by wet chemical methods in accordance with ASTM E354, by spectrographic methods in accordance with Federal Test Method Standard No. 151, Method 112, or by other approved analytical methods.

	Min.		Max.
Columbium	1.20		1.60
Hafnium	0.30		0.50
Carbon	0.015		0.030
Manganese	–		.020
Silicon	–		.10
Phosphorous	–		.010
Sulfur	–		.010
Chromium	11.9	–	12.9
Cobalt	18.00	–	19.00
Molybdenum	2.8	–	3.6
Titanium	4.15	–	4.50
Aluminum	4.80	–	5.15
Boron	0.016	–	.024
Zirconium	0.04		.08
Tungsten	–		0.05
Iron	–		0.30
Copper	–		0.07
Lead	–		0.0001 (1 ppm)
Bismuth	–		0.00005 (0.5 ppm)
Oxygen	–		0.010 (100 ppm)
Nitrogen	–		0.0050 (50 ppm)
Nickel	remainder		

3.1.1 Check Analysis: Composition variations shall meet the requirements of AMS 2269.

3.2 Thermally Induced Porosity: A sample of the product shall be heated to temperature within the range of 1171 - 1193°C (2140 - 2180°F), held at the selected temperature ±8°C (±15°F) for 4 hrs., and air cooled. Microstructure after thermal exposure shall conform to the requirements agreed upon by purchaser and vendor.

3.3 Ultrasonic Inspection: The HIP consolidation shall undergo ultrasonic inspection in accordance with ASTM 2630 using a standard agreed upon by purchaser and vendor.

3.4 Dimensional Inspection: The HIP consolidation shall undergo dimensional inspection with the data conforming to the requirements agreed upon by purchaser and vendor.

3.5 Condition: The product shall be supplied as solution, stabilization, and precipitation heat treated and descaled as follows.

3.6 Heat Treatment:

3.6.1 Solution Heat Treatment: Heat to 1163°C (2125°F), hold at this selected temperature within ± 8°C (± 15°F) for 2 hours, and oil quench.

3.6.2 Stabilization Heat Treatment: Heat to 870°C ±8 (1600°F ±15), hold at heat for 40 ±5 min., and cool to below 371°C (700°F) at a rate equivalent to air cool; heat to 982°C ±8 (1800°F ±15), hold at heat for 45 ±5 min., and cool to below 371°C (700°F) at a rate equivalent to air cool.

3.6.3 Precipitation Heat Treatment: Heat to 650°C ± 8 (1200°F ± 15), hold at heat for 24 hr., and air cool to below 371°C (700°F), heat to 760°C ± 8 (1400°F ± 15), hold at heat for 16 hrs., and air cool.

3.7 Integral Test Specimens: Shall be located so as to approximate thickest cross-sectional area and slowest cooling rate from hot isostatic pressing and heat treatment, as agreed upon by the purchaser and the vendor. Alternate location of integral test specimens and their properties shall be as agreed upon by the purchaser and the vendor.

3.7.1 Tensile Properties: Tensile test specimens cut from the product and tested at the temperatures indicated shall conform to the following requirements. Specimens to be tested at 621°C (1150°F ±10) shall be held at heat for 30 min. prior to testing. Rate of strain for testing at 621°C (1150°F ±10) shall be maintained at approximately 0.005 mm per min. (0.005 in. per in. per min.) to the 0.2% yield strength.

	Room Temperature	621°C (1150°F)
Tensile Strength, MPa, (psi), min	1482 (215,000)	1338 (194,000)
Yield Strength at 0.2% Offset, MPa (psi), min	1034 (140,000)	1014 (140,000)
Elongation, % in 4D, min	15	12
Reduction of Area, %, min	15	12

3.7.2 Stress-Rupture Properties at 732°C (1350°F): A combination smooth and notched test specimen, maintained at 732°C ±3 (1350°F ±5) under continuously applied axial stress of 92,500 psi shall not rupture in less than 23 hours. The test shall be continued to rupture with fracture occurring in the smooth section. Elongation of the smooth section after rupture, measured at room temperature, shall be not less than 5% in 4D.

3.7.2.1 As an alternate procedure, separate smooth and notched test specimens, machined from adjacent sections of the same piece may be tested individually, under the above conditions. The smooth specimen shall not rupture in less than 23 hr. and elongation after rupture, measured at room temperature, shall be not less than 5% in 4D. The notched specimens shall not rupture in less time than the smooth specimen.

3.7.3 Microstructure: Shall conform to requirements agreed upon by purchaser and the vendor.

3.7.4 Grain Size: Average shall be 5 or finer as determined by Planimetric Procedure in ASTM E112.

4. REJECTIONS: Material not conforming to this acceptance criteria or to authorized modification will be subject to rejection.

TABLE I (SI)

Specimen Number	Center Gage Diameter G, Millimeter	C	D, min	E, min	F	H	RR
1	3.18	3.18	12.70	9.53	3.18	4.50	0.10
2	3.81	3.18	15.24	9.53	3.81	5.38	0.13
3	4.06	3.18	16.51	9.53	4.06	5.74	0.13
4	4.52	3.18	19.05	9.53	4.52	6.35	0.16
5	6.40	3.18	25.40	9.53	6.40	9.07	0.23
6	9.07	3.18	38.10	9.53	9.07	12.70	0.30
Tolerance	± 0.03	± 1.59	–	–	± 0.03	± 0.08	± 0.013

TABLE I

Specimen Number	Center Gage Diameter G, Inch	C	D, min	E, min	F	H	RR
1	0.125	0.125	0.500	0.375	0.125	0.177	0.004
2	0.150	0.125	0.600	0.375	0.150	0.212	0.005
3	0.160	0.125	0.650	0.375	0.160	0.226	0.005
4	0.178	0.125	0.750	0.375	0.178	0.250	0.006
5	0.252	0.125	1.000	0.375	0.252	0.357	0.009
6	0.357	0.125	1.500	0.375	0.357	0.500	0.012
Tolerance	± 0.001	± 0.062	–	–	± 0.001	± 0.003	± 0.0005

Note 1. Radius "R" between gage and full diameter sections and between full section and thread sections shall be 0.125 - 0.250 inch (3.18 - 6.35 mm).

Note 2. Finish specimens to $\sqrt{16}$ (0.4 micrometers) or better on all "*f*" surfaces; surface roughness of notch root radius shall be substantially the same as on sides of notch as determined by examination at 10X magnification.

Note 3. The difference between dimensions "F" and "G" shall not exceed 0.0005 in. (0.013 mm) for specimens 1, 2, 3, and 4 and shall not exceed 0.001 in. (0.03 mm) for specimens 5 and 6.

Note 4. Taper gage length "D" to center so that diameter "G" at the ends of the gage length exceeds diameter "G" at the center of the gage length by 0.0005-0.0015 in. (0.013 - 0.038 mm).

Note 5. All sections shall be concentric about specimen axis within 0.001 inch (0.03 mm).

Note 6. Thread size "T" shall be such that minor diameter of the thread is greater than "H".

Note 7. Thread length "B" shall be equal to or greater than "T".

Note 8. Dimension "A" is not specified.

Note 9. Specimens 3 and 4 are the preferred specimens.

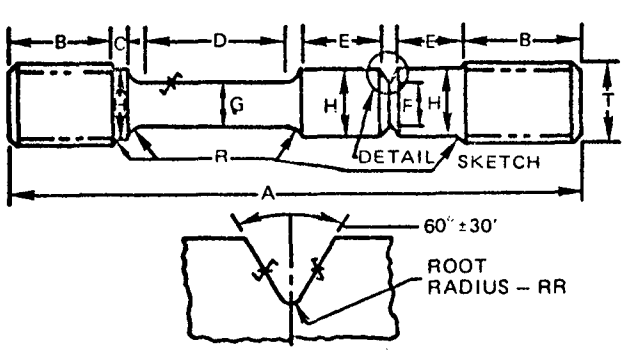

Figure 1 Combination Smooth-and-Notched Test Stress-Rupture Specimen

APPENDIX N

PROCESS CONTROL PLAN FOR POWDER ATOMIZATION/HIP PROCESS
HIP TURBINE DISK

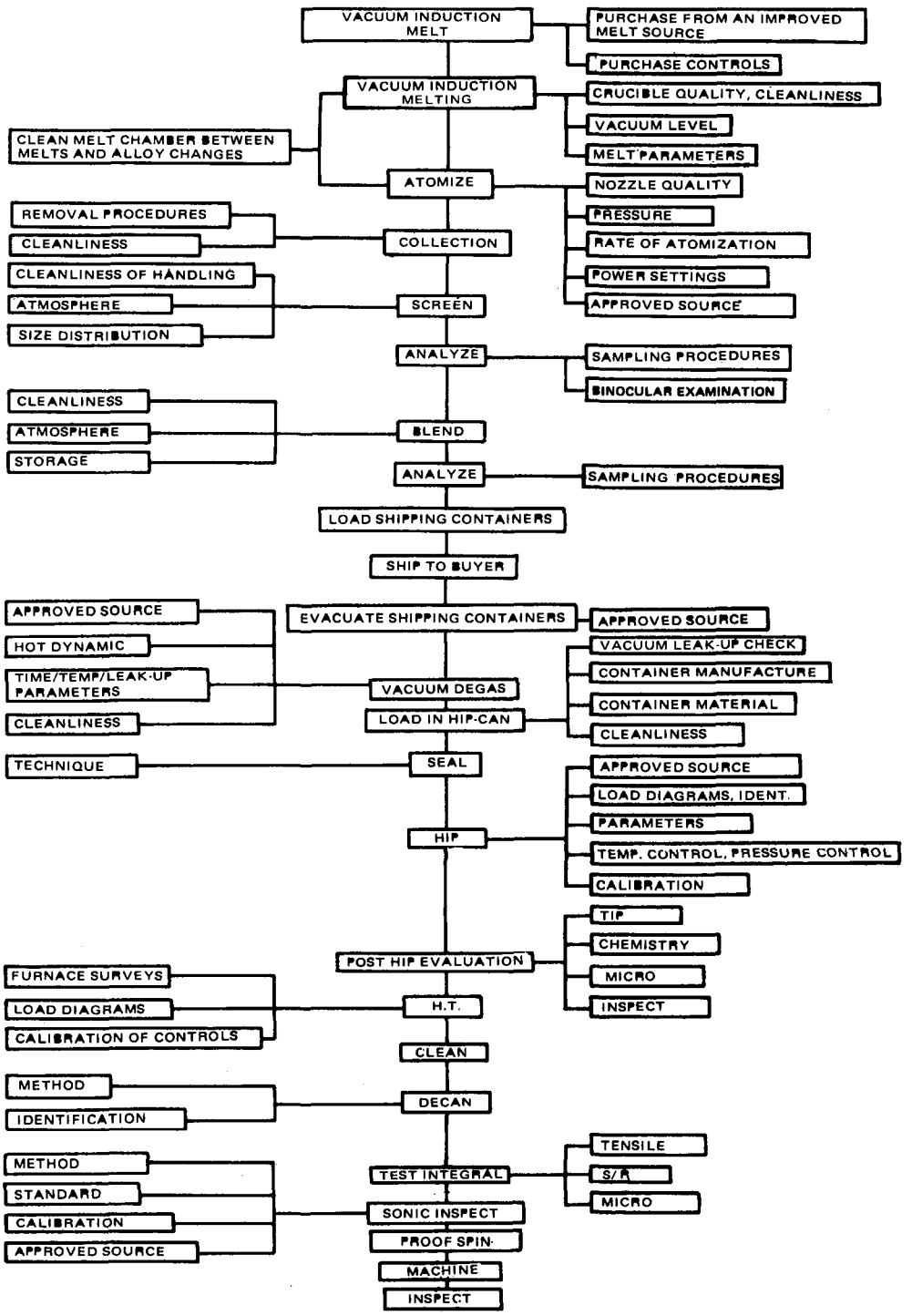

THE EXACT PARAMETERS OF EACH PROCESS STEP SHALL BE AGREED UPON BY PURCHASER AND VENDOR.

APPENDIX 0

LOWER DESIGN LIMIT PROPERTIES

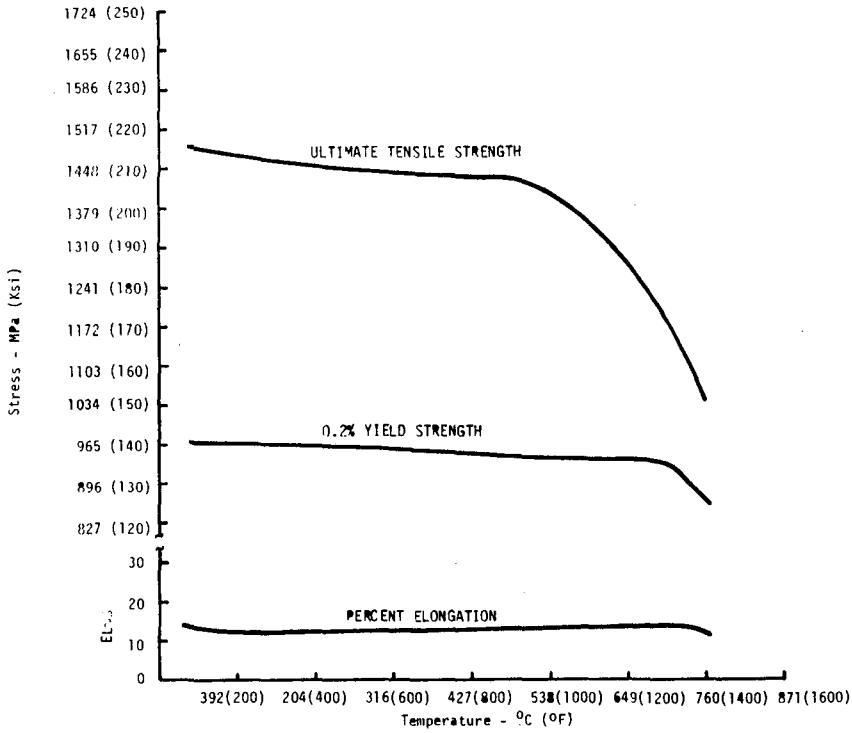

Lower Limit Tensile Properties of MERL 76

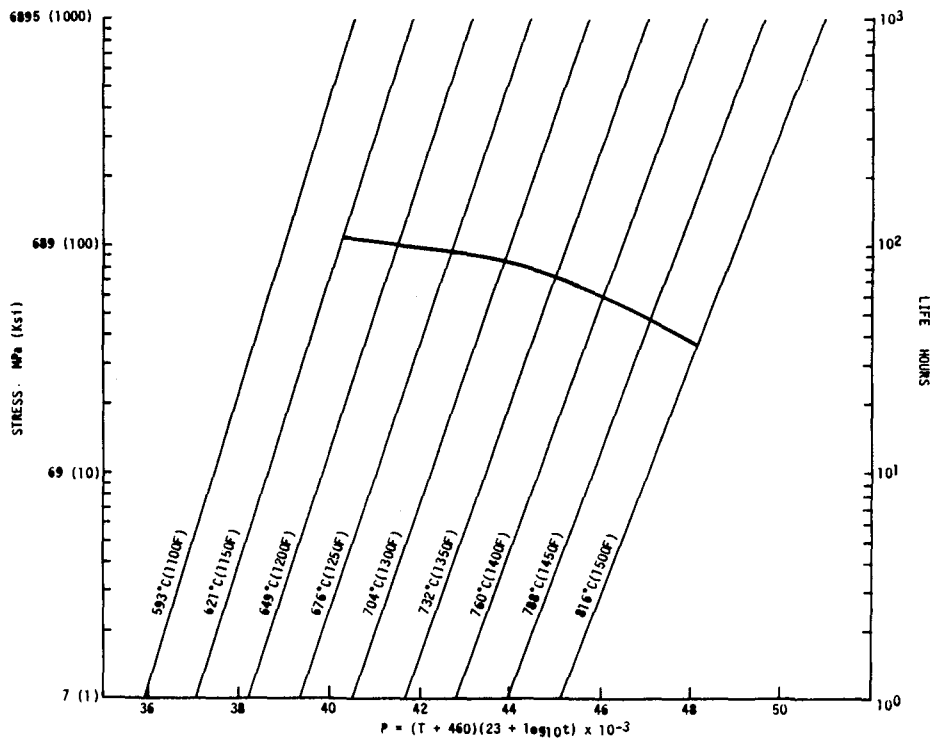

Lower Limit Stress-Rupture Properties of MERL 76

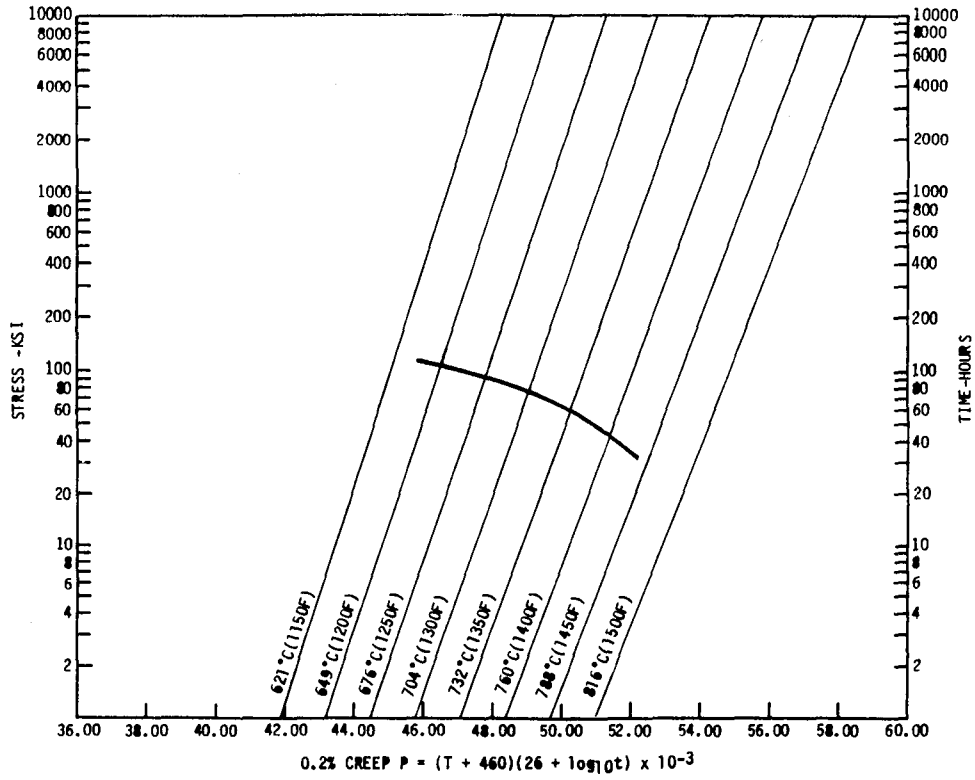

Lower Limit 0.2% Creep Properties of MERL 76

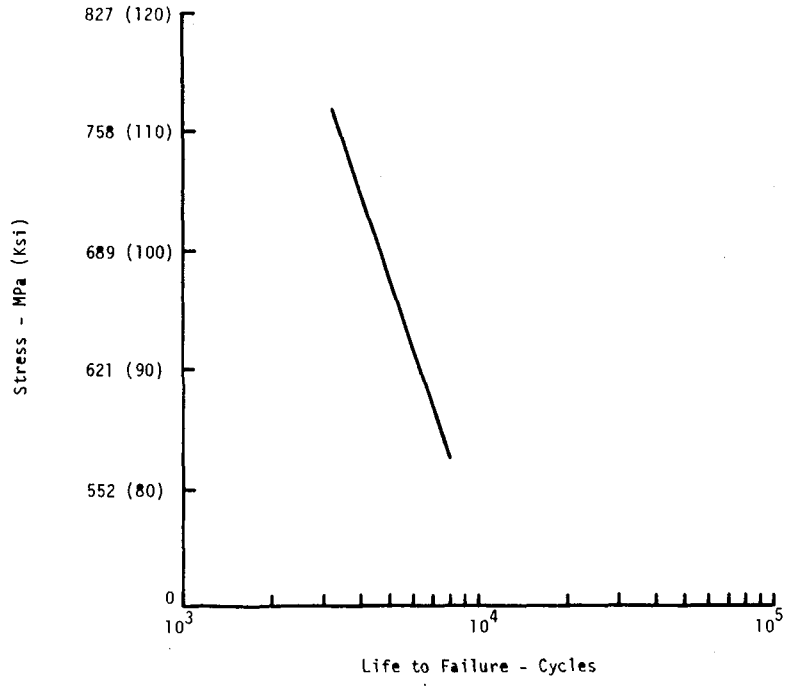

Lower Limit Notched (K_t=2.5) Low Cycle Fatigue Properties at 649°C(1200°F) for MERL 76 Temperature Range

1. Report No.	2. Government Accession No.	3. Recipient's Catalog No.
NASA CR-165549		

4. Title and Subtitle	5. Report Date
HOT ISOSTATICALLY PRESSED MANUFACTURE OF HIGH STRENGTH MERL 76 AND SEAL SHAPES	May 1982
	6. Performing Organization Code

7. Author(s)	8. Performing Organization Report No.
R. D. Eng and D. J. Evans	PWA 5574-123
	10. Work Unit No.

9. Performing Organization Name and Address	11. Contract or Grant No.
United Technologies Corporation Pratt & Whitney Aircraft Group Commercial Products Division East Hartford, Connecticut 06108	NAS3-20072
	13. Type of Report and Period Covered
12. Sponsoring Agency Name and Address	Contractor Report
National Aeronautics and Space Administration Washington, D. C. 20456	14. Sponsoring Agency Code 510-53-12

15. Supplementary Notes

Final report. Project Manager, Robert Davies, Materials Division, NASA Lewis Research Center, Cleveland, Ohio 44135.

16. Abstract

A program was conducted under Project 2 of NASA Contract NAS3-20072 to demonstrate the feasibility of using MERL 76, an advanced high strength direct hot isostatic pressed powder metallurgy superalloy, as a full scale component in a high technology, long life, commercial gas turbine engine. The component was a JT9D first stage turbine disk. The goals of Project 2 were to: 1) increase the JT9D disk rim temperature capability by at least 22°C (40°F), 2) reduce the weight of JT9D high pressure turbine rotating components by at least 35 pounds by replacement of forged Superwaspaloy® components with hot isostatic pressed MERL 76 components, and 3) reduce JT9D disk manufacturing costs by at least 30 percent relative to Superwaspaloy disks. Based on the results of Project 1 of the same contract, manufacturing processes were established which were then finalized in Project 2 to generate the process control plan and acceptance criteria for manufacture of MERL 76 HIP consolidated components. In addition, disk components were manufactured for spin/burst rig test, experimental engine test, and design data generation, which established lower design properties including tensile, stress-rupture, 0.2% creep and notched (Kt = 2.5) low cycle fatigue properties, Sonntag, fatigue crack propagation and low cycle fatigue crack threshold data. Results of Project 2 demonstrated direct HIP MERL 76, when compared to conventionally forged Superwaspaloy®, to be superior in mechanical properties, increased rim temperature capability, reduced component weight, and reduced material cost by at least 30% based on 1980 costs. These results have led to the conclusion that direct HIP MERL 76 disks are suitable for fabrication of components to be used in a commercial engine.

17. Key Words (Suggested by Author(s))	18. Distribution Statement
MERL 76; Powder metallurgy; Waspaloy; Gas turbine engines; Hot isostatic pressing; Turbine disks; Low cycle fatigue	Unclassified - unlimited STAR Category 26

19. Security Classif. (of this report)	20. Security Classif. (of this page)	21. No. of Pages	22. Price*
Unclassified	Unclassified	138	

* For sale by the National Technical Information Service, Springfield, Virginia 22161

☆USGPO: 1982 — 559-091/3234

NASA Langley Rsch Center
Attn Library
Langley Field, VA 23365

185